

KINETIC, MECHANISTIC AND SPECTROSCOPIC STUDIES OF SPORE
PHOTOPRODUCT LYASE

by

Sunshine Christine Silver

A dissertation submitted in partial fulfillment
of the requirements for the degree

of

Doctor of Philosophy

in

Biochemistry

MONTANA STATE UNIVERSITY
Bozeman, Montana

November, 2010

©COPYRIGHT

by

Sunshine Christine Silver

2010

All Rights Reserved

APPROVAL

of a dissertation submitted by

Sunshine Christine Silver

This dissertation has been read by each member of the dissertation committee and has been found to be satisfactory regarding content, English usage, format, citation, bibliographic style, and consistency and is ready for submission to the Division of Graduate Education.

Dr. Joan B. Broderick

Approved for the Department of Chemistry and Biochemistry

Dr. David Singel

Approved for the Division of Graduate Education

Dr. Carl A. Fox

STATEMENT OF PERMISSION TO USE

In presenting this dissertation in partial fulfillment of the requirements for a doctoral degree at Montana State University, I agree that the Library shall make it available to borrowers under rules of the Library. I further agree that copying of this dissertation is allowable only for scholarly purposes, consistent with “fair use” as prescribed in the U.S. Copyright Law. Requests for extensive copying or reproduction of this dissertation should be referred to ProQuest Information and Learning, 300 North Zeeb Road, Ann Arbor, Michigan 48106, to whom I have granted “the exclusive right to reproduce and distribute my dissertation in and from microform along with the non-exclusive right to reproduce and distribute my abstract in any format in whole or in part.”

Sunshine Christine Silver

November, 2010

DEDICATION

This work is dedicated to Patrick and Sienna. Thank you for your continued support and encouragement.

ACKNOWLEDGEMENTS

I would like to express my sincere gratitude to my advisor, Dr. Joan Broderick, who has provided me with an exciting project and guidance during my graduate studies. I would like to thank the members of my graduate committee for their insights and guidance, Dr. Peters, Dr. Szilagyi, Dr. Dratz, Dr. Kohler, Dr. Dooley, and Dr. Atwood.

I would like to acknowledge my collaborators for their contributions to this work, Dr. Robert Szilagyi and David Gardenghi for help with XAS studies and computational work, Dr. Vincent Huyhn and Dr. Sunil Naik for their help with the Mössbauer studies, Dr. Brian Hoffman, Dr. Nick Lees and Dr. Roman Davydov for their work on ENDOR studies, Dr. Valerie Copie for her assistance with NMR studies, and Dr. David Singel and Dr. David Schwab for assistance with EPR studies.

I would also like to thank Dr. Jeffrey Buis and Dr. Danilo Ortillo for training and helping me start the project, Dr. Egidijus Zilinskas and Shourjo Ghose for their many contributions to SPL, Dr. Tilak Chandra for his talents in synthesizing and characterizing SP substrates, and Dr. Eric Shepard and Dr. Susan Veneziano for their contributions as well as advice in many things scientific and otherwise, and my fellow lab mates.

I would like to thank Amanday Byer, Trinity Hamilton, Dr. Danilo Ortillo, Joyce Brewer Shepard, Dr. Eric Shepard, and Dr. Susan Veneziano for their friendship and support during my graduate career. I would like to thank my parents, Dan and Mary Jo, and my sister Carrie for being a source of great encouragement. A special thank you to my husband, Patrick, and my daughter, Sienna, for your support and patience while I completed this work. This goal would not have been reached without all of you!

TABLE OF CONTENTS

1. INTRODUCTION	1
Iron Sulfur Clusters	1
Radical SAM Enzymes	4
Common Mechanistic Implications	9
Structural Insights	13
Spore Photoproduct Lyase.....	15
DNA Damage, Spore Photoproduct Formation and Small, Acid Soluble Proteins	16
Repair of Pyrimidine Dimers	22
Characterization of SP Lyase.....	25
Mechanism of SP Lyase.....	28
Research Goals	36
References	39
Manuscript in Chapter 2: Contribution of Authors and Co-Authors.....	47
Manuscript Information Page.....	48
2. SPORE PHOTOPRODUCT LYASE CATALYZES SPECIFIC REPAIR OF THE 5R BUT NOT THE 5S SPORE PHOTOPRODUCT	49
Abstract	49
Acknowledgements	56
References	57
Manuscript in Chapter 3: Contribution of Authors and Co-Authors.....	58
Manuscript Information Page.....	59
3. COMPLETE STEREOSPECIFIC REPAIR OF A SYNTHETIC DINUCLEOTIDE SPORE PHOTOPRODUCT BY SPORE PHOTOPRODUCT LYASE.....	60
Abstract	60
Introduction	61
Materials and Methods	64
Biochemical Methods	64
Materials	64
Expression and Purification of SP Lyase.....	64
Protein and Iron Assays	66
Assay of SP Lyase Activity	66
HPLC Analysis	66

TABLE OF CONTENTS – CONTINUED

Mass Spectrometry.....	67
Spectroscopic Measurements.....	67
Synthetic Methods	68
Synthesis and Stereochemical Assignment of 5 <i>R</i> - and 5 <i>S</i> - Dinucleotide Spore Photoproducts	69
Results	70
Overexpression and Purification of SP Lyase	70
Spectroscopic Characterization of <i>C.a.</i> SP Lyase.....	71
Characterization of Synthetic Dinucleotide Spore Photoproducts.....	76
Enzymatic Repair of the Dinucleotide Spore Photoproducts	78
Discussion	83
Acknowledgements	88
References	89
Manuscript in Chapter 4:	
Contribution of Authors and Co-Authors.....	93
Manuscript Information Page.....	94
4. KINETIC AND MECHANISTIC INSIGHTS INTO THE REPAIR OF THE SPORE PHOTOPRODUCT CATALYZED BY SPORE PHOTOPRODUCT LYASE	95
Abstract	95
Introduction	96
Materials and Methods	99
Materials	99
Methods.....	99
Results	100
SP Repair Dependence on [4Fe-4S] ¹⁺	100
Transfer of Tritium from SP to SAM	102
Discussion	104
References	107
Manuscript in Chapter 5:	
Contribution of Authors and Co-Authors.....	109
Manuscript Information Page.....	110
5. COMBINED MÖSSBAUER AND MULTI-EDGE X-RAY ABSORPTION SPECTROSCOPIC STUDY OF THE FE-S CLUSTER IN SPORE PHOTOPRODUCT LYASE	111
Abstract	111
Introduction	112

TABLE OF CONTENTS – CONTINUED

Materials and Methods	115
Materials	115
Methods.....	115
Sample Preparation	116
Mössbauer Spectroscopy	116
X-ray Absorption Spectroscopy.....	117
X-ray Absorption Spectroscopy Data Collection and Analysis.....	118
Results and Analysis	119
Mössbauer Spectroscopic Characterization of Anaerobic SP Lyase	119
X-ray Absorption Spectroscopic Characterization of Anaerobic SP Lyase	122
Iron K-edge EXAFS	122
Iron K-edge XANES.....	125
Sulfur K-edge XAS.....	127
Discussion	133
References	141
6. CONCLUDING REMARKS.....	145
APPENDICES	151
APPENDIX A: Supporting Information for Chapter 2.....	152
APPENDIX B: Supporting Information for Chapter 5.....	155

LIST OF TABLES

Table	Page
1.1. Amount of SP repaired in the presence of varying amounts of SAM.....	33
1.2. Comparison of SP lyase from <i>B.s.</i> as compared to <i>C.a.</i>	37
3.1. Catalytic activities of SP lyase with a series of synthetic and natural substrates	87
4.1. Label transfer from SP C-6 to AdoMet at different reaction time points.....	103
5.1. Percentage of total iron present in the iron-sulfur cluster of SP lyase determined by Mössbauer spectroscopy	122
5.2. Preedge peak energies (eV) obtained from fits of the S K-edge XAS preedge features of SP lyase.....	131
5.3. Cluster changes in MoaA upon SAM binding	138

LIST OF SCHEMES

Scheme	Page
1.1. Formation of the 5'-deoxyadenosyl radical by means of reductive cleavage of <i>S</i> -adenosylmethionine.	10
1.2. DNA Photoproducts upon UV-Irradiation.....	18
1.3. UV induced SP is repaired directly by SP lyase.....	22
2.1. Formation and repair of SP.....	50
4.1. SP lyase catalyzes the repair of SP.....	96
4.2. Proposed mechanism of SP formation.....	105
4.3. Possibilities for stereospecificity of SP formation and H atom abstraction by SP lyase.....	106
5.1. SP lyase catalyzes the repair of the spore photoproduct.....	113

LIST OF FIGURES

Figure	Page
1.1. Three most common iron sulfur clusters	2
1.2. Reactions catalyzed by the radical SAM superfamily	5
1.3. Structures of adenosylcobalamin and SAM.....	8
1.4. Coordination of SAM to the radical SAM [4Fe-4S] cluster	11
1.5. Active site X-ray structures of HydE SAM-bound and [5'-dAdo + Met]- bound.....	13
1.6. X-ray crystal structures of LAM, MoaA and PFL-AE	15
1.7. Conserved CX ₃ CX ₂ C binding motif of radical SAM enzymes	16
1.8. X-ray crystal structure of SASP-DNA complex	20
1.9. UV-vis spectra of SP lyase	26
1.10. X-band EPR spectra of SP lyase.....	28
1.11. Time course repair assay of SP-DNA by SP lyase	28
1.12. Proposed mechanism for SP repair by SP lyase.	30
1.13. Tritium incorporation into SAM during SP repair.....	31
1.14. Tritium incorporation into thymine during SP repair	31
1.15. HPLC analysis of SAM cleavage by SP lyase.....	33
1.16. Sequence alignment of <i>C.a.</i> SP lyase with <i>B.s.</i> SP lyase.....	35
2.1. Chemical drawings and computational models for the 5R and 5S synthetic spore photoproduct analogues lacking a DNA backbone	52

LIST OF FIGURES – CONTINUED

Figure	Page
2.2. HPLC chromatograms showing the time-dependent formation of thymidine due to repair of 5 <i>R</i> -SP but not 5 <i>S</i> -SP and quantitation of repair.....	55
3.1. Formation and repair of SP.....	61
3.2. Structures of 5 <i>R</i> - and 5 <i>S</i> -SPTpT synthetic substrates.....	63
3.3. SDS-PAGE of <i>C.a.</i> SP lyase.....	71
3.4. UV-vis spectra of <i>C.a.</i> SP lyase.....	72
3.5. X-band EPR spectra of <i>C.a.</i> SP lyase.....	74
3.6. X-band EPR spectral evidence for unique interaction of SP lyase with AdoMet.....	76
3.7. NMR spectroscopic characterization of the purified synthetic dinucleotide spore photoproducts.....	77
3.8. HPLC chromatograms showing the time-dependent formation of thymidine due to repair of 5 <i>R</i> -SPTpT but not 5 <i>S</i> -SPTpT and quantitation of repair.....	79
3.9. Extended ESI MS of 5 <i>R</i> - thymidylyl (3'-5') thymidine (SPTpT) before and after repair with SP lyase.....	82
4.1. Proposed mechanism of SP repair by SP lyase.....	98
4.2. SP lyase HPLC-based activity assay showing repair of SP.....	101
4.3. Incorporation of ³ H atom into AdoMet after abstraction from C-6 of SP.....	103
4.4. 5 <i>R</i> -SP with the pro- <i>S</i> C-6 H atom indicated with an arrow.....	107
5.1. Mössbauer spectra of as-isolated and reduced SP lyase in the absence and presence of SAM.....	121

LIST OF FIGURES – CONTINUED

Figure	Page
5.2. Fe K-edge EXAFS of as-isolated and reduced SP lyase in the absence and presence of SAM.....	123
5.3. Fe K-edge EXAFS of as-isolated SP lyase in the presence of SAM.....	124
5.4. Fe K-edge XANES of FeCl ₂ , FeCl ₃ , FeF ₂ and FeF ₃ and as-isolated and reduced SP lyase in the absence and presence of SAM.....	125
5.5. S K-edge XANES of free S-ligands	128
5.6. Renormalized S K-edge XANES of as-isolated and reduced SP lyase in the absence and presence of SAM	129
5.7. Fits of the S K-edge spectra of the as-isolated and reduced SP lyase in the absence and presence of SAM	132

LIST OF ABBREVIATIONS

5R-SPTpT: *5R* stereoisomer of the SPTpT substrate
5S-SPTpT: *5S* stereoisomer of the SPTpT substrate
AdoMet: *S*-Adenosyl-L-methionine
dAdo: 5'-Deoxyadenosine
DFT: Density functional theory
DTT: Dithiothreitol
ENDOR: Electron nuclear double resonance
EPR: Electron paramagnetic resonance
EXAFS: Extended X-ray absorption fine structure
FAD: Flavin adenine dinucleotide
HemN: Oxygen independent coproporphyrinogen-III-oxidase
LAM: Lysine-2,3-aminomutase
MoaA: Molybdopterin cofactor biosynthesis
PFL: Pyruvate formate lyase
PFL-AE: Pyruvate formate lyase activating enzyme
SAH: *S*-Adenosyl-L-homocysteine
SAM: *S*-Adenosyl-L-methionine
SASP: Small, acid soluble protein
SP Lyase: Spore photoproduct lyase
SP: Spore photoproduct
TpT: Thymidylyl-(3'-5')-thymidine
XANES: X-ray absorption near edge structure
XAS: X-ray absorption spectroscopy

ABSTRACT

Spore forming organisms are a health threat to humans and other animals in part due to a remarkable resistance to UV irradiation. This resistance results from two events: first, the formation of a unique thymine dimer, 5-thyminyl-5,6-dihydrothymine (spore photoproduct, or SP) upon UV irradiation; and more importantly, the rapid and specific repair of this DNA photoproduct to two thymines by spore photoproduct lyase (SP lyase). Understanding the molecular basis of this radical-mediated DNA repair will ultimately allow for a better understanding of how to address the health risks caused by spore forming bacteria. SP lyase requires *S*-adenosyl-L-methionine and a [4Fe-4S]^{1+/2+} cluster to perform its catalysis. Presented in this work is a characterization of *Clostridium acetobutylicum* SP lyase and its ability to repair stereochemically defined dinucleoside and dinucleotide synthetic substrates. Careful synthesis and characterization followed by assays monitored by HPLC indicate SP lyase repairs only the 5*R* isomer of SP with an activity of 0.4 nmol/min/mg (dinucleoside substrate) and 7.1 nmol/min/mg (dinucleotide substrate). These results support the longstanding theory of SP formation by dimerization of adjacent thymines in double-helical DNA. Kinetic and mechanistic studies were pursued to further elucidate the mechanism of SP repair. Upon pre-reducing SP lyase, the specific activity increased nearly 4-fold to 1.29 μmol/min/mg. Mechanistic studies utilizing [C-6-³H] SP DNA as the substrate revealed a primary tritium kinetic isotope effect of 16.1, indicating a rate determining step during the repair reaction. These results suggest nonstereospecific SP formation regarding the C-6 position and subsequent stereospecific abstraction of the C-6 H atom by SP lyase. Mössbauer and Fe/S K-edge X-ray absorption studies of anaerobically prepared SP lyase aided in further characterization of the [4Fe-4S] cluster and its interaction with SAM. The Fe K-edge EXAFS provide evidence for a slight cluster distortion upon interacting with SAM as a new spectral feature indicative of longer Fe-Fe distances is observed. The Fe K-edge XANES provide further support that SAM is not undergoing reductive cleavage in the presence of reduced SP lyase. Our XAS studies may provide new insights into the mechanism by which radical SAM enzymes initiate their diverse catalysis.

CHAPTER 1

INTRODUCTION

Iron-Sulfur Clusters

Clusters comprised of iron and inorganic sulfide ([Fe-S] clusters) are one of the earliest prosthetic groups in nature. These clusters play an essential role for a wide array of biological reactions including photosynthesis and respiration [1-2]. It is surprising then that the first [Fe-S] proteins were not detected until 1960 as electron paramagnetic resonance signatures in mitochondrial membranes [3]. Shortly thereafter a ferredoxin was discovered in the anaerobic nitrogen-fixing bacteria *Clostridium pasteurianum* [4]. While [Fe-S] centers were discovered much later than many other biological cofactors, this can be explained by the instability of these [Fe-S] clusters in the presence of oxygen and their broad indistinct UV-visible spectra as compared to other cofactors. Since the first [Fe-S] proteins were identified, a great deal of research has been invested in this field and it is now well established that [Fe-S] proteins are present in every living organism [5]. It is fascinating that not only do these diverse and oxygen sensitive [Fe-S] proteins function in aerobic conditions, but also play essential roles in both aerobic and anaerobic environments.

The most common [Fe-S] clusters include the [2Fe-2S], [3Fe-4S] and [4Fe-4S] clusters with irons typically ligated in a tetrahedral manner through cysteine thiolate ligands with further coordination provided by inorganic sulfides (Figure 1.1). More complex [Fe-S] clusters with additional modifications are observed, such as the active

site centers found in the hydrogenase and nitrogenase enzymes [6-7]. [Fe-S] clusters demonstrate preferential ligation by thiolates and consequently cysteinyl sulfur is the most commonly observed ligand of [Fe-S] active sites, although histidine, and less often glutamine, serine, or arginine ligation has been observed in some cases [8-9].

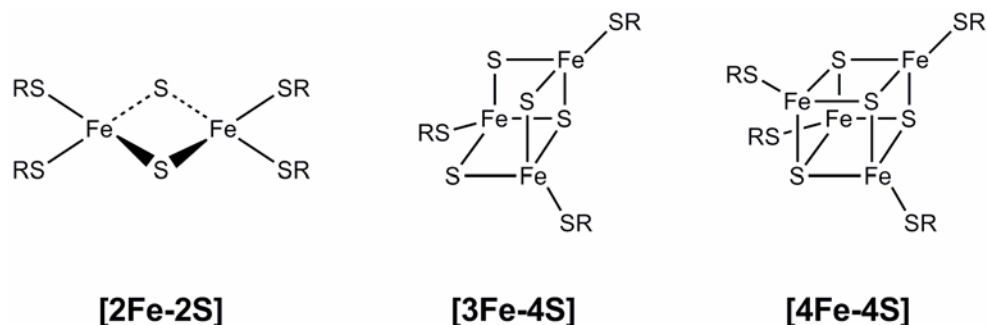


Figure 1.1. The three most common iron sulfur clusters found in biology include the [2Fe-2S], [3Fe-4S] and the [4Fe-4S].

Initially, it was suggested that [Fe-S] proteins all had the same function of facilitating biological electron transfer processes. Indeed, iron and sulfur display remarkable chemical versatility in their ability to delocalize electron density over both atoms, making them well-suited for this purpose [2, 5]. Based on the ability of iron to formally switch between +2 and +3 oxidation states and the flexibility of a proteinaceous surrounding, [Fe-S] proteins can adopt redox potentials from -500 mV to +400 mV, making them excellent candidates to donate and accept electrons in a variety of biological reactions [2, 10]. Some of the best known examples of [Fe-S] proteins displaying this function include mitochondrial respiratory complexes I-III, photosystem I, ferredoxins and hydrogenases.

While [Fe-S] proteins have long been known to function in electron transport processes, their roles have been expanded to include an assortment of diverse functions. These ubiquitous cofactors are also known to function in regulatory roles and tuning gene expression in response to environmental or intracellular conditions. Examples of this function include the bacterial transcription factors FNR, which senses O₂; IscR, which senses Fe-S cluster availability; and SoxR, which senses superoxide and NO stress [11-14]. An example for post-transcriptional regulation of gene expression by [Fe-S] clusters is provided by the mammalian cytosolic iron regulatory protein 1 (IRP1), which under iron deprivation conditions can bind to stem-loop structures (known as iron-responsive elements) in certain mRNAs of proteins involved in intra-cellular iron homeostasis [15-18]. Under iron-replete conditions, IRP1 contains a [4Fe-4S] cluster and functions as an aconitase.

An additional role of [Fe-S] proteins is enzyme catalysis, such as the role for aconitase in which a non-protein-coordinated Fe at one edge of a [4Fe-4S] cluster serves as a Lewis acid to assist in the isomerization of citrate to isocitrate. In chloroplast ferredoxin:thioredoxin reductase, the [4Fe-4S] cluster donates electrons to a redox active pair of cysteines and undergoes transient bonding to one of them [19].

While numerous other catalytic functions are known for bacterial and eukaryotic [Fe-S] enzymes involved in metabolism, the precise role of the [Fe-S] cluster is unclear in many of them and it is possible that in some proteins the [Fe-S] cluster plays merely a structural role [10, 20]. This is the suggestion for the recently discovered [Fe-S] clusters

in ATP-dependent DNA helicases involved in nucleotide excision repair including Rad3, XPD and FANCI (BRIP1) [21].

Iron-sulfur proteins also play a critical role in initiating radical catalysis, a role utilized by the members of the radical SAM superfamily of enzymes. This enzyme family utilizes *S*-adenosyl-L-methionine (SAM or AdoMet) and a site-differentiated [4Fe-4S]¹⁺ cluster to cleave non-activated C-H bonds, allowing for chemically difficult as well as diverse reactions to take place.

Radical SAM Enzymes

The radical SAM superfamily of enzymes is currently comprised of more than 2800 enzymes which require SAM and a [4Fe-4S]^{1+/2+} cluster to carry out biologically diverse reactions (Figure 1.2) [22-23]. While only a handful of radical SAM enzymes have been purified and characterized, these enzymes are found to carry out a wide diversity of reactions including the formation of protein-based glyceryl radicals, sulfur insertion reactions, rearrangement reactions, reduction of ribonucleotides, biosynthesis of complex cofactors and metal clusters, tRNA modifications, biosynthesis of antibiotics and the repair of DNA. This enzyme family typically contains a conserved CX₃CX₂C amino acid sequence which, for a number of years, was utilized to quickly identify radical SAM enzymes. However, enzymes that require SAM and a [4Fe-4S]¹⁺ cluster to carry out their catalysis but differ in their conserved cysteine sequence are now being identified (CX₂CX₄C in ThiC and CX₅CX₂C in HmdB) [24-25]. Some of the enzymes found in the radical SAM superfamily and the reactions catalyzed are shown in Figure

1.2. The role of SAM is denoted as enzymes in this superfamily utilize SAM as either a cofactor or co-substrate during catalysis.

Figure 1.2. Examples of diverse reactions catalyzed by members of the radical SAM superfamily.

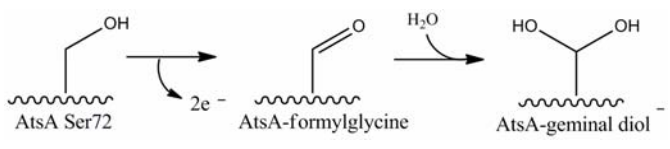
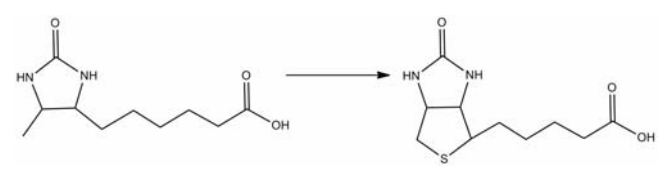

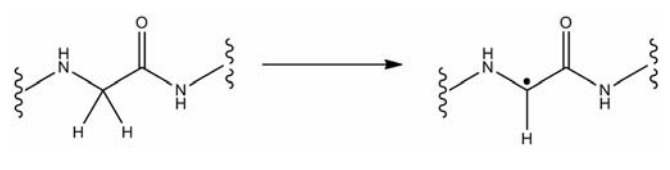
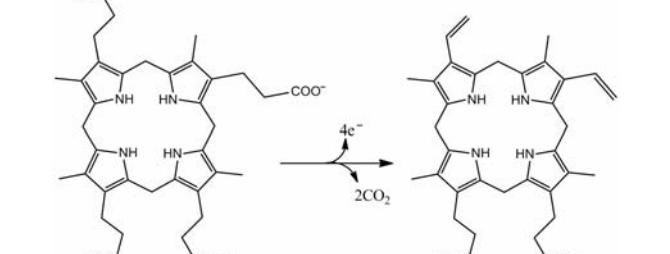
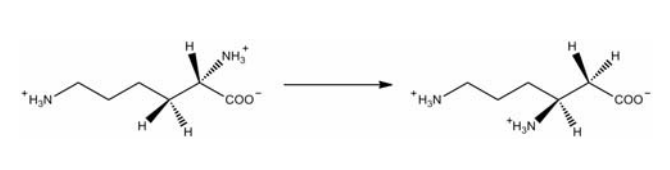

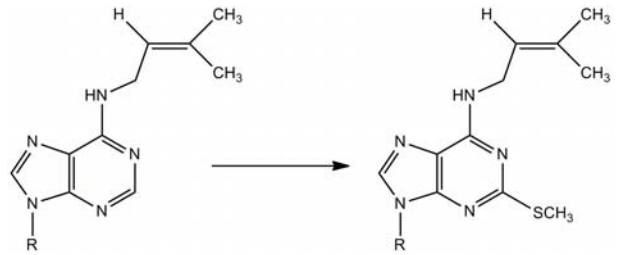
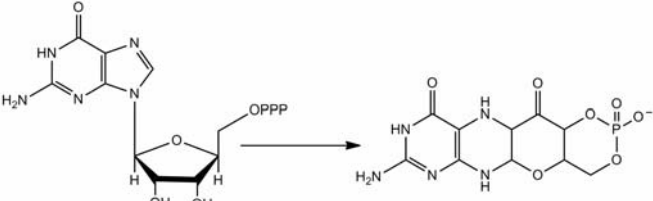
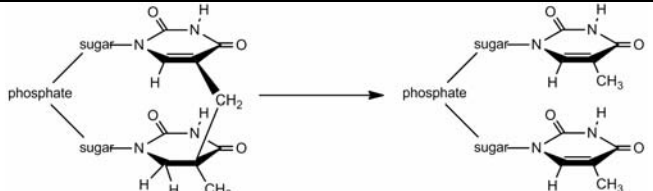
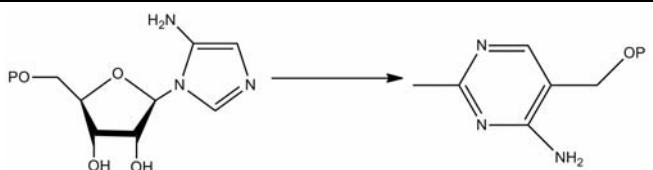
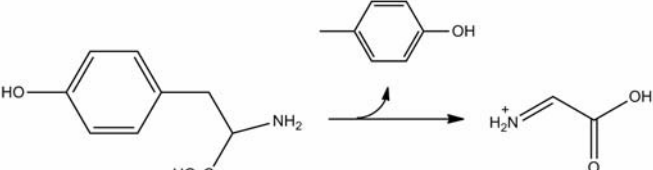
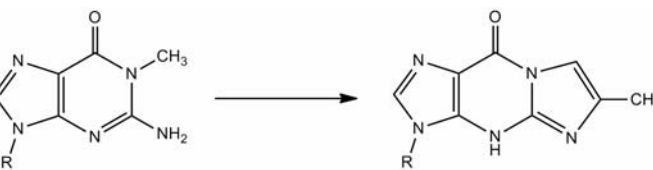
Enzyme and Function	Reaction Catalyzed	Role of SAM
AtsB Arylsulfatase activating enzyme		Substrate
BioB Biotin synthase		Substrate
BtrN Butirosin B biosynthesis		Substrate
GRE-AE Glycyl radical activating enzyme		Substrate
Hem N Coproporphyrinogen III oxidase		Substrate
LAM Lysine 2,3-aminomutase		Cofactor

Figure 1.2. Continued

Enzyme and Function	Reaction Catalyzed	Role of SAM
<p>LipA</p> <p>Lipoyl synthase</p>		Substrate
<p>MiaB</p> <p>Methylthiolation of tRNA</p>		Substrate
<p>MoaA</p> <p>Molybdopterin cofactor biosynthesis</p>		Substrate
<p>SplB</p> <p>Spore photoproduct lyase</p>		Cofactor
<p>ThiC</p> <p>Thiamine pyrophosphate biosynthesis</p>		Substrate
<p>ThiH</p> <p>Thiazole biogenesis in thiamine biosynthesis</p>		Substrate
<p>TYW1</p> <p>Wybutosine biosynthesis in tRNA</p>		Substrate

The first enzyme in the radical SAM superfamily to be discovered and characterized was lysine 2,3-aminomutase (LAM) from *Clostridium subterminale* SB4 [26]. This isomerase was found to catalyze the conversion of L-lysine to L- β -lysine (Figure 1.2) through the transfer of the α -amino group to the β -carbon. This reaction is dependent on iron, pyridoxal-5'-phosphate (PLP), SAM and reducing conditions. The dependence of this enzyme on SAM was quite surprising considering β -lysine mutase catalyzes the same reaction but is dependent on adenosylcobalamin. Adenosylcobalamin-dependent enzymes perform rearrangement reactions through a mechanism in which homolytic cleavage of the cobalt(II)-deoxyadenosine bond results in a cobalt(III) center and a 5'-deoxyadenosyl radical, which then abstracts a hydrogen atom from the substrate molecule (Figure 1.3). The mechanism of these enzymes is similar to that of the radical SAM family which utilize a $[4\text{Fe-4S}]^{1+}$ cluster to promote the reductive cleavage of SAM to produce an identical 5'-deoxyadenosyl radical which also abstracts a hydrogen atom from the substrate.

Concurrent with the characterization of LAM, another SAM-dependent enzyme was under investigation, the activating enzyme of pyruvate formate-lyase (PFL-AE) [27]. This enzyme activates pyruvate formate-lyase (PFL) in a manner dependent on flavodoxin, SAM and iron [28-32]. This reaction was determined to yield a free radical on G734 of PFL through the cleavage of SAM into methionine and 5'-deoxyadenosine [27]. The activated PFL was then found to catalyze the cleavage of pyruvate into acetyl-CoA and formate. Thus, PFL-AE provided the first evidence for SAM-dependent radical

catalysis. It has since been determined that a number of other glycy radical enzymes (GRE) are present in diverse areas of anaerobic metabolism.

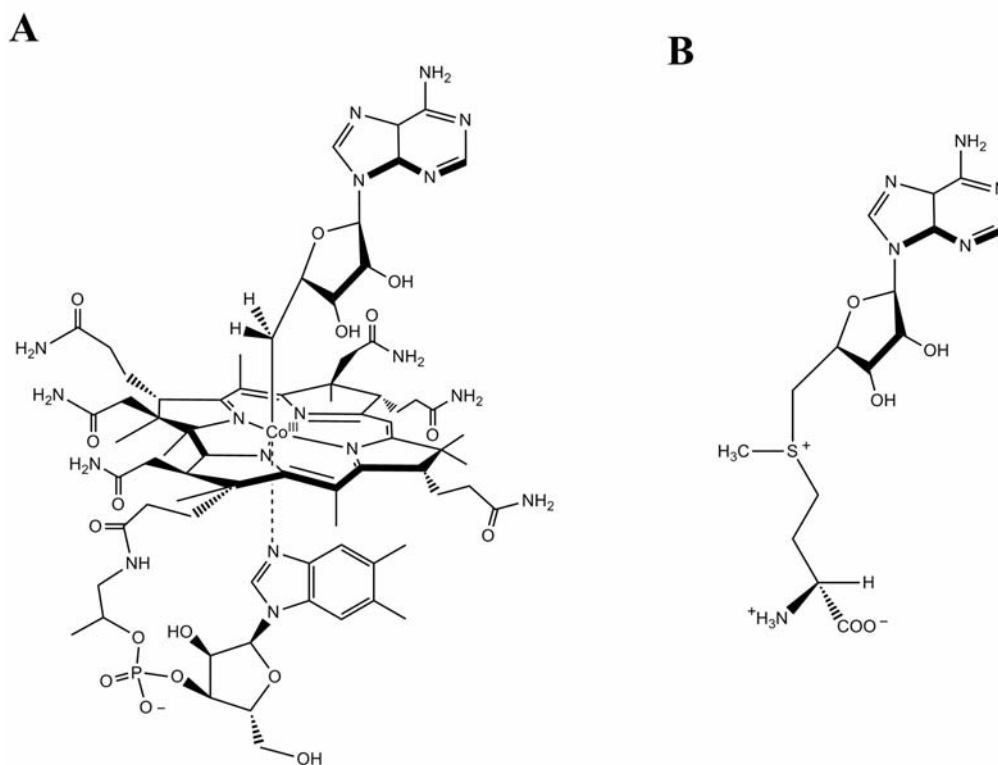


Figure 1.3. Structures of adenosylcobalamin (A) and *S*-adenosylmethionine (B).

Another radical SAM activating enzyme that has been fairly well characterized is the anaerobic ribonucleotide reductase activating enzyme (ARR-AE), which activates the glycy radical enzyme anaerobic ribonucleotide reductase (ARR). Activated ARR has a glycy radical on G681 and catalyzes the anaerobic reduction of deoxyribonucleotides [33-35]. Other GREs that require activation by radical SAM enzymes include benzylsuccinate synthase (BSS), which catalyzes the first step in anaerobic toluene degradation; the adenosylcobalamin-independent glycerol dehydratase (GDH), which is involved in a key step in glycerol fermentation; and the hydroxyphenylacetate

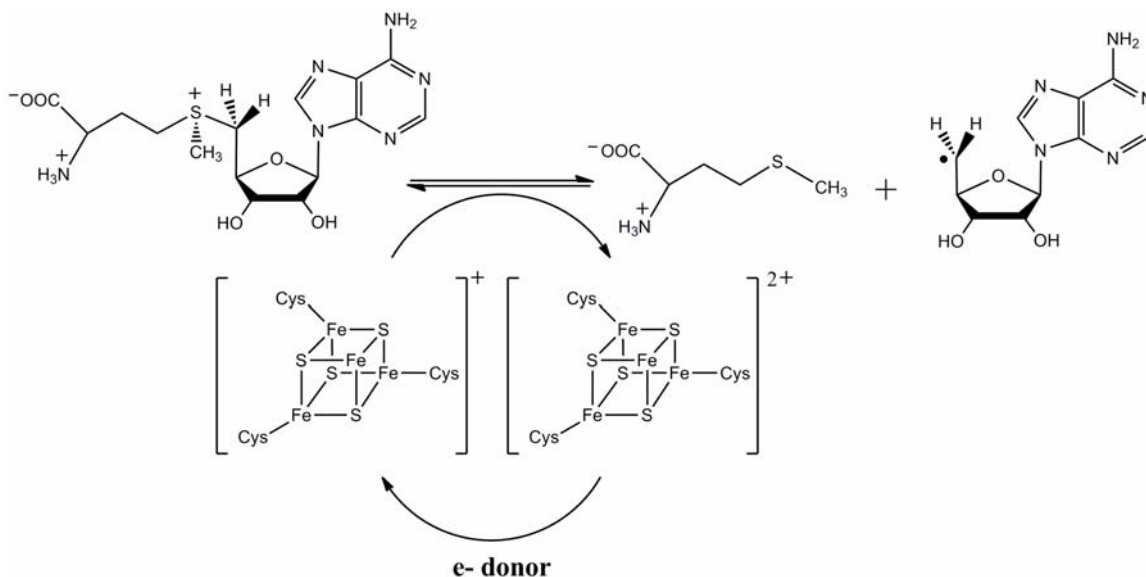
decarboxylase (HPD), which catalyzes a complicated decarboxylation reaction to produce *p*-cresol [36-39].

Biotin synthase and lipoyl synthase, both of which catalyze sulfur insertion reactions, are two other well characterized radical SAM enzymes [40-41]. Biotin synthase converts dethiobiotin into biotin (Figure 1.2) through the formation of two C-S bonds on two non-activated carbons. Lipoyl synthase catalyzes the formation of two C-S bonds of lipoyl-acyl carrier protein from octanoyl acyl carrier protein (Figure 1.2) with a mechanism similar to biotin synthase [42].

Common Mechanistic Implications

The radical SAM enzymes are suggested to have common mechanistic steps in the initiation of their radical catalysis. The enzymes all catalyze monoelectronic reductive cleave of SAM into methionine and a putative 5'-deoxyadenosyl radical (Scheme 1.1). This radical is extremely reactive and quickly oxidizes the substrate to form a carbon-based radical. The first step in the mechanism of these enzymes is the binding of SAM via the methionyl amino and carboxylate groups to the unique iron of the site-differentiated $[4\text{Fe-4S}]^{2+}$ cluster [43]. The unprecedented ligation of SAM to the unique iron of the $[4\text{Fe-4S}]$ cluster was first demonstrated for the enzyme PFL-AE by using electron nuclear double resonance (ENDOR) spectroscopy in collaborative efforts between Broderick and Hoffman [44-45]. This novel coordination has been further observed spectroscopically as well as structurally for crystal structures solved for this enzyme family (as shown for PFL-AE in Figure 1.4) [46-53]. The fourth ligand to the $[4\text{Fe-4S}]$ cluster in the absence of SAM is currently unknown.

The next step in this mechanism is the reduction of the cluster to the $[4\text{Fe-4S}]^{1+}$ catalytically active state which is often performed by flavodoxin *in vivo* [54]. It is then suggested that inner-sphere electron transfer from the $[4\text{Fe-4S}]^{1+}$ cluster to SAM promotes the homolytic cleavage of the S-C5' bond of SAM to yield methionine and a 5'-deoxyadenosyl radical. While this radical has not been observed experimentally, evidence for its existence was provided by use of a SAM analogue in the Frey laboratory [55]. The 5'-deoxyadenosyl radical is responsible for a direct H atom abstraction to form a carbon-based substrate radical and 5'-deoxyadenosine and from here the mechanisms diverge. For the activating enzymes that form glycy radical, this is the final phase of catalysis with the protein glycy radical and 5'-deoxyadenosine formed as products. For the other radical SAM enzymes the substrate radical is an intermediate on a pathway of often complex and interesting biochemical catalysis.



Scheme 1.1. Formation of the 5'-deoxyadenosyl radical by means of reductive cleavage of *S*-adenosylmethionine. Taken from reference [56].

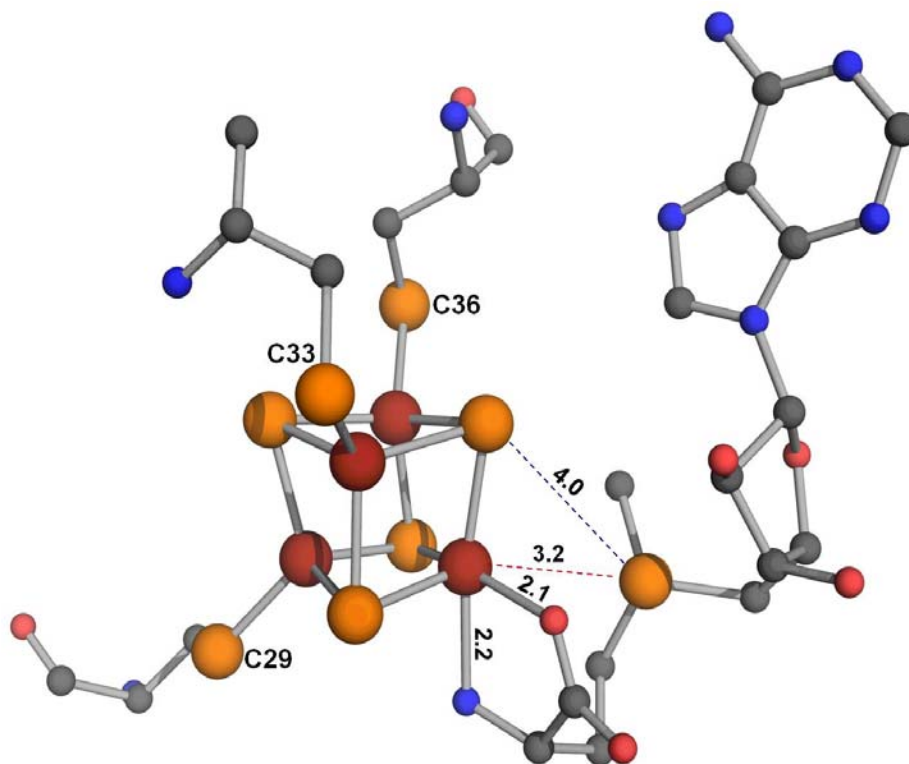


Figure 1.4. Coordination of SAM to the unique iron of the site-differentiated [4Fe-4S] cluster of PFL-AE as demonstrated by ENDOR and X-ray crystallography [43-45, 53].

A common mechanistic problem encountered in the radical SAM superfamily is the one-electron reductive cleavage of SAM. While Daley and Holm have demonstrated the inherent ability for synthetic analogues of $[4\text{Fe-4S}]^{1+/2+}$ clusters of the appropriate redox potential to cleave sulfonium cations, the redox potentials of the cluster and sulfoniums utilized in their studies made the electron transfer thermodynamically favorable [57-58]. However, in the radical SAM enzymes the reduction potentials of the $[4\text{Fe-4S}]^{1+/2+}$ clusters are in the range of ~ -450 mV whereas the reduction potential of uncoordinated SAM is suggested to be ~ -1.8 V, making the electron transfer unfavorable [59-62]. When SAM coordinates the cluster, the reduction potential for the $[4\text{Fe-4S}]^{1+/2+}$

cluster of lysine 2,3-aminomutase increases further, bringing the potential within the range of physiological reductants [59]. However, this also makes the electron transfer from the reduced cluster to SAM all the more unfavorable bringing the barrier to around -1.4 V, corresponding to ~ 32 kcal/mol. A more recent study on the reduction potential of LAM found that this barrier could be reduced to ~ 9 kcal/mol when both lysine and SAM were bound to the enzyme [63]. These studies revealed that when lysine was bound to the enzyme, the potential of the [4Fe-4S] cluster was lowered to -600 mV and the potential for bound SAM was -990 mV, a difference of 390 mV between the midpoint potentials for the [4Fe-4S] cluster and bound SAM. A mechanism to overcome this small barrier may be the transition from a pentacoordinate iron when SAM ligates the [4Fe-4S]¹⁺ cluster, to a more favorable hexacoordinate iron in [4Fe-4S]²⁺ after SAM cleavage.

This transition has recently been observed in X-ray crystal structures of HydE bound to SAM and [5'-dAdo + Met] at 1.62 Å and 1.25 Å resolution, respectively [64]. In the SAM bound structure (Figure 1.5. A), the unique Fe is coordinated by 3 sulfides from the [4Fe-4S] cluster and the methionyl amino and carboxylate groups resulting in a 5-coordinate Fe. After SAM cleavage (Figure 1.5. B), methionine remains in the active site with the Met-S providing a sixth ligand to the unique Fe, resulting in a 6-coordinate Fe with a pseudooctahedral coordination. A 6-coordinate Fe will be more stable than a 5-coordinate Fe for a variety of reasons. First, an increase in the number of bonds results in increasing stability of the complex [65]. Also, complexes with a coordination number of 5 display a delicate balance of forces and generally, their stability is not great as compared to other possible structures [66]. A 6-coordinate complex, however, can gain

stability due to Jahn-Teller distortion. A distortion from the symmetric octahedral geometry is favored by certain conditions and by definition of the Jahn-Teller theorem, lowers the energy of the complex [67-68]. The transition of the unique Fe to a hexacoordinate iron may facilitate inner sphere electron transfer to the sulfonium of SAM [63-64].

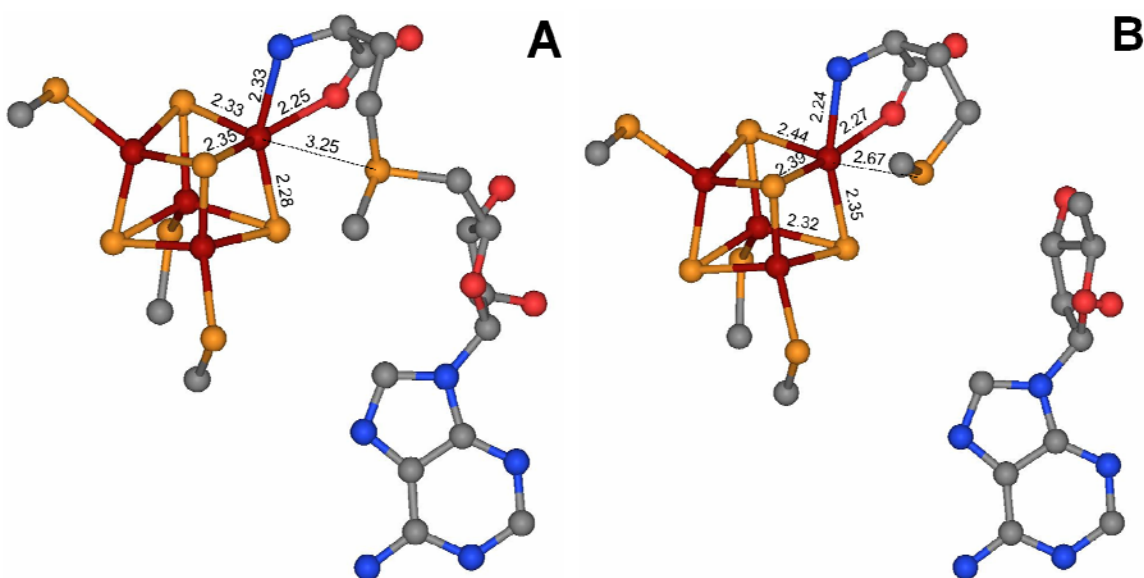


Figure 1.5. Active site X-ray structures of HydE SAM-bound (A) and [5'-dAdo + Met]-bound (B) from PDB code 3IIZ and 3IIX for (A) and (B), respectively [64].

Structural Insights

While the radical SAM superfamily catalyzes a variety of diverse biochemical reactions, the available X-ray crystal structures reveal remarkable similarity between enzymes in the superfamily (Figure 1.6). Although only a handful have been structurally characterized, all of the solved structures contain a partial or complete triosephosphate isomerase (TIM) type barrel, with BioB and HydE (one of the gene products involved in

maturation of the [Fe-Fe]-hydrogenase active site) exhibiting a complete $(\alpha/\beta)_8$ TIM barrel and the others exhibiting an incomplete $(\alpha/\beta)_6$ TIM barrel [46-47, 49-53, 69]. Those with incomplete TIM barrels provide a larger active site to allow access to larger substrates. In all of the available structures, the site-differentiated [4Fe-4S] radical SAM cluster is bound in the same location at one end of the barrel with the unique iron positioned toward the center of the barrel. The unique iron is coordinated by SAM through the amino and carboxyl groups (as described above) which allows the labile and oxygen-sensitive cluster to be partially protected from solvent. SAM is further positioned in the active site by a series of conserved residues involved in electrostatic, H-bonding, hydrophobic and π -stacking interactions which aid in optimizing the initiation and control of radical catalysis. Furthermore, the structures indicate substrate binding serves to further protect the active site and in several enzymes it has been suggested that protein loops aid in sealing off the active site during catalysis to help protect radical intermediates [70]. It is interesting to note that the adenosylcobalamin enzymes not only use a similar mechanism to promote the chemistry of the 5'-deoxyadenosyl radical, they also contain the TIM barrel architecture with adenosylcobalamin bound to a separate domain. In fact, when the barrel is superimposed on that of biotin synthase, the corrin ring occupies the same space as the [4Fe-4S] cluster of BioB, and an evolutionary relationship between the two families has been suggested [71].

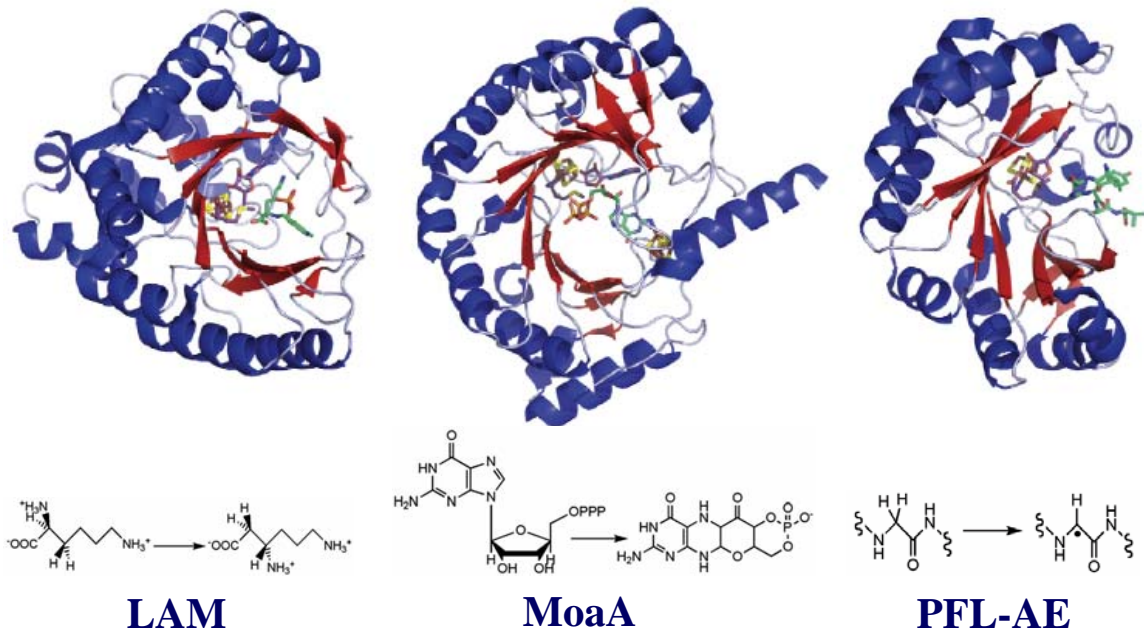


Figure 1.6. X-ray crystal structures of lysine 2,3-aminomutase (LAM, without its C-terminus), MoaA and pyruvate formate-lyase activating enzyme each with SAM and substrate bound. Adapted from reference [70].

Spore Photoproduct Lyase

Of the many diverse biochemical reactions that radical SAM enzymes catalyze, one that is particularly interesting is that of spore photoproduct lyase (SP lyase or SPL) which directly reverses a specific DNA mutation (Figure 1.2). The presence of an alternative repair mechanism for the DNA damage found in sporulating bacteria was first suggested in 1965 when a unique thymine photoproduct was discovered in bacterial spores that was not the usual thymine dimers found in vegetative cells [72]. This photoproduct was identified as 5-thyminy-5,6-dihydrothymine (later termed spore photoproduct or SP) [73] and genetic studies of the DNA repair properties of *Bacillus subtilis* spores revealed a process that specifically repaired this unique thymine dimer

[74]. When SP lyase was identified to repair SP without using light, it was differentiated from other DNA repair enzymes and determined that it must have a different and novel repair mechanism [75].

An analysis of the sequence of spore photoproduct lyase revealed a striking motif (between amino acids 80-115) rich in cysteine, histidine and aromatic residues reminiscent of iron- or zinc-binding domains [76]. Using this region of the sequence, a search of the protein sequence database revealed substantial homology to Fe-S proteins such as the activating subunits of the anaerobic ribonucleotide reductases (aRNR-AE) and pyruvate-formate lyases (PFL-AE) from *E. coli* phage T4, *Haemophilus influenza*, and *Clostridium pasteurianum* [76]. Indeed, the sequence revealed four conserved cysteine residues, three of which are clustered in the typical radical SAM motif (Figure 1.7) and SP lyase activity was found to be associated with iron [77]. Thus, SP lyase was designated as a member of the radical SAM superfamily.

SP Lyase	86	IPFATG CMGHCHYCYLQTT
PFL-AE	24	ITFFQG CLMRCLYCHNRDT
RNR-AE	20	VLFTVG CLHKCEGCYNRST
Biotin Syn	47	SIKTGAC CPQDCKYCPQTSR
Lipoate Syn	48	MILGAI CTRRCPFC DVAHG
LAM	132	LLITDM CSMYCRHCTRRRF

Figure 1.7. The amino acid sequence homology is demonstrated between SP lyase and other members of the radical SAM superfamily. The CX₃CX₂C binding motif which ligates a [4Fe-4S] cluster is indicated in bold and red.

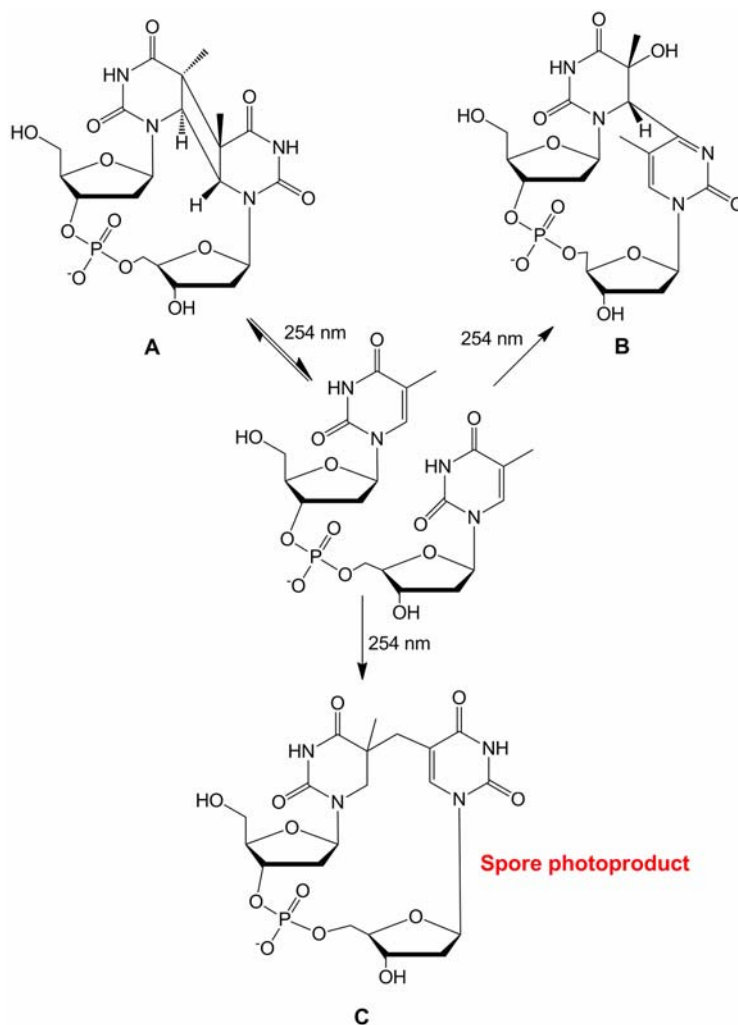
DNA Damage, Spore Photoproduct Formation and Small, Acid Soluble Proteins

Deoxyribonucleic acid (DNA) is well established as the informationally active component of nearly all organisms and was once thought to be an exceptionally stable

macromolecule [78]. However, DNA is not as stable as it was once assumed and is continually subject to change. Damage and mutations can occur as a consequence of errors introduced during replication or recombination, as well as from environmental factors including chemical and physical sources. DNA damage introduced by mismatched base pairs during replication, strand breakage by reactive oxygen species, deamination, depurination, and interstrand crosslinking by a variety of chemicals are all detrimental to cell viability. DNA repair is critical for cellular function since DNA replication and gene transcription will be prevented or will lead to DNA mutations in its absence.

Upon exposure to UV irradiation, DNA forms several photoproducts resulting in the dimerization of adjacent pyrimidine bases thymine (T) and cytosine (C). The primary photoproducts generally include *cis-syn* cyclobutane pyrimidine dimers (CPDs) (usually TT, but also CT and CC dimers) and pyrimidine-pyrimidone (6-4) photoproducts (6-4 PPs) (Scheme 1.2) [72, 79-80]. However, under certain conditions, such as within bacterial spores, the major photoproduct is a unique thymine dimer termed the spore photoproduct [72-73, 79, 81]. The remarkable photochemistry demonstrated by bacterial spores is attributed to low hydration levels of the spore core [82], a change in DNA conformation from a normal B-type to AB-like [83-84], and most importantly, a family of DNA binding proteins, known as small, acid-soluble proteins (SASPs) [85]. Despite the accumulation of UV damage, the endospores produced by bacteria of the various *Bacillus* and *Clostridium* species are metabolically dormant and are extremely resistant to

harsh treatments, including ultraviolet light. Depending on the species analyzed, spores are 10 to 50 times more resistant than vegetative cells at 254 nm UV radiation [81, 85].



Scheme 1.2. DNA Photoproducts upon UV-Irradiation A) Cyclobutane pyrimidine dimer, B) pyrimidine-pyrimidone (6-4) photoproduct, C) spore photoproduct, (5-thyminyl-5,6-dihydrothymine).

SASPs are named due to their solubility in acidic solutions and are produced at high levels during sporulation, comprising up to 20% of spore protein in various *Bacillus* species [86]. Their synthesis parallels the acquisition of UV light resistance by the developing spore and appear approximately 3-4 hours after the onset of sporulation [85-

86]. These small proteins range from 60 to 73 amino acids (5-7 kDa) and exhibit a high degree of sequence homology both within and across *Bacillus* species. It is interesting that these proteins show no sequence similarity to any other protein family and do not contain any motifs characteristic of other DNA-binding proteins [86]. These small proteins are nonspecific double-stranded DNA binding proteins that cover ~5 bp/protein, which is enough protein to saturate the spore chromosome [87-88]. Spores of *Bacillus subtilis* lacking the genes encoding the α/β -type SASPs are much more UV sensitive than are wild type spores. However, the UV resistance of these spores is largely recovered upon the overexpression of normally minor α/β -type SASPs or by the addition of an α/β -type SASPs from another species [81, 87].

Recently, a crystal structure of a complex between a 10-bp DNA duplex and an engineered α/β -type SASP originally obtained for *B. subtilis* was determined to 2.1 Å resolution (Figure 1.8) [89]. The protein was found to be ~ 65% α -helical and, in the asymmetric unit, the SASP-DNA complex is composed of three protein and one DNA molecule. Two protein molecules act as a dimer and a third protein assumes a dimeric arrangement by interacting with another protein in a similar crystallographic symmetry related complex. Each SASP protomer was found to be comprised of two long helical segments connected by a turn region and included extended N and C termini lacking secondary structure. Interestingly, these proteins were found to bind to the minor groove of the DNA via a helix-turn-helix (HTH) motif in which helix1 lies along the edge of the minor groove and helix2 lies in the minor groove along the right-hand direction of the DNA helix. Helix2 is critical in the interaction of SASPs with the DNA helix as four

conserved amino acids are found in helix2 (Ser⁻³⁴, Gly⁻³⁸, Gly⁻⁴¹ and Thr⁻⁴⁵) that directly interact with DNA through hydrogen bonds to G:C base pairs. Gly⁻⁴¹ is particularly important for the interaction of SASPs with DNA as changing this amino acid eliminates the effects of α/β -type SASPs on DNA structure and the ability to shift DNA structure from B type to AB type [89].

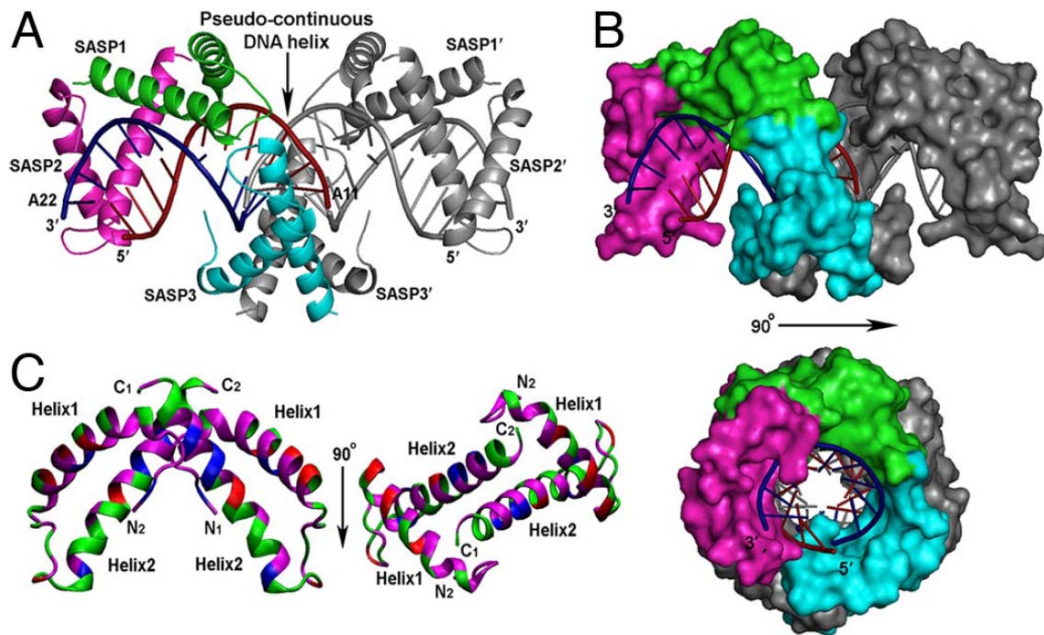


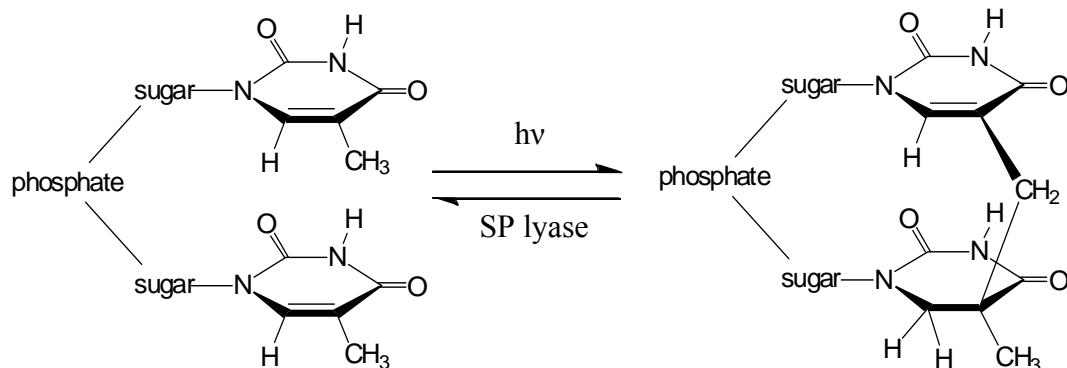
Figure 1.8. Structure of α/β -type SASP-DNA complex. A) DNA helices consisting of 10 bp are stacked end-to-end in the crystal. B) Space-filling surface diagram of the complex. C) Ribbon diagram of α/β -type SASP dimer structure. Helix2 from each subunit is located at the dimer interface contributing to hydrophobic interactions. Green, polar residues; magenta, nonpolar residues; blue, basic residues; red, acidic residues. The N- and C-termini of each subunit are labeled N1/N2 and C1/C2, respectively. Two perpendicular views of the same dimer are shown. Taken from reference [89].

The primary function of α/β -type SASPs is the protection of DNA from various types of damage. The interactions of α/β -type SASPs with DNA do not involve water molecules and therefore the proteins remain tightly bound to DNA even in dry spores,

protecting the spore DNA against glycosidic bond cleavage. The tight packing of the α/β -type SASPs around the DNA restricts access to many toxic chemicals and provides protection from temperatures greater than 90 °C [90-91]. A previous structural study of DNA bound to α/β -type SASP found a large increase in DNA persistence length, suggesting that DNA in the complex is rigid, most likely due to the many interactions of these proteins with DNA [92]. The relative rigidity aids in explaining the minimal production of cyclobutane dimers and 6,4-photoproducts between adjacent pyrimidines in DNA upon irradiation of spores [89-90]. Since the binding of α/β -type SASPs to DNA results in a change of the DNA structure from a normal B-type to an AB-type [93], this rigid complex can no longer access the conformation which favors cyclobutane dimer and 6,4-photoproduct formation. The UV photoreactivity of A-DNA is significantly lower than B-DNA because it is much more difficult to adopt the geometry necessary for cyclobutane dimer and 6,4-photoproduct formation due to the A-DNA's lower base pairs twist [94-95]. Modeling of adjacent thymidines in the DNA structure of the α/β -type SASP-DNA complex revealed that the distance between C5 of the first thymidine base and C7 of the second thymidine base (the two atoms involved in covalent bond formation in SP) is 3.4 Å [89]. This distance is shorter by more than 1 Å compared to in B-DNA [96]. This significantly shorter distance in the modeled structure, relative to that in B-DNA, coupled with the rigidity of the AB-DNA complex, indicates that SP should be formed much more readily in the α/β -type SASP-DNA complex than in B-DNA. Together, this data strongly suggests that SASP binding is the major reason for SP formation and UV resistance in bacterial spores.

Repair of Pyrimidine Dimers

While the presence of SASPs is the primary explanation for the production of SP in spores, it does not explain spore UV resistance because pyrimidine dimers, such as SP, are damaging to cells. These lesions can block replication and transcription or may result in mutations if transcription occurs past the region of the dimer. Therefore, it is crucial to repair these dimers. As a result, the other factor necessary for spore UV resistance is SP repair. There are two main systems which repair spore UV damage: 1) the nucleotide excision repair pathway (NER) and 2) the direct reversal of SP to two thymine monomers catalyzed by the enzyme SP lyase (Scheme 1.3) [74-75, 97]. These repair systems have been found to function separately, under different control pathways, and function at different phases during the development of the spores to vegetative cells. In the dormant spore core, the site of spore DNA, there is no enzyme action until the spore begins the germination process. SP lyase has been found to function in the early minutes of spore germination and its kinetics are unaffected by the presence or absence of the NER pathway [74].



Scheme 1.3. The UV-generated spore photoproduct is repaired directly by spore photoproduct lyase. The methylene bridge of SP is cleaved by SP lyase, repairing the thymine dimer back to two adjacent thymines.

The NER system in *B. subtilis* is similar to that in *E. coli*, and removes lesions from DNA, including SP and cyclobutane-type pyrimidine dimers [85]. Unlike the SP lyase mechanism, the NER pathway requires the spores to have developed further towards a vegetative state before its repair properties are observed [74]. While the NER pathway has been observed to be quite effective for removing pyrimidine dimers from vegetative cell DNA, it seems to remove SP only after cells begin to germinate and operates somewhat more slowly than the SP lyase mechanism. The kinetics of this pathway seem to be further delayed when photoproducts comprise 1 to 2% of the total thymine and fails completely when damage increases above 5% [74].

Unlike the NER system, which involves the products of a number of different genetic loci, SP-specific repair is due only to the products of the *spl* locus [74]. The *spl* locus is a two-gene operon; the first gene (*splA*) is suggested to encode a protein that regulates expression of the *spl* operon while the second gene (*splB*) encodes an SP lyase [98-99]. The *spl* operon is expressed only during sporulation in the developing forespore and is expressed in parallel with SASPs. The *spl* operon is not expressed during spore germination and is not induced by DNA damage in growing cells [100].

Currently, the only well characterized means of pyrimidine dimer direct reversal is photoreactivation, which is catalyzed by the enzyme DNA photolyase [101-102]. This family of enzymes cleave cyclobutane pyrimidine dimers or 6,4-photoproducts into monomers and are classified into two groups, either CPD photolyases or (6-4) photolyases, depending on their substrate. The photolyase family of enzymes are light activated, requiring near-UV or blue light ($\lambda = 320-500$ nm), and contain a flavin (FAD)

[103-105] and one of two chromophores, either a folate, methenyltetrahydrofolate (MTHF) [106], or deazaflavin, 8-hydroxy-5-deazariboflavin (8-HDF) [107].

The DNA photolyase enzymes are “structure-specific” DNA binding proteins with their specificity determined by the backbone structure of DNA at the binding site. This is in contrast to “sequence-specific” DNA binding proteins which depend on hydrogen-bond donors and acceptors in the grooves of the duplex [108]. As SP lyase is also a sequence-independent DNA repair enzyme, it has been suggested that the interaction between SP lyase and its substrate may be similar to that of the DNA photolyases. DNA photolyases recognize CPD lesions with rather high affinity in both single- or double-stranded DNA with dissociation constants on the order of $\sim 10^{-8}$ M for both forms of DNA for the *E. coli* photolyase [109]. Interestingly, it was determined that the binding of the thymine dimer only contributes half of the binding energy ($K_D \sim 10^{-4}$ M) while the other half is contributed by the deoxyphosphate-ribose backbone of the DNA strand. The 1.8 Å X-ray crystal structure of a complex between *A. nidulans* photolyase and a CPD lesion incorporated into duplex DNA demonstrated that the enzyme increases the CPD-induced kink in the B-type DNA upon binding the lesion from about 20-30° to 50° [110]. This large kinking of the B-type DNA is accompanied by a flip-out of the CPD lesion into the active site of the enzyme in order to be properly positioned to form hydrogen bonds between the C4 carbonyl groups of the 5'-T and the 3'-T with the adenine N6 amino group of the reduced deprotonated FADH⁻ cofactor. It is also interesting to note that the synthetic CPD lesion in this structure was comprised of a formacetal group linking the two thymines instead of the intradimer phosphate (P⁰). It

was suggested that major interactions with the missing P^0 phosphate would be unlikely since no residues close to the flipped thymine dimer could interact with the P^0 [110].

DNA photolyases repair thymidine dimers by binding to the dimer in a light-independent manner. During the repair reaction, the second chromophore absorbs a photon in the range of 350-450 nm and transfers the excitation energy to the FAD cofactor, resulting in a reduced deprotonated $FADH^-$ species, which then transfers an electron to the pyrimidine dimer. The 5-5 and 6-6 bonds of the cyclobutane ring are split generating a pyrimidine and a pyrimidine $^-$, the latter of which donates an electron back to the flavin cofactor to regenerate $FADH^-$ and the enzyme dissociates from DNA [101]. This mechanism of pyrimidine dimer repair has been shown to be absent in many species, including *Bacillus subtilis*, suggesting that alternate means of pyrimidine dimer repair might be found [84, 98]. As SP lyase is the first identified *nonphotoactivated* pyrimidine dimer reversal enzyme, it is of considerable interest to probe the detailed mechanism of thymine dimer repair by this enzyme [75].

Characterization of SP Lyase

Early work on SP lyase demonstrated the enzyme's ability to directly reverse SP to two thymines, similar to the action of DNA photolyases, with the exception that SP lyase-mediated repair is light-independent [75, 84, 97]. SP lyase was found to contain iron and sulfur and its repair activity was dependent on SAM and reducing conditions [77]. Further work demonstrated that SP lyase specifically binds to and cleaves SP but not CPDs in UV-irradiated DNA [111]. Moreover, the binding of SP lyase to SP led to significant bending or distortion of the DNA helix in the vicinity of the lesion [111].

Taking this into consideration along with the DNA photolyase structure with a CPD-DNA bound substrate [110], it is a natural extension to suggest the binding and interaction of SP lyase with its substrate may be quite similar.

More recent work on SP lyase has included characterizing the enzyme from several organisms including *Bacillus subtilis*, *Clostridium acetobutylicum*, and *Geobacillus stearothermophilus* [112-116]. In all cases, SP lyase has been determined to contain one redox-active [4Fe-4S] cluster with UV spectroscopy and EPR studies agreeing with the iron and sulfur content. Previous work from our laboratory provides support for the SplB protein to be monomeric [112]. The SplG protein from *G.s.* has been indicated to be a homodimer under anaerobic or aerobic conditions, perhaps gaining stability from an additional Cys residue not found in the SplB protein that may aid in facilitating at least two intermolecular disulfide bridges [113].

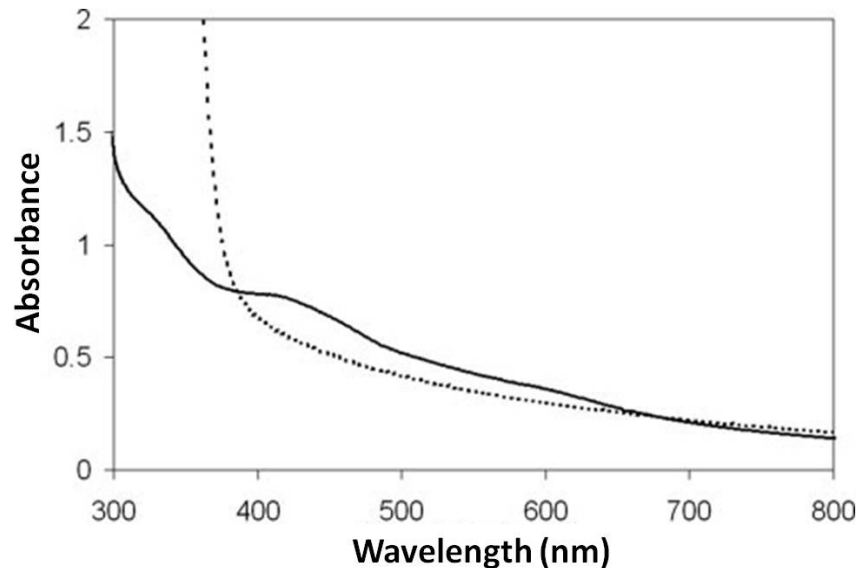


Figure 1.9. UV-visible absorption spectra of anaerobically isolated *B.s.* SP lyase. The as-isolated enzyme (solid line) and reduced with dithionite (dashed line) as shown in reference [112].

When *B.s.* SP lyase is isolated anaerobically, it elutes off a Co-Sepharose column as a dark brown band and displays a UV-vis spectrum typical of an iron-sulfur protein (Figure 1.9) [112]. The spectrum exhibits a broad shoulder with shoulders centered at 410 nm ($11.9 \text{ mM}^{-1}\text{cm}^{-1}$) and 450 nm ($10.5 \text{ mM}^{-1}\text{cm}^{-1}$), similar to what has been observed for other anaerobically purified radical SAM enzymes [42, 117]. The enzyme is redox active and can be reduced in the presence of dithionite. Anaerobically purified SP lyase contains iron (3.1 ± 0.3 mol of iron per mol of SP lyase) and acid-labile sulfide (3.0 ± 0.3 mol of S^{-2} per mol of SP lyase). The EPR signal of *B.s.* SP lyase is temperature dependent and only observable below 35 K. The as-isolated enzyme exhibits a nearly isotropic EPR signal with a g-value centered at 2.02 and is consistent with the assignment to a $[\text{3Fe-4S}]^{1+}$ cluster and accounts for between 25 and 35% of the total iron (Figure 1.10). In the presence of dithionite, SP lyase can be reduced to a $[\text{4Fe-4S}]^{1+}$ cluster, accounting for 22 to 31% of the total iron, resulting in a nearly axial signal with g-values of 2.03, 1.93 and 1.89. Upon addition of SAM to the reduced enzyme, the EPR signal is essentially identical to that of the reduced enzyme alone, but with much lower intensity.

SP lyase has been shown to be active in repair of SP in the presence of SAM and reducing conditions [77, 112, 114]. Shown in Figure 1.11 is an activity assay performed using [^3H -methyl] thymidine pUC18 DNA containing SP and *B.s.* SP lyase with a N-terminal 6-His tag. SP lyase repaired the SP-DNA with a specific activity of $0.33 \mu\text{mol}/\text{min}/\text{mg}$ over the course of 60 mins (Figure 1.11) [112]. The data suggests a possible lag time followed by acceleration of repair, possibly due to the time required to reduce the cluster to the active $[\text{4Fe-4S}]^{1+}$ state before initiating repair activity.

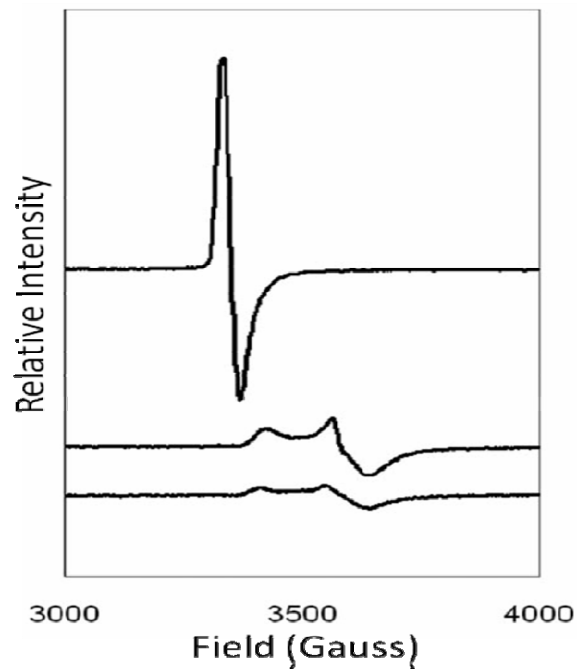


Figure 1.10. X-band EPR spectra of anaerobically isolated *B.s.* SP lyase (top), upon reduction with dithionite (middle), and with addition of SAM to the reduced enzyme (bottom). Taken from reference [112].

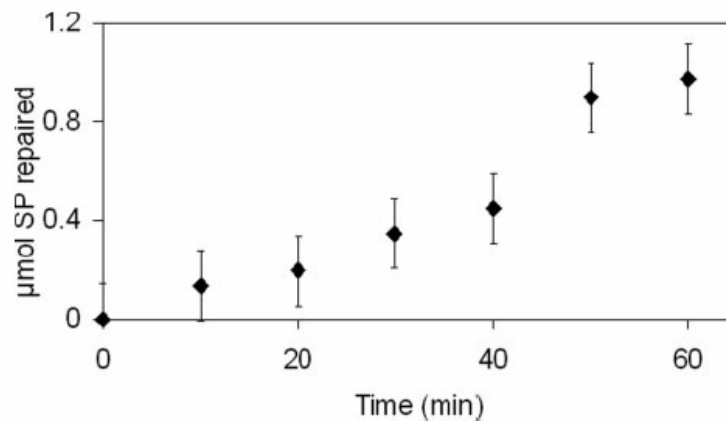


Figure 1.11. Time course repair assay of pUC18 SP-DNA by SP lyase in the presence of SAM and reducing conditions. Taken from reference [112].

Mechanism of SP Lyase

Unlike the DNA photolyase family, SP lyase does not require a flavin as a cofactor nor use light to initiate repair [77, 118]. The commonly accepted mechanism of

SP repair by SP lyase (Figure 1.12) was originally proposed by Begley and co-workers and further supported by work in the Broderick laboratory [112, 119-120]. The repair of SP [A] begins with the transfer of an electron, presumably from the $[4\text{Fe-4S}]^{1+}$ cluster of SP lyase, to SAM, resulting in reductive cleavage to form the 5'-deoxyadenosyl radical and methionine [B]. The 5'-deoxyadenosyl radical initiates catalysis by direct H atom abstraction from the C6 position of SP [B]. Previous work in our laboratory supports this step as SP prepared from irradiating [$^3\text{H-C6}$] thymidine pUC18 DNA demonstrates the incorporation of the ^3H atom into SAM after repair by SP lyase, but not when SP is prepared from [$^3\text{H-methyl}$] thymidine pUC18 DNA (Figure 1.13) [120]. A mechanism in which the substrate subsequently undergoes a radical-mediated β -scission to cleave the methylene bridge [C] to generate a thymine radical [D] is supported. It has been suggested that the thymine radical [D] subsequently re-abstracts an H-atom to re-form the putative 5'-deoxyadenosyl radical intermediate [E]. SAM could then be regenerated by the loss of an electron to the iron-sulfur cluster, and the recombination of the 5'-deoxyadenosyl radical intermediate and methionine [F]. The reabstraction of an H atom from 5'-deoxyadenosine by a thymine radical shown in [D] is supported by mechanistic work in our laboratory that used SAM ^3H labeled at the 5' position, in which we observed the transfer of the tritium atom into repaired thymine (Figure 1.14) [112]. Further work in our laboratory demonstrates support for this mechanism in the analysis of SAM as a cofactor in the repair of SP as discussed below.

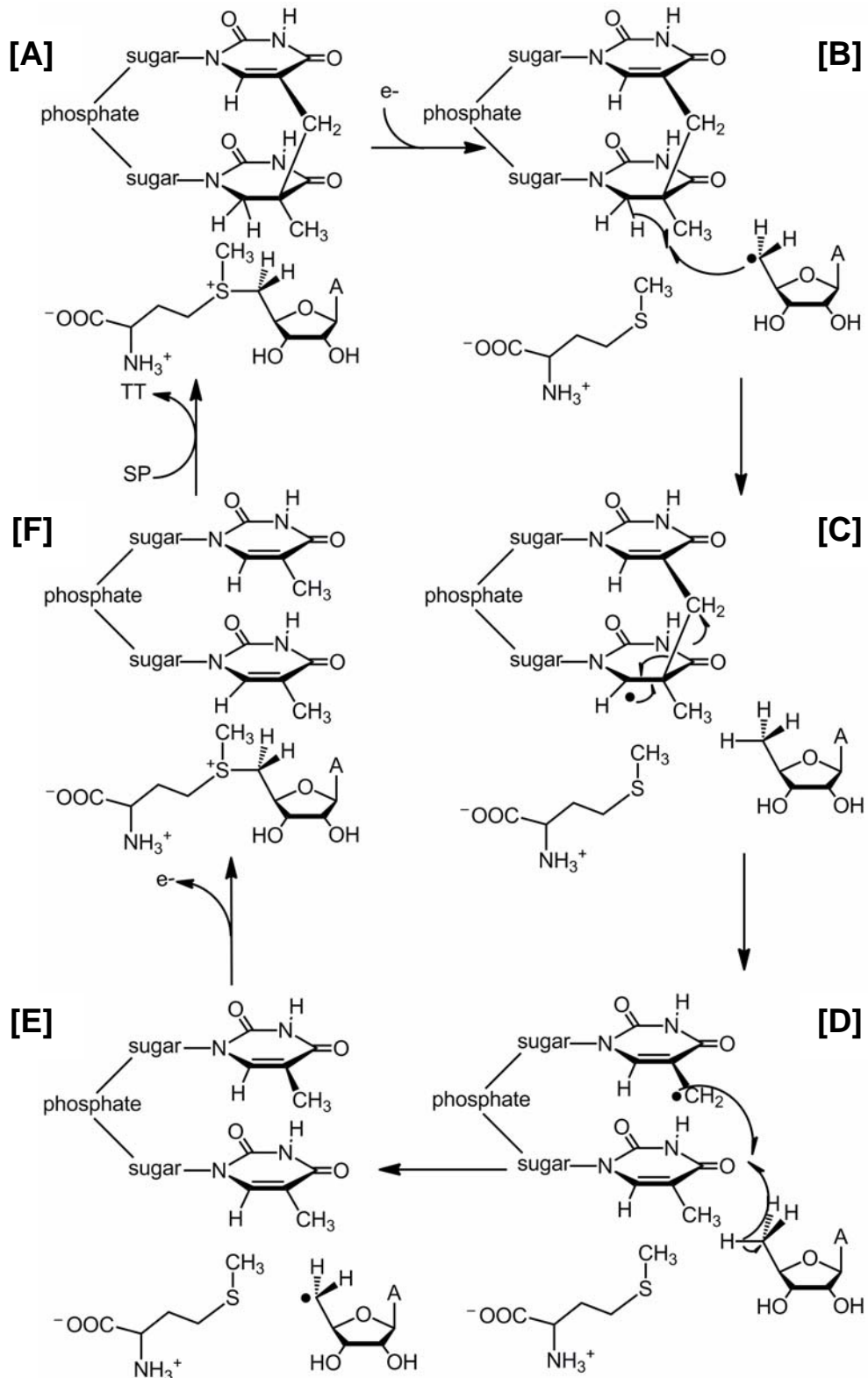


Figure 1.12. Proposed mechanism for SP repair by SP lyase. Taken from reference [112].

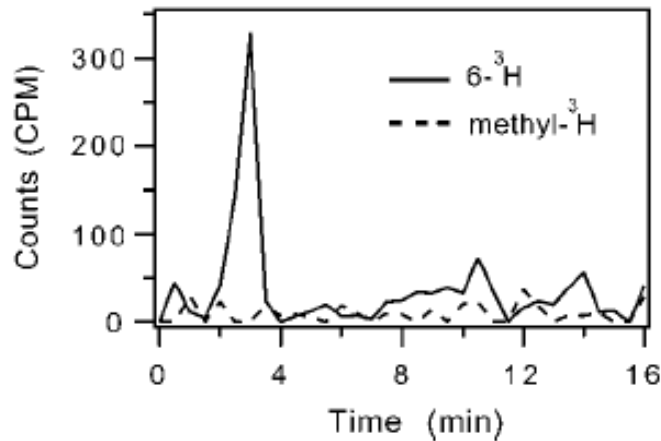


Figure 1.13. Tritium is incorporated into SAM (elution time 2.6 mins) during repair of SP when SP-DNA tritiated at the C-6 group of thymine was used as substrate (solid line), but not when SP-DNA tritiated at the methyl group of thymine was used as substrate (dashed line). Shown are difference chromatograms (assay minus control) for the C-6 tritiated and methyl-tritiated samples. The formation of 5'-deoxyadenosine is not observed (elution time 7 mins). Taken from reference [120].

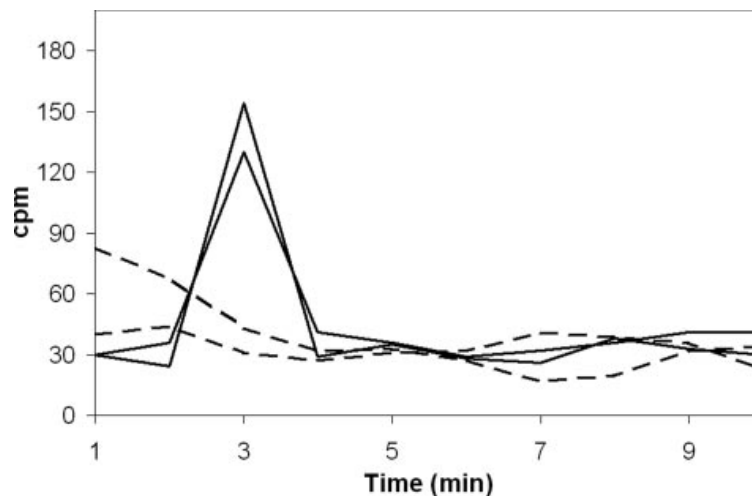


Figure 1.14. Tritium is incorporated into thymine (elution time 3 mins) when $[5'\text{-}^3\text{H}]$ SAM is used to repair SP. Shown are chromatograms for duplicate experiments in the presence of $[5'\text{-}^3\text{H}]$ SAM (solid lines) and in the absence of SP lyase (dashed lines) in which no ^3H incorporation is observed into thymine. Taken from reference [112].

The proposed mechanism was subjected to further analysis by a Hartree-Fock/density functional theory (DFT) study [121]. The analysis resulted in a slight

modification of the above proposed mechanism in which an additional inter-thymine hydrogen transfer step was proposed before the reabstraction of hydrogen to the 5'-deoxyadenosine to accommodate for the placement of SAM with respect to the SP lesion. The original proposed mechanism would result in a thymine radical on the methyl position of the 3'-thymine, while the proposed DFT modification would transfer an H atom to this radical producing a new thymine radical on the methyl position of the 5'-thymine. The DFT calculations indicate the last step (the back-transfer of the hydrogen atom from 5'-deoxyadenosine to the thymine monomer radical, shown in [D]) to be rate determining with a barrier of ~25 kcal/mol, higher than what is accepted for enzymatic reactions. However, it was suggested that the barrier was an overestimation due to the ground state being overstabilized in the simplified model being used. Another possibility suggested was that the last step is coupled to some energetically favorable step following, such as the recombination of the 5'-deoxyadenosyl radical with methionine to regenerate the SAM cofactor [121].

In the radical SAM superfamily, SAM can be used as either a cofactor (as in LAM) or co-substrate (as in PFL-AE, BioB, LipA, etc.). Whether SAM is used as a co-substrate or cofactor in SP repair has been an area of debate. While previously published data indicated that SP lyase uses SAM as a co-substrate [118, 122], recent data demonstrate that SP lyase can repair SP using catalytic amounts of SAM, supporting the role of SAM as a catalytic cofactor (Table 1.1) [112]. These results, which do not show the stoichiometric cleavage of SAM to form methionine and 5'-deoxyadenosine during SP repair (Figure 1.15), provide further support of SAM as a catalytic cofactor.

Table 1.1. Amount of SP repaired by SP lyase in 1hr in the presence of varying amounts of SAM. Taken from reference [112].

nmol of SAM	nmol of SP repaired
0.23	130 ± 10
0.46	130 ± 10
2.3	180 ± 10

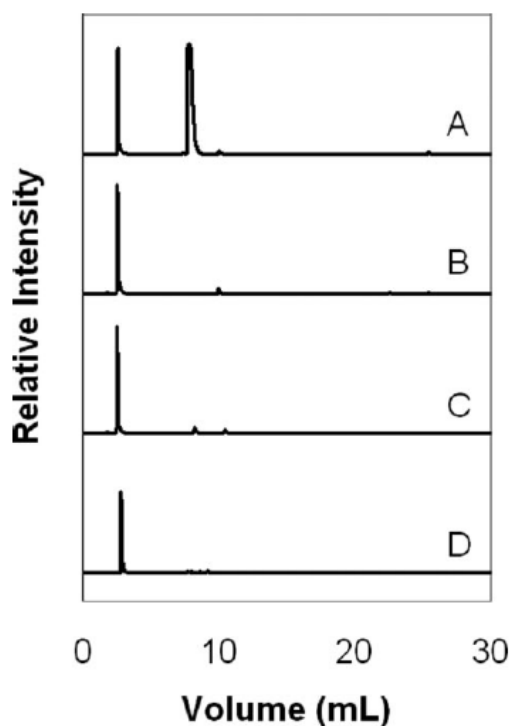


Figure 1.15. HPLC analysis of SAM cleavage to form methionine and 5'-deoxyadenosine by SP lyase during repair of SP. HPLC chromatogram of (A) a standard sample containing SAM (elution time 2.5 min) and 5'-deoxyadenosine (elution time 8 min); (B) control sample containing SAM under assay conditions without SP lyase; and assay mixtures containing SP lyase after (C) 90 min and (D) overnight. Taken from reference [112].

Interestingly, a study which utilized *B.s.* SP lyase with a single point mutation provided some insight into the mechanism of SP lyase [123]. In *Bacillus* species, SP lyase contains four highly conserved Cys residues (Figure 1.16), three of which ligate the

radical SAM [4Fe-4S] cluster. The fourth Cys residue, Cys-141, has previously been shown to be essential for maintaining UV resistance in *Bacillus* spores [124]. When Cys-141-Ala was utilized in repair assays of a dinucleotide SP substrate, the major product of the reaction was not TpT as expected, but rather a modified dinucleotide monophosphate containing one thymine and one thymine with a sulfinic moiety [123]. It was demonstrated that the sulfinic group was attached to the methyl C of the 3'-thymine and appeared to be derived from dithionite in the reaction mixture. These results suggest that Cys-141 may be important in protecting/controlling the radical chemistry that is occurring in the active site. It was further suggested that Cys-141 may act as a H atom donor to an intermediate allylic radical. However, a more likely role of Cys-141 would be to participate in the stabilization of a specific structure of the active site to prevent the intermediate radical from reacting with exogenous free radicals [123]. It is interesting to note that the observed sulfinic group was always attached to the 3'-thymine and not the 5'-thymine in this study [123]. If an H atom exchange did occur to produce a methyl radical at the 5'-thymine as proposed by the DFT study, it may be expected that the sulfinic group would be located at the 5'-thymine.

Remarkably, the essential Cys-141 in *Bacillus* species is in fact an Ala in all SP lyases from spore-forming *Clostridium* examined to date [124]. Instead, the fourth conserved Cys in SP lyases of spore-forming *Clostridium* species is Cys-74. Figure 1.16 shows the alignment of amino acid sequences of SP lyase from *B.s.* and *C.a.* as these are the two main sources from which SP lyase has been isolated in order to characterize this enzyme. Currently, no studies have been performed to determine whether the conserved

Cys-74 in *Clostridium* spore forming organisms is required for maintaining UV resistance or if it plays a similar role to that of Cys-141 in *Bacillus* SP lyase.

<i>C.a.</i>	MENMF--RRVIFEKKALDYPMGIRDILRQFENTDIEIRYSET-GRITGIPGKDE ::: . . . : . : : : : : . . . : : : : . . . : . . . : : : . . .
<i>B.s.</i>	MQNPFVLPQLVYIEPRALEYPLGQELQDKFENMGIEIRETTSHNQVRNIPGKNH 10 20 30 40 50
<i>C.a.</i>	AQSFFEGKNTLVVGVRRRELDFTCKPSANYQLPIVSGCAAMCEYCYLNTHGGK : . . .
<i>B.s.</i>	LQQYRNAKSTLVIGVRKTLKFDSSKPSAEYAIPFATGCMGHCHYCYLQTTMGS 60 70 80 90 100
<i>C.a.</i>	KPYVKINVNDDILSKAGEYIEKRKPDITVFEGAAISDPVPPERYSGALKKAI : . . .
<i>B.s.</i>	KPYIRTYNVVEEILDQADKYMKERAPFTRFEASCSTSDIVGIDHLTHTLKRAI 110 120 130 140 150
<i>C.a.</i>	EYFGKNEYSRFRFVTKYADISELLAVQHNNHTTIRFSINTPRVIKNEYHRTSS : : : : : . . . : : : . . . : . . .
<i>B.s.</i>	EHFGQSDLGKLRFVTKFHHVDHLLDAKHNGKTRFRFSINADYVIKNEFPGTSP 160 170 180 190 200 210
<i>C.a.</i>	LEDRIESAYNILNSGYKTGFIVGPVFLYENWKKEYEELLKKASDKLGD---KE . . . : : : x : . . . : : : : : : : : . . . : . . . :
<i>B.s.</i>	LDKRIEAAVKVAKAGYPLGFIVAPIYIHEGWEEGYRHLFEKLDAAALPQDVRHD 220 230 240 250 260
<i>C.a.</i>	LEFEIISRFTTSAKNKILKVFPNTKLPMDDEARKFKFGQFGYKGVYDQDDM . . . : . . .
<i>B.s.</i>	ITFELIQHRFTKPAKRVIENYPKTKLELDEEKRRYKWGRYGIGKYIYQDEE 270 280 290 300 310
<i>C.a.</i>	QEIKEFFINNINLYFNKATIKYII . . . : . . . : . : : : : . . .
<i>B.s.</i>	HALREALESYIDTFFPNAKIEYFT 320 330 340

Figure 1.16. Sequence Alignment of *C.a.* ATCC 824 SPL (top) with *B.s.* strain 168 SPL (bottom). The sequences have 42.059% identity (77.647% similarity) in 340 a.a. overlap.

Research Goals

The work presented in this dissertation was directed by two primary goals. The first objective of these studies was to provide mechanistic insight into the formation and repair of SP. Previous work has provided insight into the mechanism of SP repair providing support for the abstraction of an H atom from the C-6 position of SP as well as demonstrating the use of SAM as a cofactor in the repair process. However, much of the mechanism of SP repair remains to be elucidated. Specifically, when this work was initiated, the stereospecificity of the substrate of SP lyase was in question. While one study indicated the *5S*-SP as the substrate of SP lyase [122], another study supported the idea of a *5R*-SP as the substrate for SP lyase [125]. In pursuing our investigation for the substrate of SP lyase, the *5R*-SP and *5S*-SP substrates were synthesized and characterized in both the dinucleoside and dinucleotide forms. The ability of SP lyase to repair each of these incomplete substrates was then investigated. Through the development and implementation of an HPLC-detected repair assay, the substrate for SP lyase was identified without a doubt. These experiments also provided evidence for a correlation between catalytic activity and the completeness of the substrate.

In addition, isotope labeling experiments acted as an abundant source of information regarding both the formation and repair of SP. With respect to the formation of SP, very little is known and indeed the only suggested mechanism for SP formation was proposed in 1970. In this work we provide the first experimental glimpse regarding the stereospecificity of the formation of SP at the C-6 position. Furthermore, we provide experimental support for a kinetic isotope effect for the H atom abstraction from the C-6

position of SP, which indicates this step could be rate limiting in the repair of SP by SP lyase.

The second objective of this work was to characterize the [4Fe-4S] cluster present in SP lyase and take a closer look at its interaction with SAM. Using a variety of spectroscopic methods, including UV-Vis, low temperature electron paramagnetic resonance (EPR), Mössbauer and X-ray absorption spectroscopy (XAS), the cluster of SP lyase was investigated. As a requirement for much of this spectroscopy, SP lyase was needed in higher concentrations than was previously attainable [112]. Much of the previous work on this enzyme was performed on SP lyase cloned from *Bacillus subtilis*, but the *B.s.* SP lyase could only be concentrated to $\sim 250 \mu\text{M}$ before it would precipitate out of solution. Therefore, SP lyase was cloned from *Clostridium acetobutylicum* and overexpressed in *E.coli*. This resulted in a more stable enzyme that could be concentrated to higher concentrations without precipitation and allowed a more thorough investigation of the [4Fe-4S] cluster present in the enzyme. Table 1.2 demonstrates the observed differences between SP lyase from *B.s.* as compared to that of *C.a.* The iron content of SP lyase is consistently higher for the *C.a.* SP lyase, although, like *B.s.* SP lyase, it is preparation-dependent.

Table 1.2. Comparison of SP lyase overexpressed in *E.coli* as cloned from *Bacillus subtilis* or *Clostridium acetobutylicum*.

	<i>B.s.</i> SP Lyase	<i>C.a.</i> SP Lyase
Max Concentration	$\sim 250 \mu\text{M} - 500 \mu\text{M}$ without SAM $\sim 750 \mu\text{M}$ with SAM	$> 1 \text{ mM}$ without SAM
Fe / SP lyase	$2 - 2.5 (\pm 0.2)$	$2.5 - 3 (\pm 0.2)$
Reduction	Dithionite $\sim 25\text{-}35\%$	5-Deazariboflavin
SP lyase / 10 L growth	$\sim 25 \text{ mg}$	$\sim 100 \text{ mg}$

After *C.a.* SP lyase was obtained at higher concentrations, a more thorough investigation of the [4Fe-4S] cluster was carried out. An initial characterization of the [4Fe-4S] cluster present in SP lyase was performed using UV-Vis and X-band EPR at 12 K. A more detailed EPR study of the [4Fe-4S]-SAM complex indicates the observed EPR spectrum of reduced SP lyase in the presence of SAM is specific for the interaction of SAM with the [4Fe-4S] cluster. Mössbauer studies provided more in-depth information regarding the cluster states of SP lyase. XAS studies allowed a further characterization of the [4Fe-4S] cluster as well as the interesting observation of a change in the symmetry of the cluster upon the addition of SAM. Collectively, the results in this dissertation provide a deeper understanding of the mechanism of formation and repair of SP by SP lyase.

References

1. Beinert H (2000) *J. Biol. Inorg. Chem.* 5:2-15
2. Beinert H, Holm RH, Münck E (1997) *Science* 277:653-659
3. Beinert H, Sands RH (1960) *Biochem. Biophys. Res. Commun.* 3:41-46
4. Mortenson LE, Valentine RC, Carnahan JE (1962) *Biochem. Biophys. Res. Commun.* 7:448-452
5. Johnson DC, Dean DR, Smith AD, Johnson MK (2005) *Annu. Rev. Biochem.* 74:247-281
6. Peters JW (1999) *Curr. Opin. Struct. Biol.* 9:670-676
7. Drennan CL, Peters JW (2003) *Curr. Opin. Struct. Biol.* 13:220-226
8. Moulis JM, Davasse V, Golinelli MP, Meyer J, Quinkal I (1996) *J. Biol. Inorg. Chem.* 1:2-14
9. Rao PV, Holm RH (2004) *Chem. Rev.* 104:527-559
10. Meyer J (2008) *J. Biol. Inorg. Chem.* 13:157-170
11. Kiley PJ, Beinert H (1998) *FEMS Microbiol. Rev.* 22:341-352
12. Green J, Scott C, Guest JR (2001) *Adv. Microb. Physiol.* 44:1-34
13. Demple B, Ding H, Jorgensen M (2002) *Methods Enzymol.* 348:355-364
14. Ding H, Demple B (2000) *Proc. Natl. Acad. Sci. U.S.A.* 97:5146-5150
15. Walden WE, Selezneva AI, Dupuy J, Volbeda A, Fontecilla-Camps JC, Theil EC, Volz K (2006) *Science* 314:1903-1908
16. Rouault TA (2006) *Nat. Chem. Biol.* 2:406-414
17. Wallander ML, Leibold EA, Eisenstein RS (2006) *Biochim. Biophys. Acta.* 1763:668-689
18. Volz K (2008) *Curr. Opin. Struct. Biol.* 18:106-111

19. Dai S, Friemann R, Glauser DA, Bourquin F, Manieri W, Schurmann P, Eklund H (2007) *Nature* 448:92-96
20. Lill R (2009) *Nature* 460:831-838
21. Rudolf J, Makrantonis V, Ingledew WJ, Stark MJ, White MF (2006) *Mol. Cell.* 23:801-808
22. Frey PA, Hegeman AD, Ruzicka FJ (2008) *Crit. Rev. Biochem. Mol. Biol.* 43:63-88
23. Sofia HJ, Chen G, Hetzler BG, Reyes-Spindola JF, Miller NE (2001) *Nucleic Acids Res.* 29:1097-1106
24. McGlynn SE, Boyd ES, Shepard EM, Lange RK, Gerlach R, Broderick JB, Peters JW (2010) *J. Bacteriol.* 192:595-598
25. Chatterjee A, Li Y, Zhang Y, Grove T, Lee M, C K, Booker S, Begley T, Ealick S (2008) *Nat. Chem. Biol.* 4:758-765
26. Chirpich TP, Zappia V, Costilow RN, Barker HA (1970) *J. Biol. Chem.* 245:1778-1789
27. Knappe J, Neugebauer F, A., Blaschkowski HP, Gänzler M (1984) *Proc. Natl. Acad. Sci U.S.A.* 81:1332-1335
28. Knappe J, Schmitt T (1976) *Biochem. Biophys. Res. Commun.* 71:1110-1117
29. Knappe J, Bohnert E, Brummer W (1965) *Biochim. Biophys. Acta* 107:603-605
30. Knappe J, Schacht J, Mockel W, Hopner T, Vetter HJ, Edenharder R (1969) *Eur. J. Biochem.* 11:316-327
31. Knappe J, Blaschkowski HP, Gröbner P, Schmitt T (1974) *Eur. J. Biochem.* 50:253-263
32. Knappe J, Blaschkowski HP (1975) *Methods Enzymol.* 41:508-518
33. Harder J, Follmann H, Hantke K (1989) *Z Naturforsch C* 44:715-718
34. Eliasson R, Fontecave M, Jörnvall H, Krook M, Pontis E, Reichard P (1990) *Proc. Natl. Acad. Sci. U.S.A.* 87:3314-3318

35. Harder J, Eliasson R, Pontis E, Ballinger MD, Reichard P (1992) *J. Biol. Chem.* 267:25548-25552
36. Leuthner B, Leutwein C, Schulz H, Hörth P, Haehnel W, Schiltz E, Schägger H, Heider J (1998) *Molec. Microbiol.* 28:615-628
37. Raynaud C, Sarcabal P, Meynial-Salles I, Croux C, Soucaille P (2003) *Proc. Natl. Acad. Sci. U.S.A.* 100:5010-5015
38. O'Brien JR, Raynaud C, Croux C, Girbal L, Soucaille P, Lanzilotta WN (2004) *Biochemistry* 43:4635-4645
39. Yu L, Blaser M, Andrei PI, Pierik AJ, Selmer T (2006) *Biochemistry* 45:9584-9592
40. Duin EC, Lafferty ME, Crouse BR, Allen RM, Sanyal I, Flint DH, Johnson MK (1997) *Biochemistry* 36:11811-11820
41. Reed KE, Cronan JE, Jr. (1993) *J. Bacteriol.* 175:1325-1336
42. Miller JR, Busby RW, Jordan SW, Cheek J, Henshaw TF, Ashley GW, Broderick JB, Cronan JE, Jr., Marletta MA (2000) *Biochemistry* 39:15166-15178
43. Walsby C, Ortillo D, Yang J, Nnyepi M, Broderick WE, Hoffman BM, Broderick JB (2005) *Inorg. Chem.* 44:727-741
44. Walsby CJ, Hong W, Broderick WE, Cheek J, Ortillo D, Broderick JB, Hoffman BM (2002) *J. Am. Chem. Soc.* 124:3143-3151
45. Walsby CJ, Ortillo D, Broderick WE, Broderick JB, Hoffman BM (2002) *J. Am. Chem. Soc.* 124:11270-11271
46. Berkovitch F, Nicolet Y, Wan JT, Jarrett JT, Drennan CL (2004) *Science* 303:76-79
47. Layer G, Moser J, Heinz DW, Jahn D, Schubert W-D (2003) *EMBO J.* 22:6214-6224
48. Chen D, Walsby C, Hoffman BM, Frey PA (2003) *J. Am. Chem. Soc.* 125:11788-11789
49. Hänzelmann P, Schindelin H (2006) *Proc. Natl. Acad. Sci. U.S.A.* 103:6829-6834

50. Hänzelmann P, Schindelin H (2004) *Proc. Natl. Acad. Sci. U.S.A.* 101:12870-12875
51. Lepore BW, Ruzicka FJ, Frey PA, Ringe D (2005) *Proc. Natl. Acad. Sci. U.S.A.* 102:13819-13824
52. Nicolet Y, Rubach JK, Posewitz MC, Amara P, Mathevon C, Atta M, Fontecave M, Fontecilla-Camps JC (2008) *J. Biol. Chem.* 283:18861-18872
53. Vey JL, Yang J, Li M, Broderick WE, Broderick JB, Drennan CL (2008) *Proc. Natl. Acad. Sci. U.S.A.* 105:16137-16141
54. Henshaw TF, Cheek J, Broderick JB (2000) *J. Am. Chem. Soc.* 122:8331-8332
55. Magnusson OT, Reed GH, Frey PA (2001) *Biochemistry* 40:7773-7782
56. Booker SJ (2009) *Curr. Opin. Chem. Biol.* 13:58-73
57. Daley CJA, Holm RH (2003) *J. Inorg. Biochem.* 97:287-298
58. Daley CJA, Holm RH (2001) *Inorg. Chem.* 40:2785-2793
59. Hinckley GT, Frey PA (2006) *Biochemistry* 45:3219-3225
60. Grimshaw J (1981) In: Stirling CJM (ed) *Chemistry of the Sulphonium Group*. Wiley, Chichester, pp. 141-155
61. Saeva FD, Morgan BP (1984) *J. Am. Chem. Soc.* 106:4121-4125
62. Ugulava NB, Gibney BR, Jarrett JT (2001) *Biochemistry* 40:8343-8351
63. Wang SC, Frey PA (2007) *Biochemistry* 46:12889-12895
64. Nicolet Y, Amara P, Mouesca JM, Fontecilla-Camps JC (2009) *Proc. Natl. Acad. Sci. U.S.A.* 106:14867-14871
65. Miessler GL, Tarr DA (2004) *Inorganic Chemistry*. Pearson Prentice Hall, Upper Saddle River, NJ
66. Huheey JE, Keiter EA, Keitar RL (1993) *Inorganic Chemistry Principles of Structure and Reactivity*. HarperCollins College Publishers, New York, NY
67. Jahn HA, Teller E (1937) *Proc. R. Soc. Lond.* A161:220-225

68. Jahn HA (1938) Proc. R. Soc. Lond. A164:117-131
69. Arragain S, Garcia-Serres R, Blondin G, Douki T, Clemancey M, Latour JM, Forouhar F, Neely H, Montelione GT, Hunt JF, Mulliez E, Fontecave M, Atta M (2010) J. Biol. Chem. 285:5792-5801
70. Duschene KS, Veneziano SE, Silver SC, Broderick JB (2009) Curr. Opin. Chem. Biol. 13:74-83
71. Marsh EN, Patwardhan A, Huhta MS (2004) Bioorg. Chem. 32:326-340
72. Donnellan JE, Jr., Setlow RB (1965) Science 149:308-310
73. Varghese AJ (1970) Biochem. Biophys. Res. Commun. 38:484-490
74. Munakata N, Rupert CS (1972) J. Bacteriol. 111:192-198
75. Munakata N, Rupert CS (1974) Mol. Gen. Genet. 130:239-250
76. Nicholson WL, Chooback L, Fajardo-Cavazos P (1997) Mol. Gen. Genet. 255:587-594
77. Rebeil R, Sun Y, Chooback L, Pedraza-Reyes M, Kinsland C, Begley TP, Nicholson WL (1998) J. Bacteriol. 180:4879-4885
78. Friedberg EC, Walker GC, Siede W (1995) DNA Repair and Mutagenesis. ASM Press, Washington D.C.
79. Douki T, Laporte G, Cadet J (2003) Nucleic Acids Res. 31:3134-3142
80. Douki T, Court M, Sauvaigo S, Odin F, Cadet J (2000) J. Biol. Chem. 275:11678-11685
81. Setlow P (2001) Environ. Mol. Mutagen. 38:97-104
82. Nicholson WL, Munakata N, Horneck G, Melosh HJ, Setlow PJ (2000) Microbiol. Mol. Biol. Rev. 64:548-572
83. Stafford RS, Donnellan JE, Jr. (1968) Proc. Natl. Acad. Sci. U.S.A. 59:822-828
84. Donnellan JE, Jr., Stafford RS (1968) Biophysical J. 8:17-28
85. Setlow P (1988) Comments Mol. Cell. Biophys. 5:253-264

86. Setlow P (1988) *Ann. Rev. Microbiol.* 42:319-338
87. Setlow B, Setlow P (1987) *Proc. Natl. Acad. Sci. U.S.A.* 84:421-423
88. Driks A, Setlow P (eds) (2000) "Morphogenesis and properties of the bacterial spore" *Prokaryotic development*. American Society for Microbiology, Washington D. C.
89. Lee KS, Bumbaca D, Kosman J, Setlow P, Jedrzejewski MJ (2008) *Proc. Natl. Acad. Sci. U.S.A.* 105:2806-2811
90. Nicholson WL, Schuergler AC, Setlow P (2005) *Mutat. Res.* 571:249-264
91. Fairhead H, Setlow B, Setlow P (1993) *J. Bacteriol.* 175:1367-1374
92. Griffith J, Makhov A, Santiago-Lara L, Setlow P (1994) *Proc. Natl. Acad. Sci. U.S.A.* 91:8224-8228
93. Mohr SC, Sokolov NVHA, He C, Setlow P (1991) *Proc. Natl. Acad. Sci. U.S.A.* 88:77-81
94. Becker MM, Wang Z (1989) *J. Biol. Chem.* 264:4163-4167
95. Kundu LM, Linne U, Marahiel M, Carell T (2004) *Chemistry* 10:5697-5705
96. Huth JR, Bewley CA, Nissen MS, Evans JN, Reeves R, Gronenborn AM, Clore GM (1997) *Nat. Struct. Biol.* 4:657-665
97. Wang TC, Rupert CS (1977) *Photochem. Photobiol.* 25:123-127
98. Fajardo-Cavazos P, Salazar C, Nicholson WL (1993) *J. Bacteriol.* 175:1735-1744
99. Fajardo-Cavazos P, Nicholson WL (2000) *J. Bacteriol.* 182:555-560
100. Pedraza-Reyes M, Gutierrez-Corona F, Nicholson WL (1994) *J. Bacteriol.* 176:3983-3991
101. Sancar A (1994) *Biochemistry* 33:2-9
102. Sancar A (2003) *Chem. Rev.* 103:2203-2237
103. Iwatsuki N, Joe CO, Werbin H (1980) *Biochemistry* 19:1172-1176
104. Sancar A, Sancar GB (1984) *J. Mol. Biol.* 172:223-227

105. Eker APM, Hessels JKC, van de Velde J (1988) *Biochemistry* 27:1758-1765
106. Johnson JL, Hamm-Alvarez S, Payne G, Sancar GB, Rajagopalan KV, Sancar A (1988) *Proc. Natl. Acad. Sci. U. S. A.* 85:2046-2050
107. Eker AP, Dekker RH, Berends W (1981) *Photochem. Photobiol.* 33:65-72
108. Husain I, Sancar A (1987) *Nucleic Acids Res.* 15:1109-1120
109. Essen LO, Klar T (2006) *Cell. Mol. Life Sci.* 63:1266-1277
110. Mees A, Klar T, Gnau P, Hennecke U, Eker APM, Carell T, Essen L-O (2004) *Science* 306:1789-1793
111. Slieman TA, Rebeil R, Nicholson WL (2000) *J. Bacteriol.* 182:6412-6417
112. Buis JM, Cheek J, Kalliri E, Broderick JB (2006) *J. Biol. Chem.* 281:25994-26003
113. Pieck JC, Hennecke U, Pierik AJ, Friedel MG, Carell T (2006) *J. Biol. Chem.* 281:36317-36326
114. Chandor A, Berteau O, Douki T, Gasparutto D, Sanakis Y, Ollagnier-de-Choudens S, Atta M, Fontecave M (2006) *J. Biol. Chem.* 281:26922-26931
115. Chandor A, Douki T, Gasparutto D, Gambarelli S, Sanakis Y, Nicolet Y, Ollagnier-de-Choudens S, Atta M, Fontecave M (2007) *C. R. Chimie* 10:756-765
116. Silver SC, Chandra T, Zilinskas E, Ghose S, Broderick WE, Broderick JB (2010) *J. Biol. Inorg. Chem.* 15:943-955
117. Broderick JB, Henshaw TF, Cheek J, Wojtuszewski K, Trojan MR, McGhan R, Smith SR, Kopf A, Kibbey M, Broderick WE (2000) *Biochem. Biophys. Res. Commun.* 269:451-456
118. Rebeil R, Nicholson WL (2001) *Proc. Natl. Acad. Sci. U.S.A.* 98:9038-9043
119. Mehl RA, Begley TP (1999) *Org. Lett.* 1:1065-1066
120. Cheek J, Broderick JB (2002) *J. Am. Chem. Soc.* 124:2860-2861
121. Guo JD, Luo Y, Himo F (2003) *J. Phys. Chem. B* 107:11188-11192

122. Friedel MG, Berteau O, Pieck JC, Atta M, Ollagnier-de-Choudens S, Fontecave M, Carell T (2006) *Chem. Commun.*:445-447
123. Chandor-Proust A, Berteau O, Douki T, Gasparutto D, Ollagnier-de-Choudens S, Fontecave M, Atta M (2008) *J. Biol. Chem.* 283:36361-36368
124. Fajardo-Cavazos P, Rebeil R, Nicholson WL (2005) *Curr. Microbiol.* 51:331-335
125. Kim SJ, Lester C, Begley TP (1995) *J. Org. Chem.* 60:6256-6257

Contribution of Authors and Co-Authors

Manuscript in Chapter 2

Chapter 2: Spore Photoproduct Lyase Catalyzes Specific Repair of the 5R but Not the 5S Spore Photoproduct

Author: Tilak Chandra

Contributions: Tilak Chandra performed the synthesis of the 5R and 5S spore photoproduct dinucleosides as well as the characterization of each using NMR, NOESY and ROESY. He also aided in generating figures for the manuscript and supplemental data.

Co-author: Sunshine C. Silver

Contributions: Cloned, expressed and purified spore photoproduct lyase to use in enzymatic assays, designed and performed the repair assays and generated Figure 2.

Co-author: Egidijus Zilinskas

Contributions: Monitored the repair reactions with HPLC as well as ran standards on HPLC.

Co-author: Eric M. Shepard

Contributions: Performed DFT calculations on the dinucleoside structures and generated Figure 1.

Co-author: William E. Broderick

Contributions: Provided valuable insight and overview of the synthesis and characterization of SP dinucleosides, design of repair assays, interpretation of results and manuscript preparation.

Co-author: Joan B. Broderick

Contributions: Provided valuable insight and overview of the synthesis and characterization of SP dinucleosides, design of repair assays, interpretation of results and manuscript preparation.

Manuscript Information Page

Authors: Tilak Chandra, Sunshine C. Silver, Egidijus Zilinskas, Eric M. Shepard,
William E. Broderick, Joan B. Broderick

Journal: Journal of the American Chemical Society

Status of the manuscript:

Prepared for submission to a peer-reviewed journal

Officially submitted to a peer-reviewed journal

Accepted by a peer-reviewed journal

Published in a peer-reviewed journal

Publisher: American Chemical Society

Issue in which manuscript appears: Volume 131, 2420-2421 (2009)

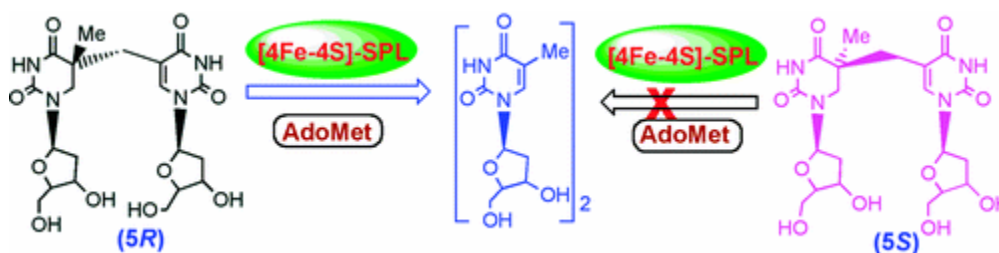
CHAPTER 2

SPORE PHOTOPRODUCT LYASE CATALYZES SPECIFIC REPAIR OF THE 5R BUT NOT THE 5S SPORE PHOTOPRODUCT

Published: *Journal of the American Chemical Society*, **2009**, *131*, 2420-2421

Tilak Chandra, Sunshine C. Silver, Egidijus Zilinskas, Eric M. Shepard, William E. Broderick, and Joan B. Broderick

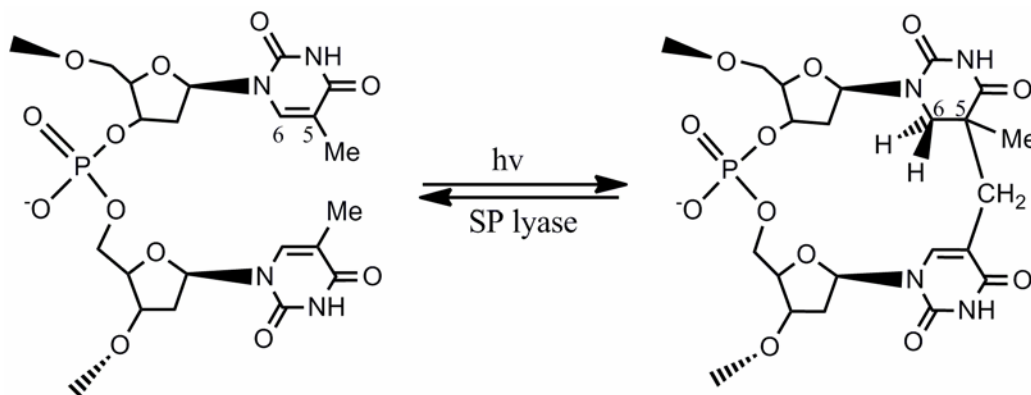
Department of Chemistry and Biochemistry and the Astrobiology Biogeocatalysis Research Center, Montana State University, Bozeman, Montana 59717

Abstract

Bacterial spores are remarkable in their resistance to chemical and physical stresses, including exposure to UV radiation. The unusual UV resistance of bacterial spores is a result of the unique photochemistry of spore DNA, which results in accumulation of 5-thyminy-5,6-dihydrothymine (spore photoproduct, or SP), coupled with the efficient repair of accumulated damage by the enzyme spore photoproduct lyase (SPL). SPL is a member of the radical AdoMet superfamily of enzymes, and utilizes an iron-sulfur cluster and *S*-adenosylmethionine to repair SP by a direct reversal mechanism initiated by H atom abstraction from C-6 of the thymine dimer. While two distinct diastereomers of SP (5*R* or 5*S*) could in principle be formed upon UV irradiation of bacterial spores, only the 5*R* configuration is possible for SP formed from adjacent thymines in double helical DNA, due to the constraints imposed by the DNA structure; the 5*S* configuration is possible in less well-defined DNA structures or as an interstrand cross-link. We report here results from HPLC and MS analysis of *in vitro* enzymatic assays on stereochemically defined SP substrates demonstrating that SPL specifically repairs only the 5*R* isomer of SP. The observation that 5*R*-SP, but not 5*S*-SP, is a substrate for SPL is consistent with the expectation that 5*R* is the SP isomer produced *in vivo* upon UV irradiation of bacterial spore DNA.

Bacterial spores are remarkable in their resistance to chemical and physical stresses, including exposure to UV radiation. The unusual UV resistance of bacterial spores is a result of the unique photochemistry of spore DNA coupled with the efficient repair of accumulated damage. Exposure of bacterial spores to UV radiation results in the formation of a methylene-bridged thymine dimer, 5-thyminyl-5,6-dihydrothymine (spore photoproduct, or SP), as the primary photoproduct.¹⁻³ SP accumulates in UV-irradiated spores; however, it is rapidly repaired upon germination, thus giving rise to the extraordinary UV resistance of bacterial spores.^{4,5} The repair of SP is catalyzed by the enzyme spore photoproduct lyase (SPL), and involves the direct reversal of SP to two thymines without base excision (Scheme 2.1).

Scheme 2.1. Formation and Repair of Spore Photoproduct



SPL is a member of the radical AdoMet superfamily, and utilizes a [4Fe-4S] cluster and *S*-adenosylmethionine (AdoMet) as essential cofactors in SP repair.⁶⁻⁹ We have previously shown that SP repair is initiated by abstraction of H \cdot from C6 of SP by an AdoMet derived 5'-deoxyadenosyl radical,^{10,11} this H-atom abstraction is thought to

initiate a radical-mediated β -scission of the C5-Cbridge bond in the photoproduct, as originally proposed by Mehl and Begley.¹²

While two distinct diastereomers of SP (*5R* or *5S*, Figure 2.1) could in principle be formed upon UV irradiation of bacterial spores, only the *5R* configuration is possible for SP formed from adjacent thymines in double helical DNA, due to the constraints imposed by the DNA structure.¹³ The *5S* configuration, therefore, is possible only in less well-defined DNA structures or as an interstrand crosslink. It was thus quite surprising when two recent reports concluded that SPL repairs only the *5S*, and not the *5R*, isomer of a synthetic SP substrate.^{14,15} We report here results from HPLC and MS analysis of *in vitro* enzymatic assays on stereochemically defined synthetic SP substrates demonstrating that SPL specifically repairs only the *5R* isomer of SP. This stereospecific repair of *5R*-SP by SPL is consistent with the longstanding hypothesis that SP is a result of UV-induced dimerization of adjacent thymines in doublehelical DNA.

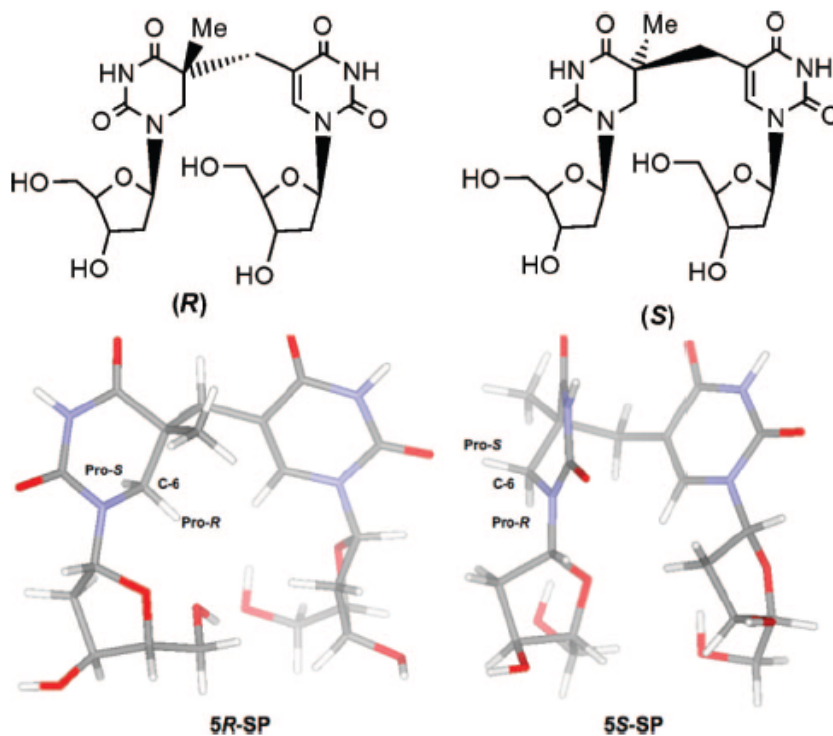


Figure 2.1. Chemical drawings (top) and computational models (bottom) for the 5*R* (left) and 5*S* (right) synthetic spore photoproduct analogues lacking a DNA backbone.

SPL was cloned from *Clostridium acetobutylicum*, overexpressed in *Escherichia coli*, and purified using a method similar to published procedures.¹¹ The enzyme contained 2.9 (\pm 0.2) Fe per SPL, and had UV-visible and EPR spectroscopic properties characteristic of an iron-sulfur enzyme. The 5*R* and 5*S* diastereomers of protected (N-SEM, O-TES, and O-TBDMS) SP were synthesized using modifications of published procedures,^{13,15} and were subsequently deprotected (Supporting Information (SI)). The structures of the fully protected, the di-SEM protected, and fully deprotected dinucleoside spore products were confirmed by ¹H and ¹³C NMR techniques, and NOESY and ROESY were used to assign the stereochemistry at C-5 (SI). To remove any potential

ambiguity associated with the assignment of stereochemistry at C-5 in the open dinucleoside forms of SP, the protected open dinucleosides (*5R* and *5S*) were converted to closed cyclic phosphotriesters, and the stereochemical assignments at C-5 were confirmed by NOESY and ROESY (SI). Stereochemical assignments were based on initially assigning the pro-*S* and pro-*R* hydrogens at C6, with the pro-*R* hydrogen appearing downfield of the pro-*S* hydrogen for nearly all of the synthetic forms of both diastereomers of SP (SI). Our assignment of pro-*R* and pro-*S* hydrogens differs from that reported previously, and may account for the disparity between our results and those previously published.^{14,15} Proper assignment of the pro-*R* and pro-*S* hydrogens is critical to the determination of stereochemistry at C5, as the coupling between these protons and the C5 methyl, as examined by 2D NOESY and ROESY, can then be used to assign the absolute configuration. Our assignments of stereochemistry are completely consistent with distances derived from our computational models of the two diastereomers of SP (SI).

Assays of SP repair were conducted at 30 °C under anaerobic conditions; details are provided in SI. Under the HPLC conditions utilized *5R*-SP elutes at 19.3 min, *5S*-SP elutes at 20.3 min, and thymidine elutes at 14.4 min. As can be seen in Figure 2.2, time-dependent formation of a peak with the retention time of thymidine is observed when *5R*-SP, but not when *5S*-SP, is used as a substrate. The identity of this emerging peak as thymidine was confirmed by co-injection with authentic thymidine and by MS analysis of HPLC fractions corresponding to the peak (SI). The synthetic SP as well as the SP peaks in Figure 2.2 (m/z) 485 (SP) and 507 (SP + Na)), as well as the peak labeled T in Figure

2.2 (m/z) 265 (T + Na)), gave rise to the expected pattern upon MS analysis. MS analysis of the small peaks eluting between 15 and 17 min show them to result from inhomogenous mixture of small peptides, presumably resulting from protein degradation during the sample workup. These assays have been performed seven different times, on two different protein samples, using two different buffers and two different reducing agents (dithionite or 5-deazariboflavin), and in all cases SPL repaired the 5R but not the 5S-SP.

Integration of the thymidine and SP peaks in the chromatograms in Figure 2.2 have allowed us to quantify the rate of SP repair in this system (Figure 2.2 C) as ~ 0.4 nmol/min/mg of SPL for the *R* isomer, and 0 nmol/min/mg of SPL for the *S* isomer. These rates can be compared to the rate of $0.33 \mu\text{mol/min/mg}$ when using *B. subtilis* SPL and UV-irradiated plasmid DNA as a substrate.¹¹ Little additional SP turnover occurs after the 4 hour time point shown in Figure 2.2 C, likely due to enzyme instability under assay conditions, and/or to enzyme inactivation. The lower rate of turnover for synthetic dinucleoside SP relative to SP generated by UV irradiation of plasmid DNA is not surprising, as the synthetic SP is not constrained to the conformation found in a DNA strand, and also lacks the phosphodiester bridge and oligonucleotide strand that likely contribute considerably to substrate binding interactions in the SPL active site. We have incorporated the protected SP phosphotriester described in the Supporting Information into an oligo; however, our initial assays on this indicated that the enzyme cannot repair the di-SEM protected SP analogue. Carell has also incorporated a synthetic SP analogue into an oligonucleotide strand, however the analogue contains no phosphodiester linkage;

no assay data on the resulting oligos were presented.¹⁶ We are currently pursuing deprotection of the SP phosphotriesters (SI) and incorporation of them into oligonucleotide DNA, to produce stereochemically defined substrates for further assay and mechanistic studies.

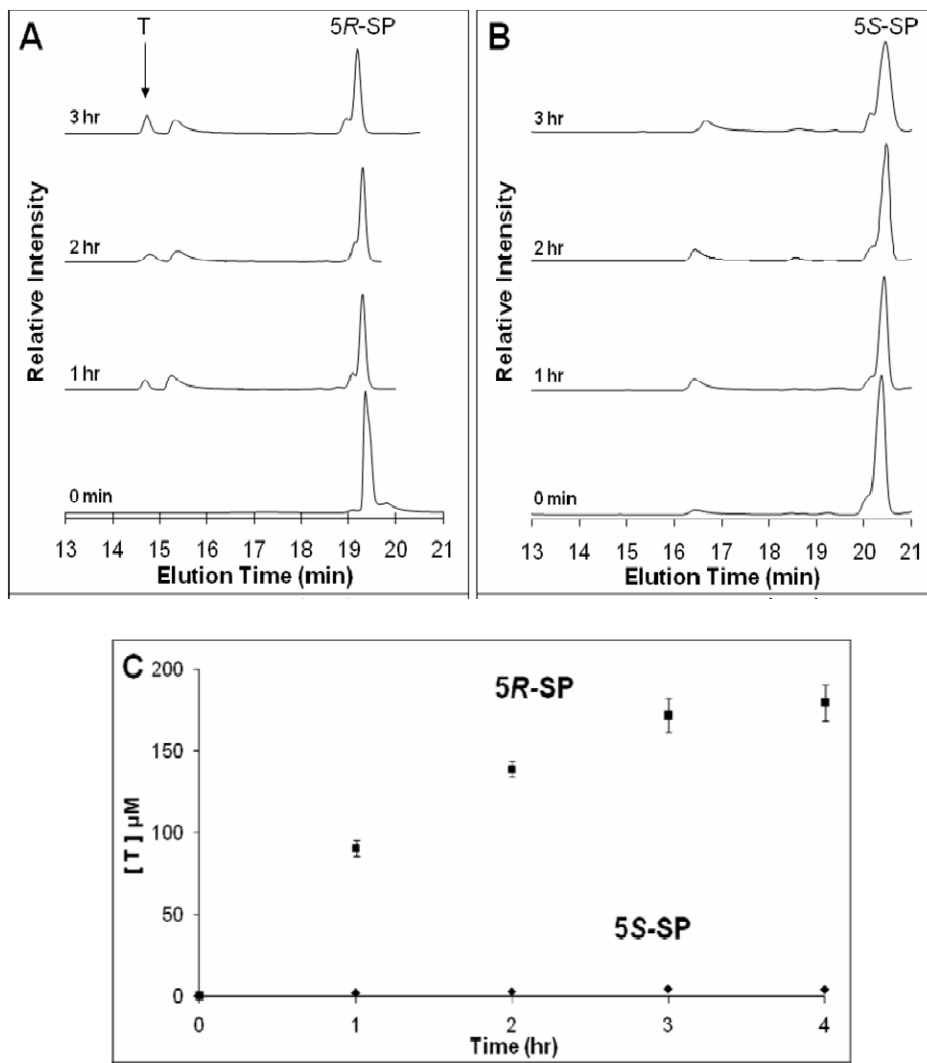


Figure 2.2. HPLC chromatograms showing the time-dependent formation of thymidine due to repair of *R*-SP (A) but not *S*-SP (B), upon incubation of 1 mM SP with SPL (50 μM), AdoMet (1 mM), DTT (5 mM), and dithionite (1 mM) in buffer (see SI) at 30 °C. SP elutes at 19.3 (5*R*) or 20.3 (5*S*) min and thymidine elutes at 14.4 min under these conditions. Integration of the thymidine and SP peaks allowed the quantitation of turnover of each isomer of SP (C).

The results presented herein provide direct and quantitative evidence for the stereochemical requirements of SP repair by SPL, demonstrating that SPL repairs specifically the 5*R* isomer of SP. The identification of 5*R*-SP as the substrate of SPL supports the premise that SP, like the more familiar cyclobutane thymine dimer, is a result of UV-induced dimerization of *adjacent* thymines in a DNA strand. Furthermore, the observation that only 5*R*-SP is a substrate for SPL is consistent with the expectation, based on the constraints imposed by the DNA double helical structure, that 5*R* is the SP isomer produced *in vivo* upon UV irradiation of bacterial spore DNA, an expectation supported by a recent report showing that 5*R* SP is the diastereomer produced upon UV irradiation of a TpT dinucleotide.¹⁷

Acknowledgments

The authors thank the National Institutes of Health for financial support of this research (GM67804). We gratefully acknowledge the assistance of Valerie Copie on NMR experiments and Robert Szilagyi on computational modeling of SP. Funds to purchase the Bruker 600 MHz NMR were provided by the NIH (SIG 1-S10RR13878) and the NSF (EPSCOR- Montana).

Supporting Information Available: Synthetic methods and NMR characterization of all synthetic SPs mentioned herein; NOESY and ROESY of selected compounds; molecular modeling of SPs; mass spec data on T and SP peaks from the HPLC-based assay. This material is available free of charge via the Internet at <http://pubs.acs.org>. The relevant mass spec data and activity assay information is located in Appendix A.

References

1. Donnellan, J. E., Jr.; Setlow, R. B. *Science* **1965**, *149*, 308–310.
2. Donnellan, J. E., Jr.; Stafford, R. S. *Biophys. J.* **1968**, *8*, 17–28.
3. Varghese, A. J. *Biochem. Biophys. Res. Commun.* **1970**, *38*, 484–490.
4. Setlow, P. *Annu. Rev. Microbiol.* **1995**, *49*, 29–54.
5. Setlow, P. *Trends Microbiol.* **2007**, *15*, 172–180.
6. Munakata, N.; Rupert, C. S. *Mol. Gen. Genet.* **1974**, *130*, 239–250.
7. Fajardo-Cavazos, P.; Salazar, C.; Nicholson, W. L. *J. Bacteriol.* **1993**, *175*, 1735–1744.
8. Rebeil, R.; Sun, Y.; Chooback, L.; Pedraza-Reyes, M.; Kinsland, C.; Begley, T. P.; Nicholson, W. L. *J. Bacteriol.* **1998**, *180*, 4879–4885.
9. Rebeil, R.; Nicholson, W. L. *Proc. Natl. Acad. Sci. U.S.A.* **2001**, *98*, 9038–9043.
10. Cheek, J.; Broderick, J. B. *J. Am. Chem. Soc.* **2002**, *124*, 2860–2861.
11. Buis, J. M.; Cheek, J.; Kalliri, E.; Broderick, J. B. *J. Biol. Chem.* **2006**, *281*, 25994–26003.
12. Mehl, R. A.; Begley, T. P. *Org. Lett.* **1999**, *1*, 1065–1066.
13. Kim, S. J.; Lester, C.; Begley, T. P. *J. Org. Chem.* **1995**, *60*, 6256–6257.
14. Friedel, M. G.; Berteau, O.; Pieck, J. C.; Atta, M.; Ollagnier-de-Choudens, S.; Fontecave, M.; Carell, T. *Chem. Commun.* **2006**, *4*, 445–447.
15. Pieck, J. C.; Hennecke, U.; Pierik, A. J.; Friedel, M. G.; Carell, T. *J. Biol. Chem.* **2006**, *281*, 36317–36326.
16. Bürckstümmer, E.; Carell, T. *Chem. Commun.* **2008**, 4037–4039.
17. Mantel, C.; Chandor, A.; Gasparutto, D.; Douki, T.; Atta, M.; Fontecave, M.; Bayle, P.-A.; Mouesca, J.-M.; Bardet, M. *J. Am. Chem. Soc.* **2008**, *130*, 16978–16984.

Contribution of Authors and Co-Authors

Manuscript in Chapter 3

Chapter 3: Complete Stereospecific Repair of a Synthetic Dinucleotide Spore Photoproduct by Spore Photoproduct Lyase

Author: Sunshine C. Silver

Contributions: Cloned, expressed and purified spore photoproduct lyase to utilize in enzymatic assays and spectroscopic studies. Designed and carried out the repair assays and spectroscopic studies of SP lyase as well as generated figures and wrote the manuscript.

Co-author: Tilak Chandra

Contributions: Performed the synthesis of the 5*R* and 5*S* spore photoproduct dinucleotides as well as the characterization of each using NMR, NOESY and ROESY. Tilak also generated Figures 7 and 9.

Co-author: Egidijus Zilinskas

Contributions: Aided in monitoring the repair of the 5*R*-SPTpT reactions with HPLC.

Co-author: Shourjo Ghose

Contributions: Aided in monitoring the repair of the 5*S*-SPTpT reactions with HPLC.

Co-author: William E. Broderick

Contributions: Provided valuable insight and overview of the synthesis and characterization of SP dinucleotides, design of repair assays, interpretation of results and manuscript preparation.

Co-author: Joan B. Broderick

Contributions: provided valuable insight and overview of the synthesis and characterization of SP dinucleotides, design of repair assays, interpretation of results and manuscript preparation.

Manuscript Information Page

Authors: Sunshine C. Silver, Tilak Chandra, Egidijus Zilinskas, Shourjo Ghose, William E. Broderick, Joan B. Broderick

Journal: Journal of Biological Inorganic Chemistry

Status of the manuscript:

- Prepared for submission to a peer-reviewed journal
- Officially submitted to a peer-reviewed journal
- Accepted by a peer-reviewed journal
- Published in a peer-reviewed journal

Publisher: Springer

Issue in which manuscript appears: Volume 15, 943-955 (2010)

CHAPTER 3

COMPLETE STEREOSPECIFIC REPAIR OF A SYNTHETIC DINUCLEOTIDE
SPORE PHOTOPRODUCT BY SPORE PHOTOPRODUCT LYASE

Published: *Journal of Biological Inorganic Chemistry*, **2010**, *15*, 943-955

Sunshine C. Silver, Tilak Chandra, Egidijus Zilinskas, Shourjo Ghose, William E. Broderick, and Joan B. Broderick

From the Department of Chemistry & Biochemistry and the Astrobiology Biogeocatalysis Research Center, Montana State University, Bozeman, MT 59717 USA

Running Title: Stereospecific Repair of Dinucleotide Spore Photoproduct

Abstract

Spore photoproduct lyase, a member of the radical *S*-adenosylmethionine superfamily of enzymes, catalyzes the repair of 5-thyminyl-5,6-dihydrothymine (spore photoproduct), a type of UV-induced DNA damage unique to bacterial spores. The anaerobic purification and characterization of *Clostridium acetobutylicum* spore photoproduct lyase heterologously expressed in *E. coli*, and its catalytic activity in repairing stereochemically-defined synthetic dinucleotide spore photoproducts was investigated. The purified enzyme contains between 2.3 and 3.1 Fe/protein. EPR spectroscopy reveals an isotropic signal centered at $g = 1.99$, characteristic of a $[3\text{Fe-4S}]^+$ cluster accounting for 3 – 4% of the iron in the sample. Upon reduction, a nearly axial signal ($g = 2.03, 1.93$ and 1.92) characteristic of a $[4\text{Fe-4S}]^+$ cluster is observed that accounts for 34 – 45% of total iron. Addition of *S*-adenosylmethionine to the reduced enzyme produces a rhombic signal ($g = 2.02, 1.93, 1.82$) unique to the AdoMet complex while decreasing overall EPR intensity. This reduced enzyme is shown to rapidly and completely repair the *5R* diastereomer of a synthetic dinucleotide spore photoproduct (SPTpT) with a specific activity of $7.1 \pm 0.6 \text{ nmol min}^{-1} \text{ mg}^{-1}$, while the *5S* diastereomer undergoes no repair.

Introduction

Bacterial spores exhibit significant resistance to a variety of environmental stresses including UV radiation. This remarkable resistance to UV radiation is due to both the intriguing photochemistry of spore DNA as well as the efficient repair of DNA damage during spore germination. The primary UV photoproduct in spore DNA is unique; rather than the cyclobutane pyrimidine dimers and pyrimidine (6-4) photoproducts formed in vegetative cells, spores accumulate 5-thyminylyl-5,6-dihydrothymine (spore photoproduct or SP, Figure 3.1) upon UV irradiation [1-3]. During germination, SP is repaired by the enzyme spore photoproduct lyase in a reaction involving radical-mediated direct reversal of damage without base excision [4-5].

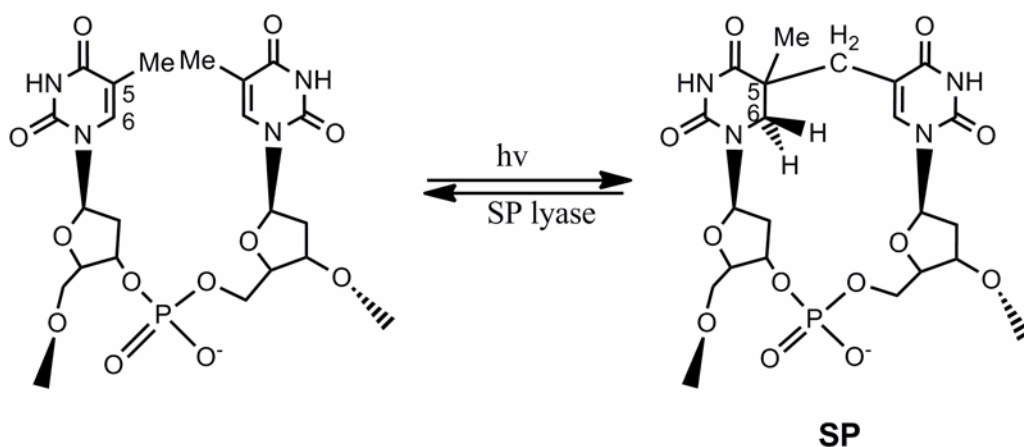


Figure 3.1. The formation of spore photoproduct (*SP*) and the repair reaction catalyzed by spore photoproduct lyase.

SP lyase is a member of the radical *S*-adenosylmethionine superfamily of enzymes and contains the characteristic three cysteine motif (CX₃CX₂C) responsible for coordinating the essential [4Fe-4S] cluster [6-8]. The fourth ligand to the [4Fe-4S] cluster in members of this superfamily is *S*-adenosyl-L-methionine (AdoMet or SAM), which

coordinates the unique iron of the cluster through the methionyl amino and carboxylate groups [9-19]. In the absence of AdoMet the fourth ligand to the [4Fe-4S] cluster is currently unknown. Common mechanistic features of these enzymes include the one-electron reductive cleavage of AdoMet by a reduced [4Fe-4S]⁺ cluster to generate methionine and a 5'-deoxyadenosyl radical intermediate, the latter of which abstracts a hydrogen atom from the substrate. We have previously presented evidence indicating that in SP lyase, the highly reactive adenosyl radical intermediate initiates catalysis by abstracting an H-atom from C-6 of SP [20-21]. The resulting substrate radical is then suggested to undergo radical-mediated β -scission to produce two thymines, reforming SAM in the process [20-22].

When the SP lesion is generated in bacterial spores, a chiral center is formed at carbon C_{5a} resulting in two possible stereoisomers, either a 5*R*- or a 5*S*-SP (Figure 3.2). Until recently, little was known regarding the stereospecificity of SP formation *in vivo*, or the stereospecificity of repair by SP lyase. Previous work has resulted in a variety of SP substrates being made both by chemical synthesis [23-28] and by UV irradiation [21, 28-30]. While the UV irradiation method of preparing substrates results in the formation of a variety of photoproducts and thus is not ideal for detailed mechanistic studies, chemical synthesis can provide pure SP substrates but is difficult, time-consuming and expensive. Further complicating both types of SP formation are the low yields for chemical characterization of the substrates.

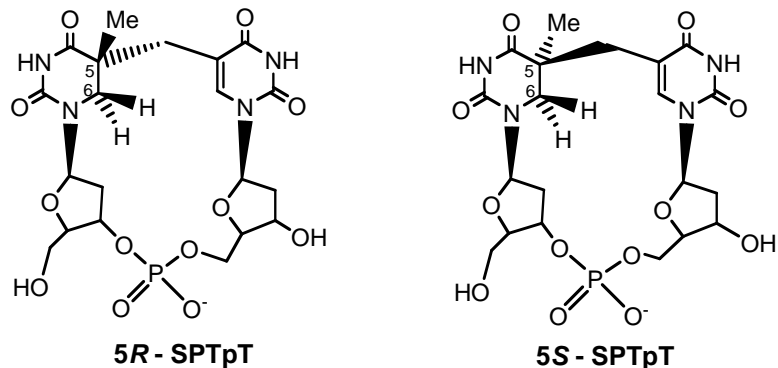


Figure 3.2. Structures of 5*R*- and 5*S*-SPTpT synthetic substrates.

The most recent progress towards defining SP lyase substrates has resulted in the conclusion that the 5*R*-SP is formed *in vivo* and that this stereoisomer is specifically repaired by SP lyase [27, 31]. These results were surprising given earlier work reporting that only the 5*S*-SP stereoisomer was a substrate for SP lyase [26, 30]. These contradicting studies were carried out on the open dinucleoside forms of SP, which could take on structures quite distinct from that for SP in DNA. We were therefore interested in characterizing the repair of both stereoisomers of a more biologically relevant substrate. We report here the anaerobic purification and characterization of SP lyase from *Clostridium acetobutylicum*. We also present the first results of enzymatic repair assays of the pure synthetic 5*R*- and 5*S*-SPTpT dinucleotides by the *C. acetobutylicum* SP lyase. Together, the results reported herein support our conclusion that only the 5*R*-spore photoproduct is repaired by SP lyase. Further, the results show that the more physiologically relevant dinucleotide SPTpT is a significantly better substrate for SP lyase than the open dinucleoside spore photoproduct.

Materials and Methods

Biochemical Methods

Materials *Clostridium acetobutylicum* genomic DNA was obtained from the ATCC (ATCC824D), *E. coli* Tuner(DE3)pLysS and the pET-14b expression vector were obtained from Novagen, and the primers from Integrated DNA Technologies. All enzymes were obtained from Promega or Invitrogen. Gel extraction and plasmid DNA purification kits were obtained from Qiagen. All chemicals were of the highest purity commercially available, unless indicated otherwise.

Expression and Purification of SP Lyase The *splB* gene was cloned from *Clostridium acetobutylicum* using ATCC824D genomic DNA as a template. Amplification of the *splB* gene was accomplished with the synthetic oligonucleotide primers 5'-GAGCGCGCGCCATATGGAAAATATGTTTAG-AAGAGTTATATTTG-3' (containing a NdeI site) and 5'-GCGCGCGCGGATCCTT-AAATTATATACTTAATTGTTGCCTTG-3' (containing a BamHI site) using standard PCR techniques. The NdeI/BamHI-digested PCR product was cloned into the same sites in pET14b, in-frame with an N-terminal hexahistidine tag. The resulting construct (pET14b/*C.a.spl*) was then transformed into NovaBlue *E. coli* for isolation and purification of the plasmid DNA. pET14b/*C.a.spl* was then transformed into Tuner(DE3)pLysS *E. coli* for protein overexpression. The fidelity of the PCR product was verified by sequencing.

A single colony of the resulting overexpression strain was used to inoculate 50 mL of LB media containing 50 µg/mL ampicillin. This culture was grown to saturation at 310 K and used to inoculate a 10-liter flask of a defined MOPS medium (MM) containing 50 µg/mL ampicillin [32]. The 10-liter culture was grown at 310 K in a New Brunswick Scientific fermentor (250 rpm, 5 p.s.i. O₂). When the culture reached an OD₆₀₀ = 0.6, isopropyl β-D-thiogalactopyranoside (IPTG) was added to a final concentration of 0.5 mM, and the medium was supplemented with 750 mg of Fe(NH₄)₂(SO₄)₂. The culture was grown for an additional 2 h, and then was cooled to 298 K and placed under N₂. The culture was further cooled to 277 K, supplemented with an additional 750 mg of Fe(NH₄)₂(SO₄)₂, and left under nitrogen for 12 h. The cells were then harvested by centrifugation and stored at 193 K until used for purification.

SP lyase was purified under anaerobic conditions as previously published [21] with the following changes: pelleted cells (12-16 g) were resuspended in lysis buffer containing 20 mM sodium phosphate, pH 7.5, 350 mM NaCl, 5% glycerol, 10 mM imidazole, 1% Triton X-100, 10 mM MgCl₂, 1 mM phenylmethylsulfonyl fluoride, 0.5 mg lysozyme/g of cells, less than 1 mg of DNase I and RNase A. SP lyase was purified using a HisTrap HP 5 mL column (GE Healthcare) that was previously equilibrated with Buffer A (20 mM sodium phosphate, 350 mM NaCl, 5% glycerol, 10 mM imidazole, pH 7.5). The column was washed with 35 mL of Buffer A followed by a step gradient of 5% Buffer B (20 mM sodium phosphate, 350 mM NaCl, 5% glycerol, 500 mM imidazole, pH 7.5) for 25 mL and then a linear gradient from 5% Buffer B to 50% Buffer B for 45 mL. The collected fractions were analyzed by SDS-PAGE, and those determined to be ≥ 95%

pure were pooled. The protein was then dialyzed against 20 mM sodium phosphate, 350 mM NaCl, 5% glycerol, pH 7.5 and concentrated using an Amicon concentrator fitted with a YM-10 membrane. The concentrated protein was placed in o-ring sealed tubes, flash-frozen and stored at 193 K.

Protein and Iron Assays Protein concentrations were determined by the Bradford method [33] using a kit sold by Bio-Rad and bovine serum albumin as a standard. Iron assays were performed using the method of Beinert [34].

Assay of SP Lyase Activity All solutions were prepared anaerobically prior to use. Assays with and without SP lyase (50 μ M) were set up in parallel in an MBraun glove box maintained at less than 1 ppm O₂. Reaction mixtures (565 μ L total volume) contained 50 μ M SP lyase, 1 mM AdoMet, 500 μ M SPTpT substrate, 5 mM dithiothreitol, and 1 mM dithionite all in 17 mM sodium phosphate, 100 mM NaCl, 6 mM KCl, pH 7.5. All reaction mixtures were incubated at 303 K with 80 μ L aliquots taken every 10 min for 60 min. The reaction was stopped by flash freezing in liquid nitrogen and protein was removed by boiling all samples for 1 min followed by centrifugation at top speed. The supernatant of each sample was then diluted 1:3 in H₂O and analyzed for TpT and SPTpT content by HPLC. All assays were run at least in duplicate, most often triplicate. Error bars represent the standard deviation of the product concentration.

HPLC Analysis Assays for repair of the spore photoproduct dinucleotides (SPTpT) to a thymine dinucleotide monophosphate (TpT) were analyzed by HPLC

(monitored at 260 nm) and were further confirmed by co-injection of authentic TpT and by mass spectrometry. Samples (20 μ L of a 1:3 dilution of each assay) were run over a C18 Waters Spherisorb 5 μ m ODS2 4.6 X 150 mm analytical column at 1 mL/min with a linear gradient of acetonitrile in 2 mM TEAA (0% to 10% from 0 min to 20 min, then 10% to 20% from 20 min to 30 min). Integration of the TpT and SPTpT peaks allowed for quantification of repair as compared to control samples.

Mass Spectrometry Thymidylyl (3'-5') thymidine (TpT) formation in repair assays was confirmed by subjecting the isolated TpT peak from HPLC to electrospray-ionization (ESI) mass spectrometry on a Quattro II mass spectrometer.

Spectroscopic Measurements Low temperature X-band CW (continuous wave) EPR spectra were recorded using a Varian E-109 spectrometer modified with a National Instruments computer interface (for data collection and field control) and equipped with an Air Products and Chemicals LTD-3-110 Heli-Tran Liquid Helium Transfer Refrigerator (Allentown, PA). EPR parameters were as follows: sample temperature 12 K; microwave frequency 9.24 GHz; microwave power 2 mW; time constant 0.50; each spectrum shown is the average of 2 scans. Samples were prepared in an MBraun glove box maintained at less than 1 ppm O₂ with protein concentrations between 560 μ M and 640 μ M. Reduced samples were prepared by adding 5 mM DTT, 50 mM Tris, 100 μ M 5-deazariboflavin and illuminating the sample with a 300 W halogen lamp for 1 h in an EPR tube placed in an ice-water bath. Spin concentration was determined by double integration of the EPR signals arising from samples and from a Cu(II)-EDTA standard of

known concentration under identical conditions. UV-visible spectra were recorded at room temperature on a Cary 6000i UV-Vis-NIR (Varian) spectrophotometer. Samples were prepared inside an anaerobic MBraun chamber and transferred to anaerobic Spectrosil quartz 1.4 mL cuvettes (Starna Cells, Inc., Atascadero, CA).

Synthetic Methods

All reactions were carried out in oven- or flame-dried glassware under a nitrogen atmosphere. Solvents were distilled prior to use. Dichloromethane and pyridine were distilled from calcium hydride. Tetrahydrofuran (THF) was distilled on sodium/benzophenone prior to use. Purification of reaction products was carried out by flash chromatography using silica gel (230-400 mesh). All reagents were commercially available and used without further purification. All reactions were monitored by thin-layer chromatography (TLC) using silica gel 60, F-254. ^1H NMR and ^{13}C NMR spectra were recorded on Bruker DPX-300, Bruker DRX-500 or on Bruker DRX-600. NMR spectra were recorded on solutions in deuterated chloroform (CDCl_3), with residual chloroform (δ 7.27 ppm for ^1H NMR and δ 77.0 ppm for ^{13}C NMR) or deuterated dimethyl sulfoxide ($\text{DMSO-}d_6$), with residual dimethyl sulfoxide (δ 2.50 ppm for ^1H NMR and δ 35.0 ppm for ^{13}C NMR) taken as the standard, and were reported in parts per million (ppm). Abbreviations for signal coupling are as follows: s, singlet; d, doublet; t, triplet; q, quartet; m, multiplet. The multiplicities of the ^{13}C NMR signals were determined by HMQC and DEPT techniques. Mass spectra (high resolution FAB or ESI) were recorded on a Q-Tof and 70-VSEs spectrometer at the Mass Spectrometry Laboratory, Noyes Laboratory, University of Illinois Urbana-Champaign.

Synthesis and Stereochemical Assignment

of 5*R*- and 5*S*- Dinucleotide Spore Photoproducts

The synthesis of 5*R*- and 5*S*-spore photoproducts with the phosphate backbone (SPTpT) was achieved from their corresponding pure 5*R*- and 5*S*-dinucleoside substrates [27] using published procedures [23] after separation of the diastereomers after the first step in the synthesis as described in [27]. The structures of synthesized 5*R*-SPTpT & 5*S*-SPTpT were fully characterized using NMR techniques. The stereochemistry of each of the two diastereomers was assigned based on NOESY and ROESY cross-peaks of precursors as well as the pure phosphotriester [27]. The structures of the fully deprotected 5*R*-SPTpT and 5*S*-SPTpT were confirmed by ¹H NMR, ³¹P NMR, ¹³C NMR and mass spectrometry.

(5*R*-SPTpT) Synthesized as a white solid; *R_f*: 0.1; ¹H NMR (CD₃OD): δ 1.24 (s, 3H, Me), 2.1 (dd, 1H, CH₂, 2'), 2.2-2.9 (m, 1H, CH, 2'), 2.3-2.38 (m, 1H, CH, 2'), 2.4-2.49 (m, 1H, CH, 2'), 2.60 (d, *J* = 14 Hz, 1H, CH₂, bridge), 2.8 (d, *J* = 14 Hz, 1H, CH₂, bridge), 3.3 (d, *J* = 14 Hz, 1H, CH₂, base), 3.4 (d, *J* = 13.5 Hz, 1H, CH₂, base), 3.62-3.67 (m, 2H, CH₂, 5'), 3.7 (dd, *J* = 3.5, 10 Hz, 2H, CH₂, 5'), 3.9 (bt, 1H, CH, 4'), 4.0 (bs, 1H, 4'), 4.5-4.53 (m, 1H, 3'), 4.6-4.67 (m, 1H, 3'), 6.1-6.17 (m, 2H, 1'), 7.8 (s, 1H, base); ¹³C NMR (CD₃OD): δ 24.2 (CH₃, C5), 36.5 (CH₂ bridge), 37.2 (CH₂), 39.9 (CH₂), 41.9, 47.3 (CH₂-base), 61.5 (CH₂), 65.2 (CH₂), 71.2 (C 3'), 73.2 (C 3'), 83.8 (C 4'), 84.3 (C, 1'), 85.2 (C 1'), 86.5 (C 4'), 112.0 (Cquat), 140.1 (CH), 152.5 (Cquat), 155.5 (Cquat), 165.4 (Cquat), 176.9 (Cquat); ³¹P NMR (CD₃OD): 0.064; HRMS: *m/z*: 547.1420 (calcd. for C₂₀H₂₈N₄O₁₂P; 547.1441) (M + H); MS: (TOF, MS, ESI) *m/z* 547, 449, 362, 314.

(5*S*-SPTpT): Synthesized as a white solid; *R_f*: 0.1; ¹H NMR (D₂O): δ 1.02 (s, 3H, Me), 1.93-1.95 (m, 1H, CH₂, 2'), 2.0-2.08 (m, 1H, CH, 2'), 2.12-2.22 (m, 2H, CH, 2'), 2.5

(d, J = 15 Hz, 1H, CH₂, bridge), 2.6 (d, J = 15 Hz, 1H, CH₂, bridge), 3.2 (d, J = 13.5 Hz, 1H, CH₂, base), 3.3 (d, J = 13.5 Hz, 1H, CH₂, base), 3.83-4.0 (m, 6H, CH₂, 5' & 3'), 4.2 (bt, 1H, 3'), 4.4 (bt, 1H, 3'), 6.1 (t, 1H, 1'), 6.2 (t, 1H, 1'), 7.6 (s, 1H, base); ³¹P NMR (D₂O): 0.91; HRMS: *m/z*: 547.1438 (calcd. for C₂₀H₂₈N₄O₁₂P; 547.1441) (M + H); MS: (TOF, MS, ESI) *m/z* 547, 569.

Results

Overexpression and Purification of SP Lyase

The *Clostridium acetobutylicum splB* gene was cloned into pET-14b containing a N-terminal hexahistidine tag. The resulting construct was used to transform *E. coli* Tuner(DE3)pLysS for overproduction of histidine-tagged SP lyase. Under this IPTG-inducible system, *C.a.* SP lyase overexpression can be easily observed (Figure 3.3 lane 3); the overproduced protein migrates around 41 kDa on SDS-PAGE, consistent with the amino acid sequence of SP lyase. The crude extract (Figure 3.3 lane 4) was loaded onto a Ni HisTrapTM HP affinity column and eluted with an imidazole gradient. SP lyase elutes between 150 and 250 mM imidazole as a dark brown band, consistent with the presence of an iron-sulfur cluster in the protein. Pure fractions (Figure 3.3 lane 5) were identified by SDS-PAGE, pooled, dialyzed to remove the imidazole and then concentrated. About 80-100 mg of pure SP lyase could be obtained from 10 L of culture, which is 3-4 times the amount we previously obtained for the growth and purification of His₆-SP lyase from *B. subtilis* [21].

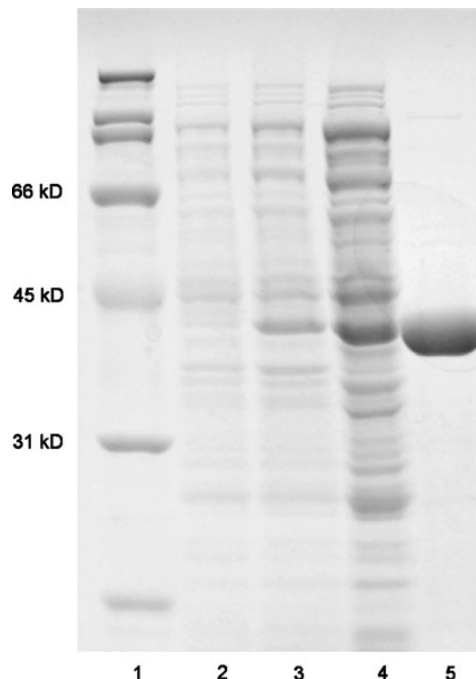


Figure 3.3. SDS-PAGE analysis of *C.a.* SP lyase expression and purification. SP lyase was expressed in *E. coli* Tuner(DE3)pLysS/pET14b as described in the text. Samples were run on a 12% Tris-HCl gel. *Lane 1*, molecular mass standards; *lane 2*, pre-induced culture; *lane 3*, post-induced culture, *lane 4*, clarified crude lysate; *lane 5*, purified SPL.

Spectroscopic Characterization of *C.a.* SP Lyase

The UV-visible spectrum of the purified enzyme (Figure 3.4, solid line) is characteristic of the presence of an iron-sulfur cluster. The spectrum exhibits a broad shoulder with a maximum at 413 nm, similar to what has previously been observed for *B.s.* SP lyase [21], as well as for anaerobically purified pyruvate formate-lyase-activating enzyme and lipoyl synthase [35-36]. Anaerobically purified SP lyase contains iron (between 2.3 – 3.1 (\pm 0.2) depending on preparation) and is stable at concentrations greater than 1 mM in the absence of SAM. This is in contrast to *B.s.* SP lyase which was highly susceptible to precipitation at concentrations greater than 250 μ M [21]. SP lyase can be photoreduced under anaerobic conditions in the presence of DTT, Tris, and 5-

deazariboflavin, and reduction is accompanied by a decrease in the visible absorption to produce a spectrum more characteristic of a $[4\text{Fe-4S}]^+$ cluster (Figure 3.4, dashed line).

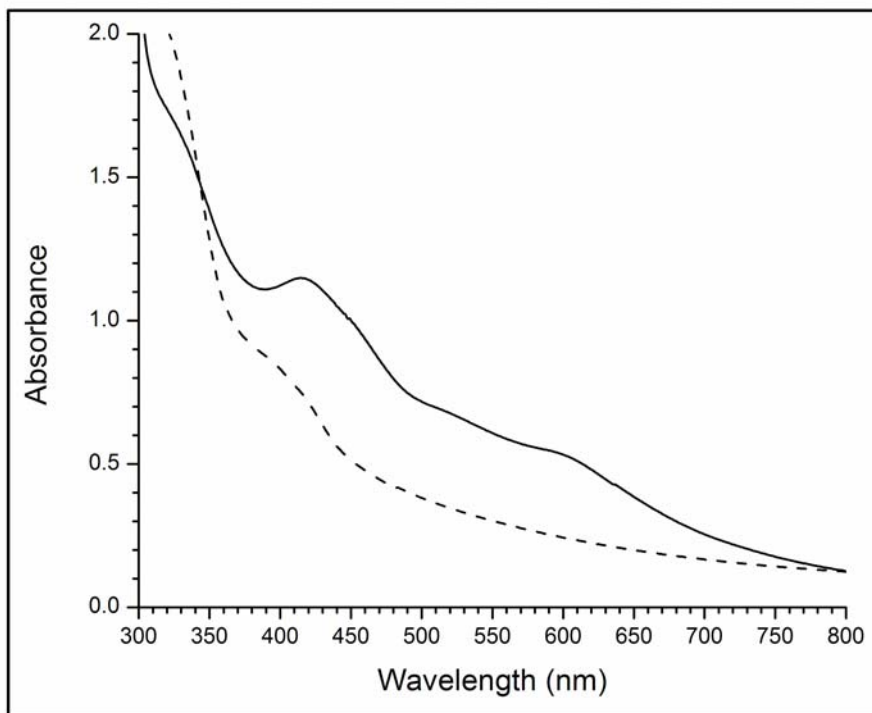


Figure 3.4. UV-visible absorption spectra of SP lyase. Presented are spectra of the as-isolated (solid line) and reduced with 5-deazariboflavin (dashed line). For both spectra, the protein was 150 μM in 20 mM sodium phosphate, 350 mM NaCl, 5 mM dithiothreitol, 5% glycerol, pH 7.5. The reduced protein also contained 100 μM 5-deazariboflavin. The spectra were recorded in a 1 cm path length cuvette under anaerobic conditions at room temperature.

The as-isolated SP lyase EPR spectrum exhibits an isotropic signal that is centered at a g -value of 1.99 (Figure 3.5A). This signal is similar to what has previously been observed for *B.s.* SP lyase and is consistent with the assignment of a $[3\text{Fe-4S}]^+$ cluster being present in the as-isolated form of the enzyme. Spin quantification of this signal, however, shows that it accounts for only about 3 to 4% of the total iron, a very small amount compared to the 25 – 35% $[3\text{Fe-4S}]^+$ we observed for *B.s.* SP lyase [21].

Upon photoreduction of SP lyase, significant changes in the EPR spectral properties are observed (Figure 3.5B). The reduced enzyme displays a nearly axial signal with g values of 2.03, 1.93 and 1.92, similar to what has previously been reported for *B. subtilis* SP lyase reduced with sodium dithionite [21, 30] and for reconstituted *C. acetobutylicum* SP lyase reduced with sodium dithionite [29], although the signal shown here is significantly stronger than those reported previously. This signal in Figure 3.5B is consistent with the presence of a $[4\text{Fe-4S}]^+$ cluster in the reduced form of the enzyme which accounts for between 32% and 45% of the total iron, indicating incomplete reduction. When AdoMet is added to the reduced enzyme (Figure 3.5C), a similar signal is observed but with much lower intensity (between 5 and 13% of total iron as $[4\text{Fe-4S}]^+$) and slightly altered g-values (2.03, 1.92, and 1.82). Both the reduced signal intensity and the altered g-values are presumably indicative of the interaction of AdoMet with the active-site $[4\text{Fe-4S}]^+$ cluster, as has been observed for other radical AdoMet enzymes.

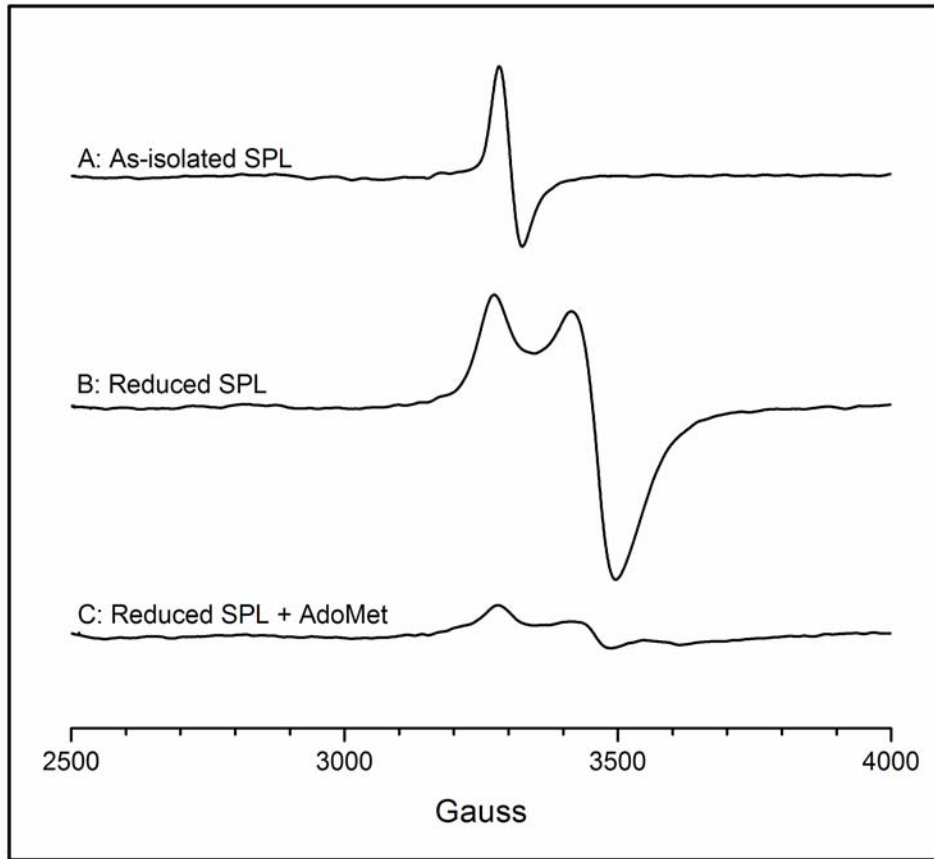


Figure 3.5. X-band EPR spectra of SP lyase. Presented are spectra of the as-isolated enzyme (A), enzyme photoreduced with 5-deazariboflavin (B), and photoreduced enzyme to which AdoMet has been added (C). The protein was in 20 mM sodium phosphate, 350 mM NaCl, 5% glycerol, pH 7.5. The as-isolated protein was 640 μ M; the reduced sample was 600 μ M and prepared with the addition of 5 mM dithiothreitol and 100 μ M 5-deazariboflavin; the reduced + AdoMet sample was 560 μ M and prepared by adding AdoMet to 3 mM final concentration after reduction with 5-deazariboflavin. Conditions of measurement: T = 12 K; microwave power 2 milliwatts; microwave frequency 9.24 GHz; modulation amplitude 10.00; receiver gain 1.6×10^3 , average of 2 scans presented. *SPL* SP Lyase

To further probe the nature of the EPR spectral changes observed in the presence of AdoMet, we investigated the effects on the EPR spectrum of the $[4\text{Fe-4S}]^+$ state of SP lyase in the presence of AdoMet cleavage products and an AdoMet analog (Figure 3.6). The enzyme was subjected to deazariboflavin-mediated photoreduction and was then

mixed with AdoMet, L-methionine, 5'-deoxyadenosine, or *S*-adenosyl-L-homocysteine (SAH) and the 12 K EPR spectrum was recorded. In order to accurately compare the spectra, the samples were prepared from the same stock of SP lyase. The reduced enzyme and reduced enzyme in the presence of methionine display similar features with a nearly axial signal with *g*-values of 2.03 and 1.92 (Figure 3.6A, 3.6C). In the presence of 5'-deoxyadenosine and SAH, the enzyme displays an axial signal with sharpening of the spectral lines, but maintains *g*-values of 2.03 and 1.92 (Figure 3.6D, 3.6E). In the presence of AdoMet (Figure 3.6B and inset), the spectrum changes once again to a rhombic signal with *g*-values of 2.03, 1.92 and 1.82. It is fascinating that the rhombic signal observed for the reduced enzyme in the presence of AdoMet is not observed with any of these similar molecules, and suggests that this spectral change is specific to the AdoMet-cluster interaction.

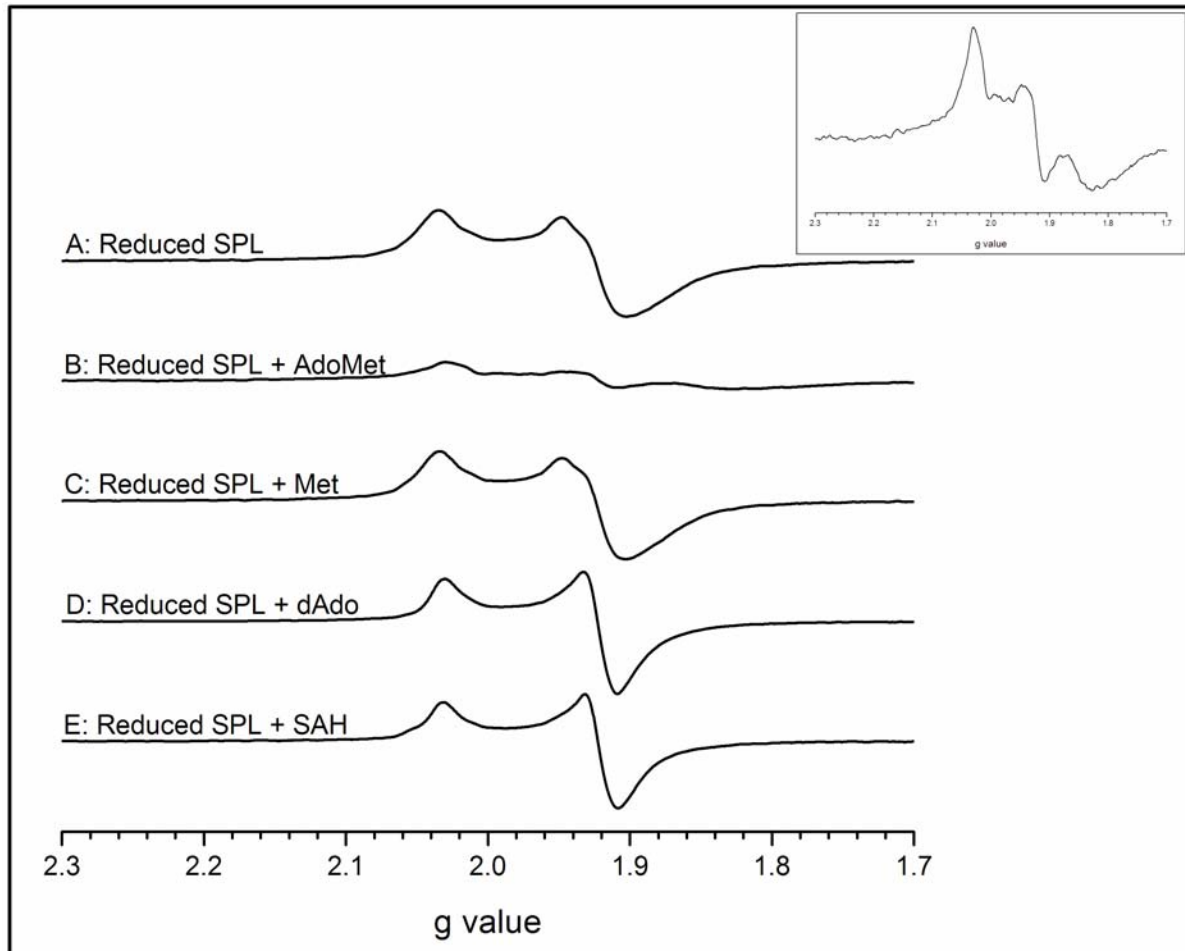


Figure 3.6. X-band EPR spectral evidence for a novel interaction of SP lyase with AdoMet. Presented are spectra of spore photoprodut lyase acquired at 12 K normalized to 570 μM : (A) enzyme photoreduced with 5-deazariboflavin; (B) photoreduced enzyme plus 1.5 mM AdoMet; (C) photoreduced enzyme plus 1.5 mM methionine; (D) photoreduced enzyme plus 1.5 mM dAdo; (E) photoreduced enzyme plus 1.5 mM SAH. Inset: magnification of the spectrum as shown in (B). The protein was in 20 mM sodium phosphate, 350 mM NaCl, 5% glycerol, pH 7.5. Conditions of measurement: T = 12K; microwave power 2 milliwatts; microwave frequency 9.24 GHz; modulation amplitude 10.00; receiver gain 1.6×10^3 , average of 2 scans presented. *SPL* SP Lyase

Characterization of Synthetic Dinucleotide Spore Photoproducts

The structures of the fully deprotected 5*R*- and 5*S*-dinucleotide spore photoproducts were confirmed by ^1H NMR (Figure 3.7A), ^{13}C NMR, ^{31}P NMR (Figure

3.7B), and mass spectrometry. In addition the structures of these two closely related products were based on our recent report where we used 2D ROESY and NOESY spectroscopy of open and closed forms, as well as of the 5*R*- and 5*S*-dinucleosides, to confirm the stereochemistry [27, 37].

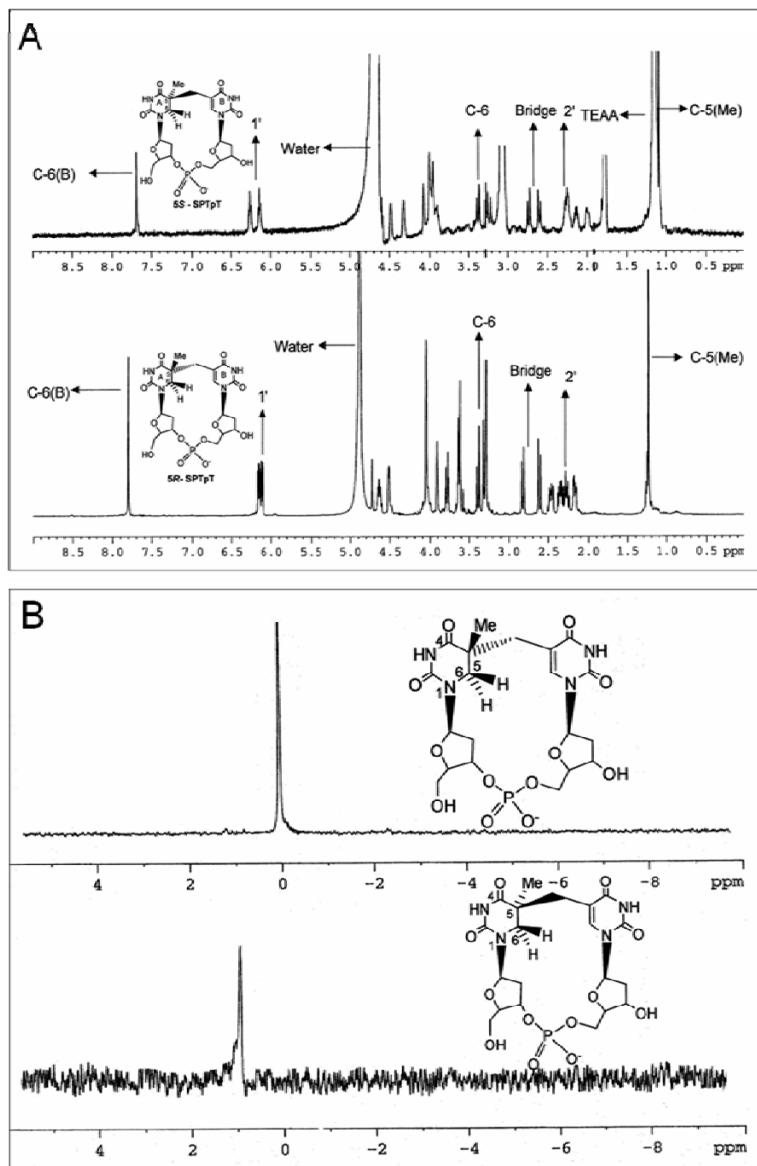


Figure 3.7. NMR spectroscopic characterization of the purified synthetic dinucleotide spore photoproducts. (A) ^1H NMR spectra of 5*S*-SPTpT in D_2O (top) and 5*R*-SPTpT in CD_3OD (bottom). (B) ^{31}P NMR spectra of 5*R*-SPTpT (top) and 5*S*-SPTpT (bottom) in $\text{CD}_3\text{OD}/\text{D}_2\text{O}$.

Enzymatic Repair of the Dinucleotide Spore Photoproducts

We have previously demonstrated that SP lyase repairs the 5*R*-SP synthetic dinucleoside but not the 5*S*-SP synthetic dinucleoside; turnover of the 5*R*-SP was, however, quite slow ($0.4 \text{ nmol min}^{-1} \text{ mg}^{-1}$) and did not proceed to completion [27]. Using the techniques described herein, we have now synthesized both the 5*R*- and 5*S*-SP dinucleotide monophosphate (SPTpT) and for the first time have performed repair assays on both diastereomers. These synthetic dinucleotide substrates contain a phosphodiester bond linking the sugar groups of the thymidine dimer, providing a more biologically relevant substrate for the enzyme to act upon (Figure 3.2). Activity assays were carried out anaerobically and analysis by HPLC allowed for the quantification of TpT product formation over time to obtain a rate of repair.

These assays clearly demonstrate the *complete* repair of the 5*R*-SPTpT to form the TpT product with ten turnovers in about 40 min (Figure 3.8A). The complete repair of the 5*R*-SPTpT substrate to form the TpT product is indicated by a significant decrease in the 5*R*-SPTpT peak (eluting at 8.5 min) and a significant increase in the TpT peak (eluting at 16.2 min). Formation of TpT was confirmed by co-injection with authentic TpT as well as by MS analysis [$m/z = 547$ (M + H); 569 (M + Na)] of the HPLC fractions corresponding to the TpT peak (Figure 3.9B). There was no detectable 5*R*-SPTpT substrate in the reaction at 40 min or later time points. That this conversion of 5*R*-SPTpT to TpT was dependent on SP lyase and AdoMet was demonstrated by control reactions lacking either enzyme or cofactor; in neither case was any formation of TpT detected (data not shown).

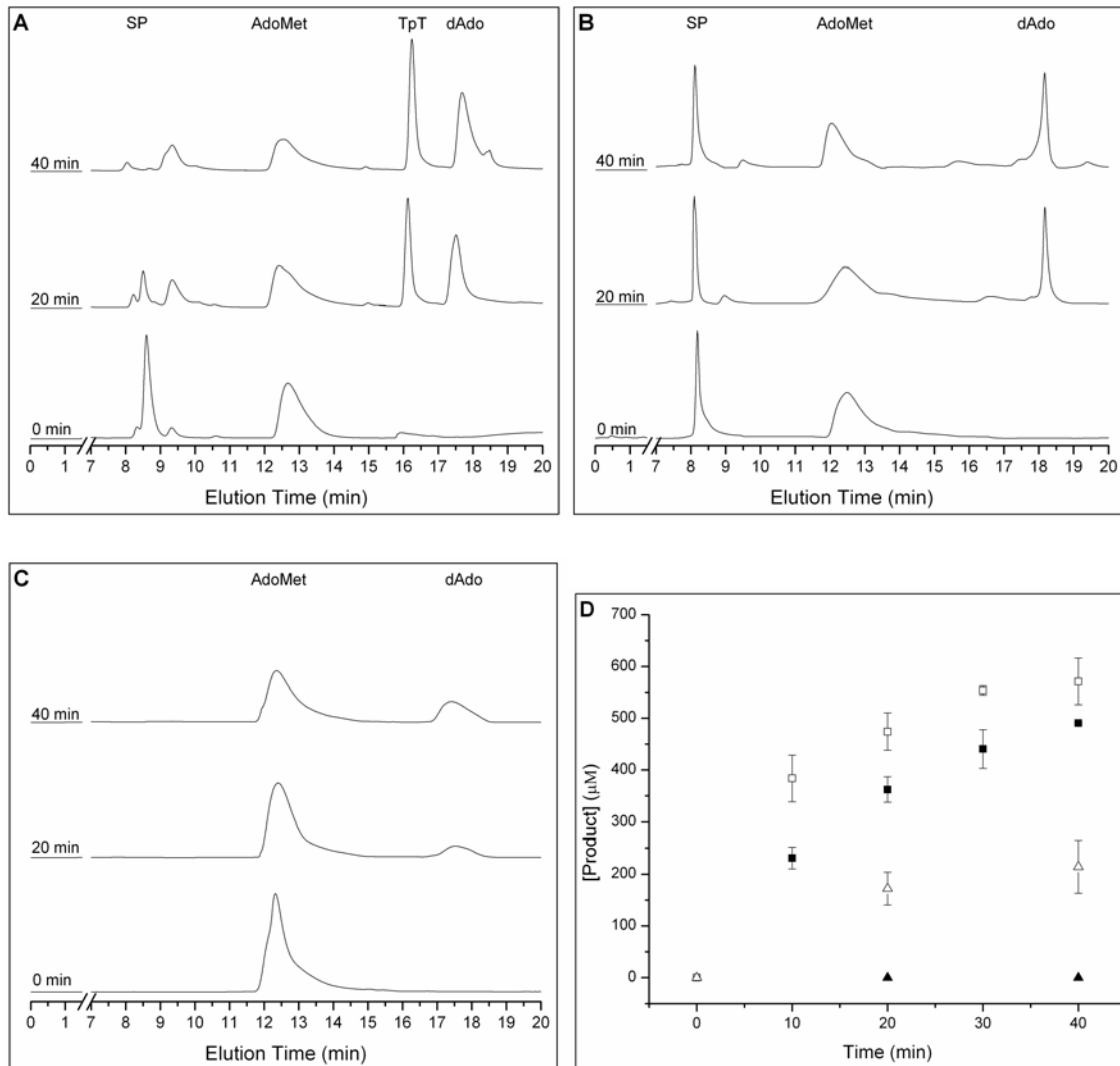


Figure 3.8. HPLC chromatograms demonstrating the time-dependent formation of TpT due to repair of 5R-SPTpT (A) but not the 5S-SPTpT (B), upon incubation of 500 μ M SP with SPL (50 μ M), AdoMet (1 mM), DTT (5 mM) and dithionite (1 mM) in 17 mM sodium phosphate, 100 mM NaCl, 6 mM KCl, pH 7.5 at 303 K. SPTpT elutes at 8.5 min (5R) or 8.1 min (5S) and TpT elutes at 16.2 min under these conditions. HPLC chromatograms of the negative control (lacking substrate) (C) demonstrating the time-dependent cleavage of AdoMet by SP lyase (50 μ M) incubated with AdoMet (1 mM), DTT (5 mM) and dithionite (1 mM) in 17 mM sodium phosphate, 100 mM NaCl, 6 mM KCl, pH 7.5 at 303 K. Integration of the TpT, SPTpT, AdoMet and dAdo peaks allowed for the quantification of each isomer of SP and AdoMet cleavage (D). The repair of the 5R-SPTpT (solid squares) demonstrates the repair over the course of 40 min while assays of 5S-SPTpT (solid triangles) resulted in no detectable formation of TpT. Formation of dAdo is shown for the 5R-SPTpT (open squares) as well as for the 5S-SPTpT (open triangles).

In contrast to these results with the *5R*-SPTpT, in assays with the *5S*-SPTpT no significant decrease in peak intensity for the substrate (eluting at 8.1 min) or increase in peak intensity for the product TpT was observed (Figure 3.8B). Co-injection of the *5S*-SPTpT reaction mix with authentic TpT results in the formation of a new peak not previously observed in the reaction mix. These results demonstrate that the *5R*-SPTpT is a substrate for SP lyase, while the *5S*-SPTpT is not. For assays with either diastereomer of the synthetic dinucleotide spore photoproduct, dAdo formation is observed (Figure 3.8A and 3.8B); such dAdo production is also observed under these assay conditions in the absence of the synthetic substrates, indicating an uncoupling between substrate turnover and the reductive cleavage of AdoMet (Figure 3.8C). Such uncoupling is common among radical AdoMet enzymes in the presence of non-physiological reducing agents.[38]. Similar quantities of dAdo are observed for the experiments shown in Figure 3.8B (with the non-substrate *5S*-SPTpT) and in Figure 3.8C (with no substrate), indicating that the nonsubstrate synthetic dinucleotide has no effect on the rate of uncoupled AdoMet cleavage. The dAdo production in the presence of the synthetic substrate *5R*-SPTpT, however, is greater than these other two cases (Figures 3.8A and 3.8D). A comparison between the rates of turnover of the synthetic dinucleotides and the rates of reductive cleavage of AdoMet in each assay is provided in Figure 3.8D. While the AdoMet cleavage in the assays of *5S*-SPTpT is clearly uncoupled, as no substrate turnover is observed, the observation of only a small excess of dAdo produced over repaired *5R*-SPTpT could lead one to believe that AdoMet is acting as a substrate (accounting for 1 dAdo per *5R*-SPTpT repaired), with the remaining dAdo produced as a

result of uncoupling. We have, however, demonstrated previously with “native” substrate that SP lyase uses AdoMet catalytically and not as a substrate.[21] We therefore conclude that the approximately 1.3:1 ratio of dAdo to TpT in the assays of 5*R*-SPTpT is simply a result of enhanced uncoupled AdoMet cleavage in the presence of a “poor” substrate for SP lyase.

Under the given assay conditions, SP lyase was found to have a specific activity for the repair of the 5*R*-SPTpT of $7.1 \pm 0.6 \text{ nmol min}^{-1} \text{ mg}^{-1}$ (or $0.29 \pm 0.02 \text{ mol mol}^{-1} \text{ min}^{-1}$), comparable to the $0.24 \text{ mol mol}^{-1} \text{ min}^{-1}$ previously observed for repair of an SPTpT substrate produced by irradiation [30]. Furthermore, the k_{cat} for the repair of the dinucleotide 5*R*-SPTpT substrate by SP lyase was $0.30 \pm 0.01 \text{ min}^{-1}$, significantly higher than the $0.021 \pm 0.004 \text{ min}^{-1}$ determined for the repair of the 5*R*-SP dinucleoside. Together, these results illustrate that while the stereochemical requirement for the *R* configuration is maintained as the substrate gains both complexity and physiological relevance in going from dinucleoside to dinucleotide, significantly higher rates of catalysis are achieved by the simple introduction of a phosphodiester bridge.

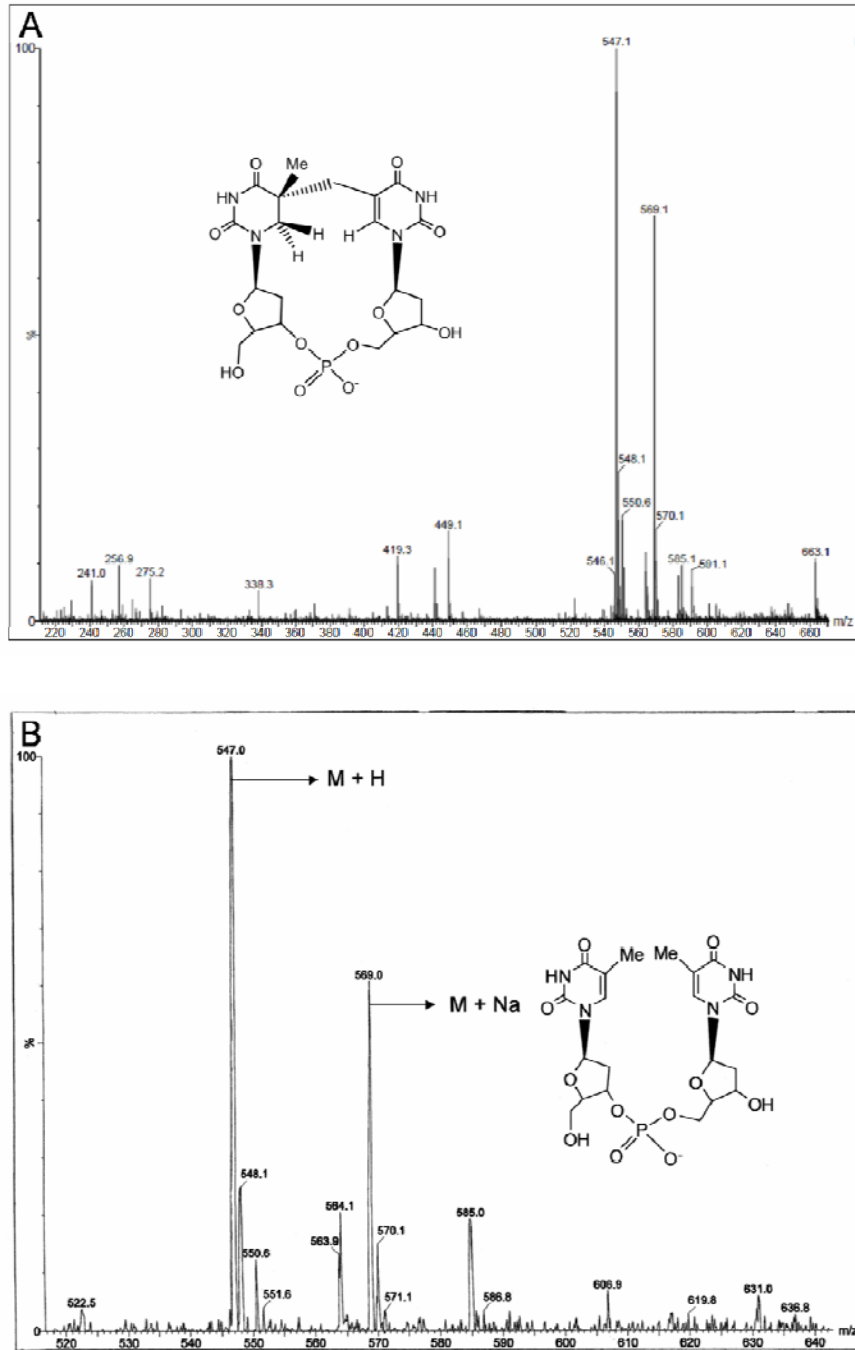


Figure 3.9. Extended ESI MS of 5R- thymidylyl (3'-5') thymidine (SPTpT) before repair by SP lyase (A) and after repair by SP lyase as isolated from the assay mixture (TpT) (M + H = 457; M + Na = 569; M + K = 585).

Discussion

We provide here the first detailed investigation of the repair activity of SP lyase towards stereochemically-defined dinucleotide spore photoproducts. We have expressed *C. acetobutylicum* SP lyase in *E. coli* and following anaerobic purification, an active enzyme with an iron-sulfur cluster is obtained. This enzyme has proved to be much more stable and soluble than the enzyme from *B. subtilis* [21]. Furthermore, the *C.a.* SP lyase yields significantly more protein, about 80 to 100 mg from a 10 L culture, as compared to about 25 mg per 10 L for the *B.s.* SP lyase.

The clone of *C. acetobutylicum* SP lyase used for these studies included an N-terminal six-histidine tag to aid in purification on a Ni affinity column. Our strictly anaerobic isolation of SP lyase yields a brown protein containing between 2.3 to 3.1 iron per protein monomer, depending on the preparation. The observation that SP lyase is being isolated with less than 4 iron atoms per monomer indicates the enzyme does not contain a fully loaded [4Fe-4S] cluster, an observation not uncommon among radical AdoMet enzymes. This purified protein has UV-visible spectroscopic features characteristic of an iron-sulfur cluster (Figure 3.4), although is not indicative of which type of cluster the enzyme contains. EPR spectroscopy reveals only a minor amount (about 3 to 4% of total iron) being present as a [3Fe-4S]⁺ cluster (Figure 3.5A), which suggests the isolated enzyme contains a mixture of EPR-silent clusters (most likely [2Fe-2S]²⁺ and [4Fe-4S]²⁺) in addition to the minor [3Fe-4S]⁺ component giving rise to the characteristic EPR signal. EPR spectroscopy of the reduced enzyme shows that a significant proportion of the iron is present in EPR-active [4Fe-4S]⁺ clusters (Figure

3.5B), with the remainder being EPR-silent and presumably in a $[4\text{Fe-4S}]^{2+}$ state based on observations of other radical AdoMet enzymes. Reductive cluster conversions (from $[3\text{Fe-4S}]^+$ and $[2\text{Fe-2S}]^+$ states to $[4\text{Fe-4S}]^{2+/+}$) have previously been reported for several enzymes in the radical AdoMet superfamily, including pyruvate formate-lyase activating enzyme [32, 39-41], biotin synthase [42-44], lysine 2,3-aminomutase [45-46], lipoyl synthase [47-48] and anaerobic ribonucleotide reductase activating enzyme [49], although the physiological relevance of these cluster conversions remains unknown.

Addition of AdoMet to the reduced enzyme produces a decreased signal intensity in the EPR spectrum, similar to previous observations with *B.subtilis* SP lyase [21]. However, we also observe a change in the line shape to a rhombic signal not previously observed for SP lyase in the presence of AdoMet (Figure 3.5C). This novel signal appears to be unique to the interaction of AdoMet with the reduced enzyme, as the addition of AdoMet cleavage products or AdoMet analogs to the reduced SP lyase did not produce the rhombic signal observed when AdoMet is present (Figure 3.6). The decrease in $[4\text{Fe-4S}]^+$ signal intensity upon addition of AdoMet, which is also not observed upon addition of AdoMet analogs or cleavage products, has previously been suggested to be due to the reductive cleavage of AdoMet (which would be accompanied by cluster oxidation to the EPR-silent $[4\text{Fe-4S}]^{2+}$ state) [50]; we do not however observe significant SAM cleavage in the absence of substrate and dithionite while being incubated in an ice bath (conditions in which EPR sample is prepared; data not shown), suggesting that the cluster is *not* being oxidized. While a small amount (30 μM) of dAdo is observed to form, this amount does not fully account for the change in signal intensity upon the addition of AdoMet.

Another possibility is that the addition of AdoMet results in conversion of the $[4\text{Fe-4S}]^+$ cluster from $S=1/2$ to a higher spin state which we are not observing under our current EPR parameters. The reason behind this dramatic reduction in signal intensity is currently under active investigation.

We have recently demonstrated the repair of the synthetic *5R*-SP, but not the *5S*-SP, dinucleoside (lacking a phosphodiester bridge) by SP lyase [27]. This rudimentary substrate provided the first definitive evidence for the stereochemical requirements for spore photoproduct repair by SP lyase, although repair was quite slow ($0.4 \text{ nmol min}^{-1} \text{ mg}^{-1}$) and did not proceed to completion. In the present work, we characterize for the first time the ability of SP lyase to repair the pure stereochemically defined dinucleotide substrates. The *5R*- and *5S*-SPTpT synthetic dinucleotides, which include a phosphodiester bridge linking the sugars, provide more complete and biologically relevant spore photoproducts with which to further investigate the stereochemical requirements for repair by SP lyase. Our results clearly demonstrate that only the *5R*-SPTpT acts as a substrate for SP lyase, and that repair is relatively rapid, with a specific activity 18-fold greater ($7.1 \text{ nmol min}^{-1} \text{ mg}^{-1}$) than that observed when the *5R*-dinucleoside SP was used as a substrate. The turnover rate is lower, however, than that observed with “native” substrate ($0.33 \text{ } \mu\text{mol min}^{-1} \text{ mg}^{-1}$), generated by irradiating DNA with UV light under appropriate conditions, indicating that the incorporation of SPTpT into a DNA strand is necessary for optimal substrate efficiency. We observe multiple turnovers of our *5R*-SPTpT substrate, with 100% repair (10 turnovers) of the *5R*-SPTpT

over the course of 40 min, consistent with more efficient repair, and with less enzyme inactivation occurring during turnover, relative to assays with the dinucleoside substrate.

Our results provide the most convincing evidence to date for the stereospecificity of the repair reaction catalyzed by SP lyase, and support our previous conclusions based on assays with the minimal dinucleoside substrate. Our results however contradict earlier reports that the *5S*- but not the *5R*-SP is a substrate for SP lyase [26, 28]. While it is not possible for us to determine precisely what led to a different conclusion in this previously published work, the turnover of *5R*-SPTpT reported here is both rapid and complete, allowing for complete characterization of turnover and providing definitive evidence for our conclusion that SP lyase is stereospecific for the *5R*- spore photoproduct (Figure 3.8). Our conclusion that the *5R*- isomer of spore photoproduct is the only one repaired by SP lyase is further supported by a recent report that UV irradiation of TpT produced only the *5R*-SPTpT [31].

A comparison of specific activities for SP lyase from different sources with different synthetic and naturally-occurring substrates is provided in Table 3.1. Assays in which the synthetic SP dinucleoside is used as substrate show the lowest activity, consistent with this being a minimal substrate lacking structural features required for efficient turnover. The addition of the phosphodiester bridge to make the SPTpT dinucleotide substrate, whether generated synthetically (this work) or by UV irradiation of TpT [29-30], considerably enhances the observed activity for SP lyase, increasing the k_{cat} 14-fold. Substrates in which the SP lesion is generated by UV irradiation of a single-stranded oligo [28] or double-stranded DNA [21], give rise to the highest specific

activities measured for SP lyase. Comparison of these rates indicates that both the phosphodiester bridge between the sugars of the SP lesion, and the nucleotides adjacent to the SP lesion, and possibly the overall structure and conformation of the DNA in which the SP lesion resides, contribute to rates of catalysis. Further insight into these effects will require investigation of binding thermodynamics with different substrates, as well as full kinetic analysis of each substrate, both of which are currently underway.

Table 3.1. Catalytic activities of SP lyase with a series of synthetic and natural substrates.

Substrate	Specific Activity (mol mol ⁻¹ min ⁻¹) ^{a,b}	k _{cat} (min ⁻¹)	Temperature	Source of SP Lyase ^c	Reference
Dinucleoside	0.02 ^d	0.021 ^f	303 K	<i>C.a.</i>	27
	0.007 ^d	NR	NR	<i>B.s.</i>	26
Dinucleotide	0.29 ^d	0.30	303 K	<i>C.a.</i>	This study
	0.24 ^e	NR	293 K or 310 K	<i>B.s.</i>	30
	0.2 ^e	NR	NR	<i>C.a.</i>	29
ss 6-mer	100 ^e	NR	NR	<i>G.s.</i>	28
Oligo DNA	14 ^e	NR	310 K	<i>B.s.</i>	21

NR not reported

^aActivities for SP lyase observed in our laboratory have been converted to the same units for previously published results to allow for direct comparisons. ^bThe activity for *G.s.* SP lyase was converted to the same units to allow direct comparison using the literature value of 40.5 kDa as the molecular mass. ^c*C.a.* *Clostridium acetobutylicum*, *B.s.* *Bacillus subtilis*, *G.s.* *Geobacillus stearothermophilus* ^dStereochemically-defined synthetic substrates. ^eSubstrates produced by UV irradiation. ^fk_{cat} calculated and reported in this study.

In conclusion, we report here the anaerobic purification and characterization of SP lyase from *C. acetobutylicum*, showing that it contains a reducible iron-sulfur cluster that reacts in a very specific manner with AdoMet. The spectroscopic signatures of *C. acetobutylicum* SP lyase are consistent with its membership in the radical SAM

superfamily, and are similar to observations for SP lyase from other sources. However, we observe a novel change in the EPR signal with the addition of AdoMet to the reduced enzyme not previously observed for SP lyase from other sources. We have also synthesized the pure stereochemically-defined dinucleotide lesions *5R*-SPTpT and *5S*-SPTpT, and demonstrate that the *5R*- isomer is efficiently repaired to TpT while no repair of the *5S*- isomer is detected. The rapid and complete repair of the more physiologically relevant *5R*-SPTpT substrate, relative to the earlier report of *5R*- dinucleoside substrate, provides for a convincing demonstration of not only the stereospecificity of SP lyase, but also the importance of the phosphodiester bridge of the lesion for efficient enzymatic repair.

Acknowledgements

We would like to thank David Schwab and Eric Shepard for assistance in running EPR samples, and David Singel for use of his EPR instrument. This research has been supported by the NIH (GM67804 to J.B.B.). The Astrobiology Biocatalysis Research Center is supported by the NASA Astrobiology Institute (NAI05-19). The authors acknowledge support for the Mass Spectrometry Laboratory at the University of Illinois at Urbana-Champaign. The 70-VSE mass spectrometer was purchased in part with a grant from the Division of Research Resources, National Institutes of Health (RR 04648). The Q-ToF Ultima mass spectrometer was purchased in part with a grant from the National Science Foundation, Division of Biological Infrastructure (DBI-0100085).

References

1. Donnellan JE, Jr., Setlow RB (1965) *Science* 149:308-310
2. Varghese AJ (1970) *Biochem. Biophys. Res. Commun.* 38:484-490
3. Nicholson WL, Setlow B, Setlow P (1991) *Proc. Natl. Acad. Sci. U.S.A.* 88:8288-8292
4. Munakata N, Rupert CS (1972) *J. Bacteriol.* 111:192-198
5. Munakata N, Rupert CS (1974) *Mol. Gen. Genet.* 130:239-250
6. Fajardo-Cavazos P, Salazar C, Nicholson WL (1993) *J. Bacteriol.* 175:1735-1744
7. Nicholson WL, Chooback L, Fajardo-Cavazos P (1997) *Mol. Gen. Genet.* 255:587-594
8. Sofia HJ, Chen G, Hetzler BG, Reyes-Spindola JF, Miller NE (2001) *Nucleic Acids Res.* 29:1097-1106
9. Walsby C, Ortillo D, Yang J, Nnyepi M, Broderick WE, Hoffman BM, Broderick JB (2005) *Inorg. Chem.* 44:727-741
10. Walsby CJ, Hong W, Broderick WE, Cheek J, Ortillo D, Broderick JB, Hoffman BM (2002) *J. Am. Chem. Soc.* 124:3143-3151
11. Walsby CJ, Ortillo D, Broderick WE, Broderick JB, Hoffman BM (2002) *J. Am. Chem. Soc.* 124:11270-11271
12. Layer G, Moser J, Heinz DW, Jahn D, Schubert W-D (2003) *EMBO J.* 22:6214-6224
13. Chen D, Walsby C, Hoffman BM, Frey PA (2003) *J. Am. Chem. Soc.* 125:11788-11789
14. Berkovitch F, Nicolet Y, Wan JT, Jarrett JT, Drennan CL (2004) *Science* 303:76-79
15. Hänzelmann P, Schindelin H (2004) *Proc. Natl. Acad. Sci. U.S.A.* 101:12870-12875
16. Hänzelmann P, Schindelin H (2006) *Proc. Natl. Acad. Sci. U.S.A.* 103:6829-6834

17. Lepore BW, Ruzicka FJ, Frey PA, Ringe D (2005) *Proc. Natl. Acad. Sci. U.S.A.* 102:13819-13824
18. Nicolet Y, Rubach JK, Posewitz MC, Amara P, Mathevon C, Atta M, Fontecave M, Fontecilla-Camps JC (2008) *J. Biol. Chem.* 283:18861-18872
19. Vey JL, Yang J, Li M, Broderick WE, Broderick JB, Drennan CL (2008) *Proc. Natl. Acad. Sci. U.S.A.* 105:16137-16141
20. Cheek J, Broderick JB (2002) *J. Am. Chem. Soc.* 124:2860-2861
21. Buis JM, Cheek J, Kalliri E, Broderick JB (2006) *J. Biol. Chem.* 281:25994-26003
22. Mehl RA, Begley TP (1999) *Org. Lett.* 1:1065-1066
23. Kim SJ, Lester C, Begley TP (1995) *J. Org. Chem.* 60:6256-6257
24. Friedel MG, Pieck JC, Klages J, Dauth C, Kessler H, Carell T (2006) *Chem. Eur. J.* 12:6081-6094
25. Bürckstümmer E, Carell T (2008) *Chem. Commun.*:4037-4038
26. Friedel MG, Berteau O, Pieck JC, Atta M, Ollagnier-de-Choudens S, Fontecave M, Carell T (2006) *Chem. Commun.*:445-447
27. Chandra T, Silver SC, Zilinskas E, Shepard EM, Broderick WE, Broderick JB (2009) *J. Am. Chem. Soc.* 131:2420-2421
28. Pieck JC, Hennecke U, Pierik AJ, Friedel MG, Carell T (2006) *J. Biol. Chem.* 281:36317-36326
29. Chandor A, Douki T, Gasparutto D, Gambarelli S, Sanakis Y, Nicolet Y, Ollagnier-de-Choudens S, Atta M, Fontecave M (2007) *C. R. Chimie* 10:756-765
30. Chandor A, Berteau O, Douki T, Gasparutto D, Sanakis Y, Ollagnier-de-Choudens S, Atta M, Fontecave M (2006) *J. Biol. Chem.* 281:26922-26931
31. Mantel C, Chandor A, Gasparutto D, Douki T, Atta M, Fontecave M, Bayle P-A, Mouesca J-M, Bardet M (2008) *J. Am. Chem. Soc.* 130:16978-16984
32. Krebs C, Henshaw TF, Cheek J, Huynh B-H, Broderick JB (2000) *J. Am. Chem. Soc.* 122:12497-12506

33. Bradford M (1976) *Anal. Biochem.* 72:248-254
34. Beinert H (1978) *Methods Enzymol.* 54:435-445
35. Miller JR, Busby RW, Jordan SW, Cheek J, Henshaw TF, Ashley GW, Broderick JB, Cronan JE, Jr., Marletta MA (2000) *Biochemistry* 39:15166-15178
36. Broderick JB, Henshaw TF, Cheek J, Wojtuszewski K, Smith SR, Trojan MR, McGhan RM, Kopf A, Kibbey M, Broderick WE (2000) *Biochem. Biophys. Res. Comm.* 269:451-456
37. Chandra T, Broderick WE, Broderick JB (2009) *Nucleosides, Nucleotides & Nucleic Acids* 28:1016-1029
38. Duschene KS, Veneziano SE, Silver SC, Broderick JB (2009) *Curr. Opin. Chem. Biol.* 13:74-83
39. Broderick JB, Duderstadt RE, Fernandez DC, Wojtuszewski K, Henshaw TF, Johnson MK (1997) *J. Am. Chem. Soc.* 119:7396-7397
40. Krebs C, Broderick WE, Henshaw TF, Broderick JB, Huynh BH (2002) *J. Am. Chem. Soc.* 124:912-913
41. Yang J, Naik SG, Ortillo DO, Garcia-Serres R, Li M, Broderick WE, Huynh BH, Broderick JB (2009) *Biochemistry* 48:9234-9241
42. Ugulava NB, Gibney BR, Jarrett JT (2000) *Biochemistry* 39:5206-5214
43. Duin EC, Lafferty ME, Crouse BR, Allen RM, Sanyal I, Flint DH, Johnson MK (1997) *Biochemistry* 36:11811-11820
44. Tse Sum Bui B, Florentin D, Marquet A, Benda R, Trautwein AX (1999) *FEBS Letters* 459:411-414
45. Lieder KW, Booker S, Ruzicka FJ, Beinert H, Reed GH, Frey PA (1998) *Biochemistry* 37:2578-2585
46. Petrovich R, Ruzicka F, Reed G, Frey P (1992) *Biochemistry* 31:10774-10781
47. Busby RW, Schelvis JPM, Yu DS, Babcock GT, Marletta MA (1999) *J. Am. Chem. Soc.* 121:4706-4707
48. Ollagnier-de Choudens S, Fontecave M (1999) *FEBS Lett.* 453:25-28

49. Ollagnier S, Meier C, Mulliez E, Gaillard J, Schuenemann V, Trautwein A, Mattioli T, Lutz M, Fontecave M (1999) *J. Am. Chem. Soc.* 121:6344-6350
50. Rebeil R, Nicholson WL (2001) *Proc. Natl. Acad. Sci. U.S.A.* 98:9038-9043

Contribution of Authors and Co-Authors

Manuscript in Chapter 4

Chapter 4: Kinetic and Mechanistic Insights into the Repair of the Spore Photoproduct Catalyzed by Spore Photoproduct Lyase

Author: Sunshine C. Silver

Contributions: Performed initial studies utilizing *B.s.* SP lyase to determine the rate of H atom abstraction by SP lyase. Generated the figures and wrote the manuscript in preparation for submission.

Co-author: Shourjo Ghose

Contributions: Currently performing repair assays on SP lyase utilizing [methyl ^3H] thymidine pUC18 DNA to determine a rate of repair for *C.a.* SP lyase.

Co-author: Jeffrey M. Buis

Contributions: Performed initial studies utilizing *B.s.* SP lyase to determine the rate of H atom abstraction by SP lyase.

Co-author: Joan B. Broderick

Contributions: Joan B. Broderick provided valuable insight and overview of repair assays, interpretation of results and manuscript preparation.

Manuscript Information Page

Authors: Sunshine C. Silver, Shourjo Ghose, Jeffrey M. Buis, Joan B. Broderick

Journal: Biochemistry

Status of the manuscript:

- Prepared for submission to a peer-reviewed journal
- Officially submitted to a peer-reviewed journal
- Accepted by a peer-reviewed journal
- Published in a peer-reviewed journal

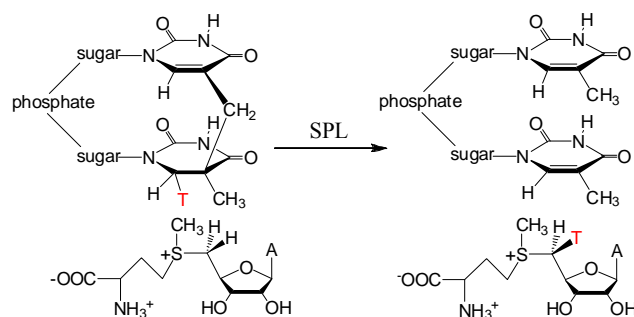
CHAPTER 4

KINETIC AND MECHANISTIC INSIGHTS INTO THE REPAIR OF THE SPORE
PHOTOPRODUCT CATALYZED BY SPORE PHOTOPRODUCT LYASE

The following work is currently in progress to be submitted for publication.

Sunshine C. Silver, Shourjo Ghose, Jeffrey M. Buis, Joan B. Broderick

*Department of Chemistry and Biochemistry and the Astrobiology Biogeochemistry
Research Center, Montana State University, Bozeman, Montana 59717*

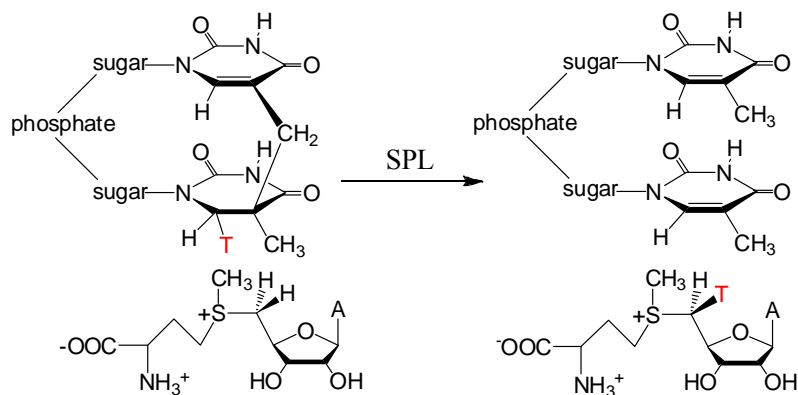
Abstract

Spore photoproduct lyase (SP lyase) catalyzes the repair of 5-thymine-5,6-dihydrothymine, a methylene-bridged thymine dimer which accumulates in UV-irradiated bacterial spores. The kinetic parameters of the repair assay were investigated utilizing pre-reduced SP lyase and resulted in linear repair without a previously observed lag time in the assay. The specific activity was found to increase nearly 4-fold from previously published results to 1.29 $\mu\text{mol}/\text{min}/\text{mg}$. Mechanistic studies were performed to investigate the rate of abstraction of the C-6 H atom from the substrate by the AdoMet cofactor using [C-6- ^3H] SP DNA as the substrate. The results indicate a kinetic isotope effect for the abstraction of a tritium atom of 16.1, demonstrating that C6 H atom abstraction is a rate determining step in the repair reaction. The results of the tritium transfer experiment also suggest the nonstereospecific formation of SP with regards to the C-6 position and the subsequent stereospecific abstraction of the C-6 H atom by SP lyase.

Introduction

Spore photoproduct lyase (SP lyase) catalyzes the repair of 5-thyminy1-5,6-dihydrothymine (spore photoproduct or SP), a methylene-bridged thymine dimer which accumulates in UV-irradiated bacterial spores (Scheme 4.1) [1-3]. The enzyme belongs to the radical SAM superfamily of enzymes which require AdoMet and a $[4\text{Fe-4S}]^{1+/2+}$ cluster to catalyze surprisingly diverse reactions [4-6]. Recent studies have determined the substrate for SP lyase to be the 5*R*-SP [7-9]. While a variety of mechanistic studies have been performed on this enzyme, we still lack detailed information regarding the formation of SP as well as intermediates and kinetic parameters of the key steps during the mechanism.

Scheme 4.1. SP lyase catalyzes the repair of SP. When SP is specifically labeled at the C-6 position, the tritium label is transferred to AdoMet during the repair reaction.



Members of the radical SAM enzyme family are proposed to share a common mechanism to initiate radical catalysis through the one-electron reductive cleavage of AdoMet by a reduced $[4\text{Fe-4S}]^{1+}$ cluster to yield methionine and a 5'-deoxyadenosyl radical intermediate. For the repair of SP, the 5'-deoxyadenosyl radical was suggested to

directly abstract a H atom from the C-6 position of SP (Figure 4.1) [10]. In a subsequent step of the proposed mechanism, the substrate radical undergoes radical-mediated β -scission to cleave the methylene bridge, to generate a product thyminyl radical. The thyminyl radical is then suggested to abstract an H atom from 5'-deoxyadenosine, producing the repaired thymines and reforming the 5'-deoxyadenosyl radical. The regeneration of AdoMet is achieved by the recombination of the 5'-deoxyadenosyl radical intermediate and methionine with the loss of an electron to the iron-sulfur cluster, completing the reaction cycle.

This proposed mechanism is supported by several studies carried out in our laboratory. The abstraction of an H atom from C-6 of SP is supported by a previous study in which SP prepared by irradiating [*C*-6-³H] thymidine pUC18 DNA demonstrates the incorporation of the ³H atom into SAM after repair by SP lyase, but not when SP is prepared from [*methyl*-³H] thymidine pUC18 DNA [11]. The reabstraction of a H atom from 5'-deoxyadenosine by a thymine radical is supported by mechanistic work in our laboratory that utilized [*5'*-³H] AdoMet and demonstrated the transfer of the tritium atom into repaired thymine [12]. Further work in our laboratory provided support for this mechanism in the analysis of AdoMet as a cofactor in the repair of SP [12]. Studies were performed utilizing a catalytic amount of AdoMet with multiple turnovers of SP observed. The lack of formation of 5'-deoxyadenosine (an AdoMet cleavage product) during turnover conditions also provides support for the role of AdoMet as a cofactor during the repair of SP [12].

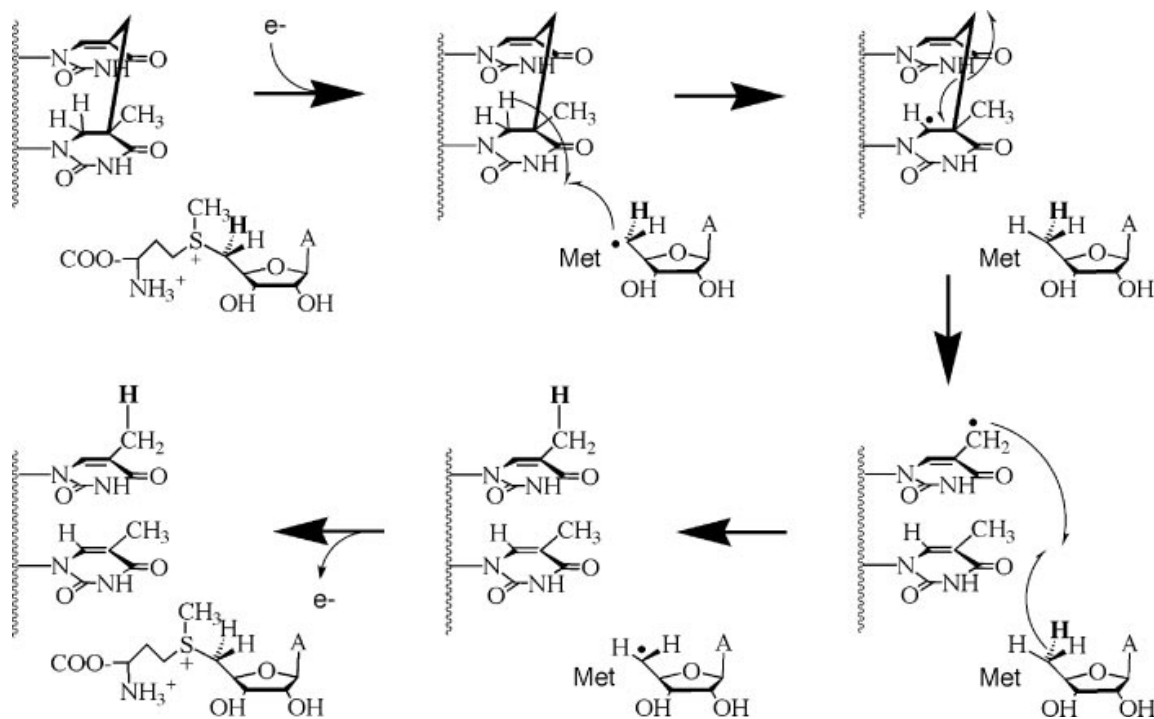


Figure 4.1. Proposed mechanism of SP repair by SP lyase as proposed by Mehl and Begley [10].

In this study, we present kinetic and mechanistic characterizations of SP lyase to provide insights into the formation and repair of SP. We provide here experimental evidence concerning the formation of SP in bacterial spores. Our results suggest that SP formation is non-stereospecific at the C-6 position. It is also suggested that subsequently, SP lyase catalyzes stereospecific H atom abstraction from the C-6 position. With regards to the H atom abstraction from C-6 of SP, we report here a tritium kinetic isotope effect of 16.1, indicating that this is a rate limiting step during the repair reaction. Collectively, these results provide a deeper understanding regarding the formation as well as repair of SP by SP lyase.

Materials and Methods

Materials

All chemicals and other materials were obtained from commercial sources and were of the highest purity commercially available, unless indicated otherwise.

Methods

The *N*-terminal His₆-tagged SP lyase from *Bacillus subtilis* was expressed using *Escherichia coli* Tuner(DE3)pLysS cells transformed with a pET14b expression plasmid, containing the *spIB* gene, and purified anaerobically by Ni-HisTrap HP chromatography and FPLC as previously described [12]. Protein, iron, and sulfide assays were performed as previously described [13-15]. SspC from *B. subtilis* was expressed using *E. coli* Tuner(DE3)pLacI cells transformed with a pETBlue1 expression plasmid containing the *sspc* gene and purified aerobically using an acid extraction and CM-cellulose column and FPLC as previously described [12]. AdoMet was prepared as previously described [16]. SP-containing DNA was prepared as previously described using either [*methyl*-³H] thymidine or [*C*-6-³H] thymidine enriched LB media [12]. SP lyase activity assays were performed as previously described in 20 mM sodium phosphate, 500 mM NaCl, pH 7.0. Assays using pre-reduced SP lyase were carried out as previously described except that SP lyase was reduced under anaerobic conditions by the addition of 10 mM sodium dithionite and 10 mM DTT prior to the addition to the reaction mix [12]. Activity assays of [*methyl*-³H] thymidine SP-DNA were acid hydrolyzed and reaction components separated on a HPLC with a Waters Spherisorb S5P 4.0 x 250 mm analytical column with fractions collected for scintillation counting every min for 25 min as previously described

[12]. Activity assays of [*C*-6-³H] thymidine SP-DNA were quenched and the reaction mixture was filtered through a YM-3 micron centrifugal filtration device. The filtrate was then loaded onto a Waters Spherisorb C18 ODS2 4.6 x 150 mm column and eluted with a step gradient (4 mL H₂O with 0.1% trifluoroacetic acid (TFA), 13 mL 82% H₂O with 0.1% TFA, 18% acetonitrile with 0.1% TFA, 14 mL acetonitrile with 0.1% TFA) while collecting fractions for scintillation counting as previously described [11]. Under these conditions, AdoMet elutes at 2.6 min and 5'dAdo elutes at 7.0 min.

Results

SP Repair Dependence on [4Fe-4S]¹⁺

Previous work in our laboratory demonstrated SP lyase activity using [*methyl*-³H] SP DNA as a substrate. The specific activity for the repair of SP in these assays was observed to be 0.33 μmol/min/mg. The results were suggestive of an increasing activity over the 60 min time course. The apparent “lag” was attributed to the time it took to reduce the [4Fe-4S] cluster to the active [4Fe-4S]¹⁺ state. In this work, we repeated the assay using SP lyase that had been reduced with sodium dithionite prior to adding it into the reaction mixture. Aliquots were taken at 10 min intervals for 60 min, quenched with TFA and the DNA was then hydrolyzed. Reaction components were separated using a HPLC and Waters Spherisorb S5P analytical column and the amount of SP remaining in each fraction was determined using liquid scintillation counting (LSC).

The results of these assays are presented in Figure 4.2. SP elutes around 10.5 min under the given conditions. LSC of this fraction for each aliquot taken during turnover

demonstrates the decreasing peak for SP, with repair complete at 60 min (Figure 4.2A). Repair was linear over the course of 50 min, at which point the substrate was almost completely repaired (Figure 4.2B). The specific activity observed for this assay was $1.29 \pm 0.05 \mu\text{mol}/\text{min}/\text{mg}$, almost 4-fold higher than that observed previously. This observation is not surprising and provides support for the $[\text{4Fe-4S}]^{1+}$ state as the active state of SP lyase.

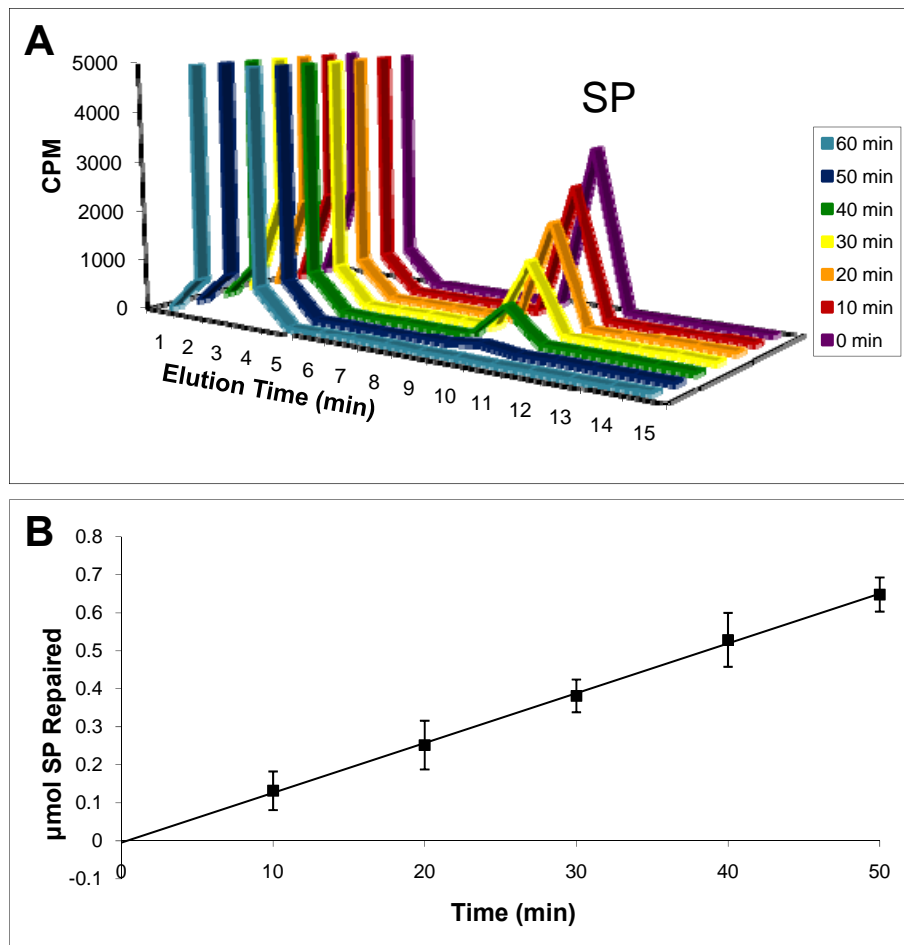


Figure 4.2. SP lyase HPLC-based activity assay showing a decrease in SP (elution time 10.5 min) as the reaction goes to completion (A) and a plot of SP repaired as a function of time (B). SP lyase displays a higher specific activity of $1.3 \mu\text{mol}/\text{min}/\text{mg}$ of SP lyase when pre-reduced to the $[\text{4Fe-4S}]^{1+}$ state.

Transfer of Tritium from SP to SAM

While previous studies demonstrated the transfer of a tritium atom from C-6 of SP to AdoMet during turnover, the overall amount and rate of transfer was not determined [11]. If the amount of tritium is quantified during repair, insight can be gained into the formation of SP as well as mechanistic parameters of the repair of SP. The main objective of these studies was to determine a primary tritium kinetic isotope effect for the C-6 H atom abstraction. For these studies, pUC18 DNA was prepared from medium enriched with [C-6-³H] thymidine. The purified DNA was then subjected to UV irradiation under low hydration conditions in the presence of SspC to produce SP. The repair reaction was performed using sufficient SP lyase in order for the reaction to be complete in 10 minutes, over which time activity has been shown to be linear. Aliquots were taken at 0, 2.5, 5 and 10 minutes, and the amount of tritium incorporated into AdoMet was quantified after separation of reaction components by HPLC (Figure 4.3). AdoMet elutes from the Waters Spherisorb ODS2 column at 3 min under the given conditions. Based on the initial amount of tritium contained in SP, we would expect 15060 CPM of tritium incorporation into SAM after the repair reaction was complete, assuming the stereochemistry of SP formation and repair allows 100% tritium transfer to SAM. At the time point corresponding to 100% turnover, we observe only 5928 CPM transferred to SAM. This corresponds to 79% recovery if at maximum only half the tritium is able to transfer to SAM. Because of the complex techniques involved, it would be expected to lose some of the tritium in the work up of the reaction mixture. Therefore, a yield of 79%

is not unreasonable, and for these experiments we have thus taken 5928 CPM in SAM as representing 100% repair.

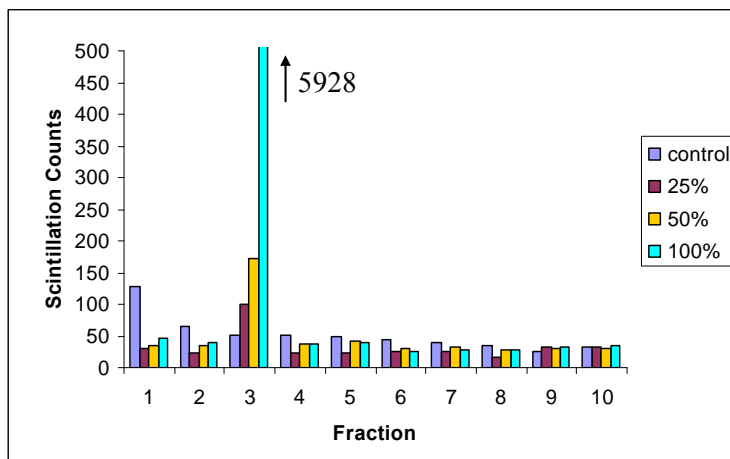


Figure 4.3. Incorporation of ^3H atom into AdoMet after abstraction from C-6 of SP. The bar graph above shows the number of counts present in AdoMet (elution time 3 min) after a repair assay with $[\text{C}-6\text{-}^3\text{H}]$ -thymine SP. Aliquots were taken at 0, 2.5, 5 and 10 minutes. A kinetic isotope effect between 15 and 17.2 can be calculated for tritium during SP repair and H atom abstraction.

Table 4.1. Label transfer from SP C-6 to AdoMet at different reaction time points. The “theoretical” numbers are calculated assuming nonstereospecific SP formation and are scaled to 5928 CPM corresponding to 100% repair.

% SP repaired	Theoretical SAM CPM with KIE = 1.00	Theoretical SAM CPM with KIE = 15.8	Observed SAM CPM	Calculated KIE
0	0	0		N/A
25	1482	94	99	15
50	2964	188	172	17.2
100	5928	5928	5928	N/A

Aliquots taken at 2.5 min and 5 min during the reaction (corresponding to 25% and 50% reaction time points) demonstrate 99 CPM and 172 CPM transferred to AdoMet, respectively. Using the 5928 CPM as our 100% repair, we calculated the expected amount of ^3H transfer into AdoMet for the 2.5 and 5 min reaction time points

using a KIE of 1 and 15.8, the theoretical value for a primary tritium kinetic isotope effect (Table 4.1). The observed transfer of ^3H from SP to AdoMet during the course of the reaction correlates well with the theoretical KIE of 15.8 and clearly indicates a tritium kinetic isotope effect. The calculated tritium isotope effect was determined to be 15 and 17.2 for the respective time points, or 16.1 for the overall reaction.

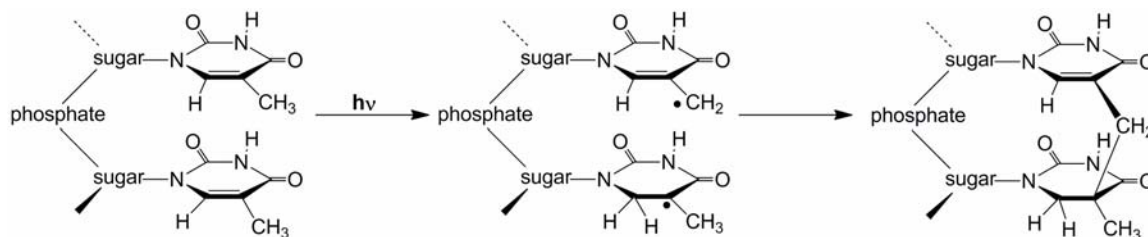
Discussion

In this work, we provide kinetic and mechanistic studies to further investigate the formation and repair of SP by SP lyase. We demonstrate linear repair of SP over the course of 50 min utilizing pre-reduced SP lyase. The observation of linear repair supports the previous suggestion of an apparent lag time in the assay being due to the time it took to reduce the $[\text{4Fe-4S}]$ cluster to the active $[\text{4Fe-4S}]^{1+}$ state. The observed specific activity also increased nearly 4-fold to $1.29 \pm 0.05 \mu\text{mol}/\text{min}/\text{mg}$, suggesting activity is dependent on the amount of enzyme with a fully intact reduced cluster.

To further understand the mechanism of formation as well as repair of the unique SP substrate, we pursued studies to investigate the kinetics and mechanism of the DNA-repair activity for SP lyase. Previous work provided evidence for the direct H atom abstraction from the C-6 position of SP by the putative 5'-deoxyadenosyl radical (Figure 4.1) [11]. However, these studies did not quantify the amount or rate at which ^3H was transferred to AdoMet. If the ^3H transfer is quantified during the course of the reaction, we can explore the possibility of a primary kinetic isotope effect for the H atom abstraction by SP lyase.

By quantifying the final amount of tritium transfer, we can probe the stereospecific parameters of SP formation. When SP is generated (Scheme 4.2), a prochiral center is formed at the C-6 position; it is unknown, however, if this center is formed stereospecifically. It is expected that the abstraction of the C6 H atom by SP lyase is stereospecific as is the case for other radical SAM enzymes including PFL-AE, which stereospecifically abstracts the pro-*S* H atom of Gly 734 [17] and LAM, which stereospecifically abstracts the 3-pro-*R* H atom of α -lysine [18]. In the case of SP lyase, it is unknown which H atom (either the pro-*R* or pro-*S*) is abstracted.

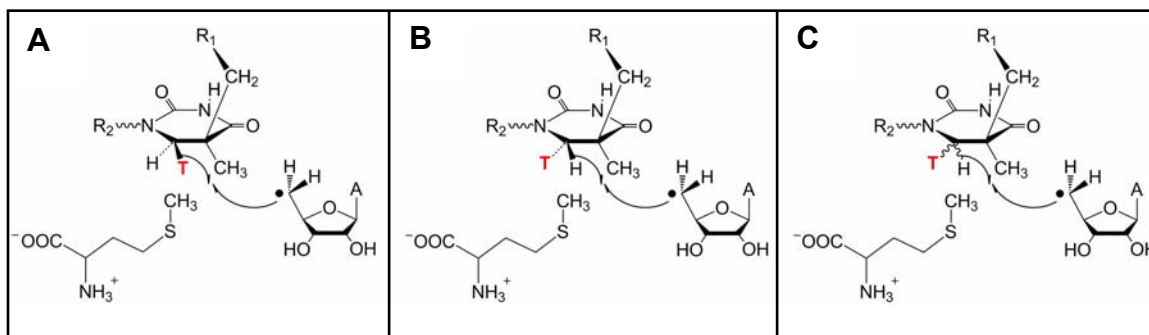
Scheme 4.2. Proposed mechanism of SP formation. Taken from reference [3].



Based on these results, we hypothesize three likely scenarios for the transfer of the C-6 tritium from SP to AdoMet during the course of repair (Scheme 4.3). If SP formation is stereospecific in regards to the H atom at C-6 (meaning the H atom will be specifically added to either the pro-*R* or pro-*S* position) and H atom abstraction is stereospecific during SP repair (either the pro-*R* or pro-*S* H atom is specifically abstracted), it would be expected that either (A) 100% transfer would be observed, or (B) no transfer would be observed. However, if SP formation is nonstereospecific, the ^3H atom would be located in both the pro-*R* and pro-*S* in a racemic mix (C). It would be expected in this case that about half of the tritium label would be incorporated into

AdoMet if H atom abstraction is stereospecific during SP repair. Furthermore, if the H atom abstraction step is rate-limiting, it would be expected that a kinetic isotope effect would be observed during the repair process with SP lyase favoring H atom abstraction over a heavier ^3H atom. Therefore, the incorporation of the ^3H atom into AdoMet from SP was investigated during different reaction time points as well as the overall transfer at the completion of the reaction.

Scheme 4.3. Possibilities for stereospecificity of SP formation and H atom abstraction by SP lyase.



The results demonstrate that about half of the overall available tritium was transferred to AdoMet over a time course that should have allowed 100% repair. This suggests that the formation of SP with regards to the C-6 position is nonstereospecific. As a result, when SP is formed, the original H atom present on thymine is moving to either the pro-*R* or pro-*S* position in a 1:1 ratio. SP lyase is subsequently expected to abstract the H atom stereospecifically and we expect the pro-*S* H atom will be abstracted. Based on modeling of the 5*R*-SPTpT substrate, the H atom in this position is the most accessible (Figure 4.4). The primary KIE of 16.1 is well within the expected range for enzymes catalyzing reactions where the isotopically sensitive step is significantly rate limiting

[19]. Therefore, the observed KIE for the ^3H atom abstraction from C-6 of SP by AdoMet indicates a rate determining step in the mechanism of SP repair by SP lyase.

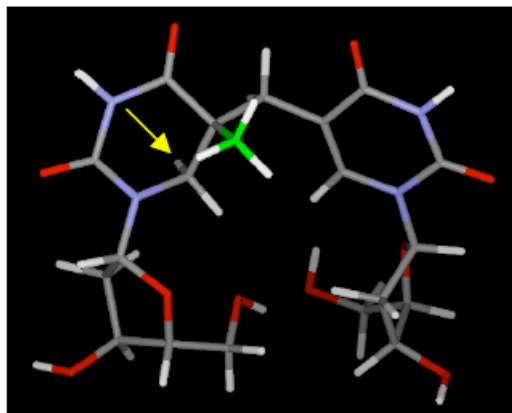


Figure 4.4. 5R-SP with the pro-S C-6 H atom indicated with an arrow.

References

1. Donnellan JE, Jr., Setlow RB (1965) *Science* 149:308-310
2. Donnellan JE, Jr., Stafford RS (1968) *Biophysical Journal* 8:17-28
3. Varghese AJ (1970) *Biochem. Biophys. Res. Commun.* 38:484-490
4. Sofia HJ, Chen G, Hetzler BG, Reyes-Spindola JF, Miller NE (2001) *Nucleic Acids Res.* 29:1097-1106
5. Frey PA, Hegeman AD, Ruzicka FJ (2008) *Crit. Rev. Biochem. Mol. Biol.* 43:63-88
6. Duschene KS, Veneziano SE, Silver SC, Broderick JB (2009) *Curr. Opin. Chem. Biol.* 13:74-83
7. Chandra T, Silver SC, Zilinskas E, Shepard EM, Broderick WE, Broderick JB (2009) *J. Am. Chem. Soc.* 131:2420-2421
8. Silver SC, Chandra T, Zilinskas E, Ghose S, Broderick WE, Broderick JB (2010) *J. Biol. Inorg. Chem.* 15:943-955

9. Mantel C, Chandor A, Gasparutto D, Douki T, Atta M, Fontecave M, Bayle P-A, Mouesca J-M, Bardet M (2008) *J. Am. Chem. Soc.* 130:16978-16984
10. Mehl RA, Begley TP (1999) *Org. Lett.* 1:1065-1066
11. Cheek J, Broderick JB (2002) *J. Am. Chem. Soc.* 124:2860-2861
12. Buis JM, Cheek J, Kalliri E, Broderick JB (2006) *J. Biol. Chem.* 281:25994-26003
13. Bradford M (1976) *Anal. Biochem.* 72:248-254
14. Beinert H (1978) *Methods Enzymol.* 54:435-445
15. Beinert H (1983) *Anal. Biochem.* 131:373-378
16. Walsby CJ, Hong W, Broderick WE, Cheek J, Ortillo D, Broderick JB, Hoffman BM (2002) *J. Am. Chem. Soc.* 124:3143-3151
17. Frey M, Rothe M, Wagner AFV, Knappe J (1994) *J. Biol. Chem.* 269:12432-12437
18. Aberhart DJ, Gould SJ, Lin HJ, Thiruvengadam TK, Weiller BH (1983) *J. Am. Chem. Soc.* 105:5461-5470
19. Marsh EN (1995) *Biochemistry* 34:7542-7547

Contribution of Authors and Co-Authors

Manuscript in Chapter 5

Chapter 5: Combined Mössbauer and Multi-Edge X-Ray Absorption Spectroscopic Study of the Fe-S Cluster in Spore Photoproduct Lyase

Author: Sunshine C. Silver

Contributions: Prepared SP lyase samples for Mössbauer, Fe and S K-edge X-ray absorption spectroscopy. Performed data analysis on S K-edge XAS samples and wrote the manuscript.

Co-author: David J. Gardenghi

Contributions: Aided in data collection and analysis of XAS samples. David also helped in writing the manuscript and data for generating figures.

Co-author: BoiHanh Huynh

Contributions: Collected and analyzed data for Mössbauer spectroscopy as well as generated Figure 1.

Co-author: Robert K. Szilagy

Contributions: Aided in data collection and analysis of XAS samples. Provided critical discussions of results and implications for research presented. Provided feedback on manuscript at all stages of writing.

Co-author: Joan B. Broderick

Contributions: Provided valuable insight and overview of the sample preparation, interpretation of results and preparation of the manuscript.

Manuscript Information Page

Authors: Sunshine C. Silver, David J. Gardenghi, BoiHanh Huynh, Robert K. Szilagy, Joan B. Broderick

Journal: Biochemistry

Status of the manuscript:

- Prepared for submission to a peer-reviewed journal
- Officially submitted to a peer-reviewed journal
- Accepted by a peer-reviewed journal
- Published in a peer-reviewed journal

**Combined Mössbauer and Multi-Edge X-Ray Absorption Spectroscopic Study of
the Fe-S Cluster in Spore Photoproduct Lyase**

Sunshine C. Silver, David J. Gardenghi, BoiHanh Huynh, Robert K. Szilagyi, Joan B. Broderick

*Astrobiology Biogeocatalysis Research Center, Department of Chemistry & Biochemistry
Montana State University, Bozeman, MT 59717 USA*

Abstract

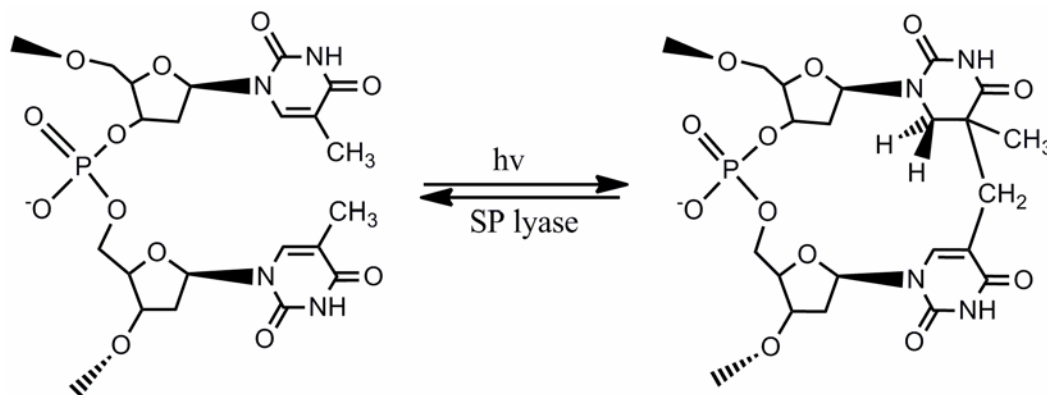
Spore photoproduct lyase (SP lyase) is a member of the radical SAM superfamily and catalyzes the direct reversal of the spore photoproduct (SP, 5-thyminy-5,6-dihydrothymine), a specific DNA photoproduct found in bacterial spores, to two thymines. SP lyase requires *S*-adenosyl-L-methionine (SAM) and a [4Fe-4S]^{1+/2+} cluster for catalysis. In the absence of a crystal structure, much remains unknown regarding the active site of SP lyase. In order to gain a better understanding of the electronic and geometric structures of the [4Fe-4S] cluster we carried out a Mössbauer analysis of anaerobically prepared SP lyase. These results indicate a mixture of cluster states in the anaerobically purified enzyme. Furthermore, iron and sulfur K-edge X-ray absorption spectroscopic measurements were performed to further characterize the [4Fe-4S] cluster as well as study the interaction between the cluster and SAM. The Fe K-edge EXAFS provide evidence for a slight distortion of the cluster upon interacting with SAM as a new Fe...Fe scatterer at 3.0 Å is observed. The Fe K-edge XANES also provide further support that SAM is not undergoing reductive cleavage in the presence of reduced SP lyase. Due to the mixture of Fe-S cluster states the S K-edge results provided only limited insights into the metal-ligand bonding.

Introduction

Members of the radical SAM superfamily require *S*-adenosylmethionine (SAM) and a redox active [4Fe-4S] cluster to carry out diverse radical reactions [1]. This enzyme family is typically found to contain a conserved CX₃CX₂C sequence which ligates three of the iron atoms in the cluster. The fourth iron in the cluster is ligated by the amino and carboxylate groups of the methionine moiety of SAM, which has been demonstrated for a number of these enzymes through spectroscopy as well as X-ray crystallography [2-12]. Members of this superfamily catalyze an extensive variety of radical reactions including the formation of DNA precursors, rearrangement reactions, sulfur-insertion reactions, activation reactions, vitamin and antibiotic biosynthesis reactions and the assembly of complex metallocofactors.

Spore photoproduct lyase (SP lyase), a member of the radical SAM superfamily, catalyzes the direct reversal of a specific DNA photoproduct, the 5-thymine-5,6-dihydrothymine (spore photoproduct or SP), back to two thymines in a SAM-dependent manner (Scheme 5.1) [13-16]. This methylene-bridged thymine dimer results as the primary photoproduct when sporulating bacteria are subjected to UV radiation [17-18]. We have previously demonstrated that SP lyase initiates repair by H atom abstraction from C6 of SP by the 5'-deoxyadenosyl radical [16, 19]. The resulting substrate radical is suggested to initiate radical-mediated β-scission of the C-C bond linking the two thymines resulting in the repaired thymines and reforming SAM in the process [16, 19-20]. More recent work has elucidated the substrate for SP lyase as the enzyme has been observed to stereospecifically repair the 5*R*-SP dinucleoside and dinucleotide [21-23].

Scheme 5.1. SP lyase catalyzes the repair of the spore photoproduct.



Previous work on SP lyase has shown the enzyme to contain a single iron-sulfur cluster [13] which appears to be isolated as a mixture of cluster states [19, 22, 24-25]. While various spectroscopic techniques have been utilized to characterize the cluster in SP lyase, very little work characterizing the interaction between the [4Fe-4S] cluster and SAM has been performed. HYSCORE, a two-dimensional pulsed EPR technique, has previously been utilized to probe the [4Fe-4S]-SAM complex [25]. The results of this study indicate the amino group of SAM is coordinated to the unique Fe of the [4Fe-4S] cluster of SP lyase in a manner similar to other radical SAM enzymes.

The [4Fe-4S] cluster of *C.a.* SP lyase has previously been characterized using UV-visible and EPR spectroscopies. The UV-visible absorbance spectrum of purified SP lyase shows a broad shoulder with a maximum of 413 nm, similar to other members of the radical SAM superfamily [22, 26-27]. The broad feature around 600 nm may indicate the presence of [2Fe-2S] clusters in the enzyme [28]. Upon reduction in the presence of DTT and 5-deazariboflavin, the UV-vis spectral features decrease in intensity resulting in a lower intensity broad peak ~410 nm. These spectra indicate a redox-active Fe-S

cluster, but it is difficult to determine the types and concentrations of the clusters which may be present.

X-band EPR spectroscopy performed at 12K was also utilized to characterize SP lyase [22]. The as-isolated enzyme exhibits an isotropic signal centered at a g value of 1.99 and is characteristic of a $[3\text{Fe-4S}]^{1+}$ cluster. Spin quantification revealed that only about 3-4% of the total iron present is in this state. Upon reduction of SP lyase, the EPR spectrum displays a nearly axial signal with g values of 2.03, 1.93 and 1.92, and is consistent with the presence of a $[4\text{Fe-4S}]^{1+}$ cluster present in the reduced form of the enzyme. Spin quantification indicated that between 32-45 % of the total iron is accounted for in this form, indicating incomplete reduction. Upon the addition of SAM to the reduced enzyme, a similar signal is observed as compared to the reduced enzyme, but with a much lower intensity and broadening of the spectral features. This rhombic signal has g-values of 2.03, 1.92 and 1.82 and is specific for the interaction of SAM with the cluster as similar molecules do not yield equivalent EPR signals in the presence of reduced SP lyase [22].

A general spectroscopic problem in the study of the $[4\text{Fe-4S}]$ cluster of SP lyase interacting with SAM is the presence of various Fe-S clusters in the as-isolated enzyme. This enzyme typically contains a mixture of cluster types, making it difficult to determine the amounts of each type of cluster present. Further complicating this problem is the observed EPR signal of the $[4\text{Fe-4S}]^{1+}$ which broadens and decreases in intensity in the presence of SAM, making ENDOR studies difficult to investigate the interaction of the cluster with SAM. Because of these obstacles and in the absence of a crystal structure, we have been left with a few outstanding questions regarding the active site present in

anaerobically purified SP lyase: What cluster types are present in the as-isolated and reduced forms of this enzyme? Do these cluster states change in the presence of SAM? Is SAM interacting with the cluster in the same manner as previously observed for other members of the radical SAM superfamily? Does the sulfonium atom of SAM interact with the [4Fe-4S] cluster? In order to address these questions and gain a better understanding of the active site of SP lyase, a variety of spectroscopic studies were pursued. Mössbauer studies were performed to identify and quantify the various cluster types that are present in the as-isolated enzyme and reduced enzyme both in the absence and presence of SAM. Fe and S K-edge XAS studies were initiated to further characterize the cluster states as well as the interaction of SAM with the [4Fe-4S] cluster. In this study, we report the first characterization of the [4Fe-4S] cluster in anaerobically purified SP lyase using a combination of Mössbauer and X-ray absorption spectroscopic techniques. Our Mössbauer results indicate SP lyase is isolated with a mixture of [Fe-S] clusters, while our EXAFS results provide evidence for the unique Fe site in SP lyase. Together, these results provide a better understanding of the mechanism for [4Fe-4S] cluster initiated reductive cleavage of SAM.

Materials and Methods

Materials

All chemicals and other materials were obtained from commercial sources and were of the highest purity commercially available, unless indicated otherwise.

Methods

The *N*-terminal His₆-tagged SP lyase from *Clostridium acetobutylicum* (*C.a.*) was expressed using *Escherichia coli* Tuner(DE3)pLysS cells transformed with a pET14b

expression plasmid, containing the *spIB* gene, grown in minimal media and purified anaerobically by Ni-HisTrap HP chromatography and FPLC as previously described [22]. To prepare selenomethionine (SeMet) labeled SP lyase, the *N*-terminal His₆-tagged SP lyase from *C.a.* was expressed using *Escherichia coli* B834(DE3)pLysS cells transformed with a pET14b expression plasmid, containing the *spIB* gene, grown in SeMet media base (Molecular Dimensions/AthenasES) and purified anaerobically by Ni-HisTrap HP chromatography and FPLC as previously described [22]. Following anaerobic dialysis in 20 mM sodium phosphate, 350 mM NaCl, 5% glycerol, pH 7.5, the enzyme was concentrated using an Amicon concentrator fitted with a YM-10 membrane to a final concentration of 0.49 – 0.67 mM. All XAS samples had glycerol added to them in a final concentration of 30%. All protein samples used for spectroscopic analysis were prepared in an MBRAUN glove box maintained at less than 1 ppm O₂ and immediately frozen in liquid N₂. Protein, iron and sulfide assays were performed as previously described [29-31]. SAM was synthesized as previously described [2].

Sample Preparation

Mössbauer Spectroscopy

⁵⁷Fe was purchased from Cambridge Isotope Laboratories, Inc., and dissolved in hot concentrated hydrochloric acid. The pH was adjusted with NaOH. SP lyase as-isolated ⁵⁷Fe samples were prepared from 10 L cultures using the defined minimal medium previously described with ⁵⁷Fe substituted at the same molar concentrations for ⁵⁶Fe. ⁵⁷Fe (191 μM) was also added at induction with IPTG. SP lyase was anaerobically purified, dialyzed and concentrated as described above. Reduced samples were prepared by adding 5 mM DTT, 50 mM tris(hydroxymethyl) aminomethane, 100 μM 5-deazariboflavin and

illuminating the sample with a 300 W halogen lamp for 1 hr in an EPR tube placed in an ice-water bath. SAM was added to appropriate samples at a final concentration of 3 mM as a final step in preparation. Protein samples (640 μ M) were loaded into 450 μ L cups and immediately stored under liquid nitrogen. Mössbauer spectra were recorded on a Mössbauer spectrometer equipped with a Janis 8DT variable temperature cryostat and operated at a constant acceleration mode in transmission geometry. The zero velocity refers to the centroid of a room-temperature spectrum of a metallic iron foil. Analysis of the spectra was performed with WMOSS (WEB Research).

X-ray Absorption Spectroscopy

Iron K-edge XAS samples were prepared in two different ways. The samples were first prepared using SP lyase protein (0.59 mM) expressed in Tuner(DE3)pLysS *E. coli* cells as described above. As-isolated samples were prepared from the anaerobically purified/dialyzed enzyme in the absence and presence of SAM (3 mM). Reduced samples were prepared by the method described above and SAM (3 mM) was added to the photoreduced enzyme as a final step in preparation. A second set of samples were prepared for Fe K-edge XAS as duplicates of the S K-edge XAS SeMet SP lyase (0.67 mM) and reduced by the addition of methyl viologen (3 mM) and SAM (3 mM) was added to appropriate samples. After each sample was prepared, \sim 100 μ L was loaded into a XAS cell (Delrin) sealed with thin iron-free Kapton tape and frozen in liquid N₂.

Sulfur K-edge XAS samples were prepared on two separate occasions using SeMet labeled SP lyase (0.49 or 0.67 mM). Reduced samples were prepared by the addition of methyl viologen (3 mM) and SAM (3 mM) was added to appropriate samples. After each

sample was prepared, ~100 μL was loaded into a XAS cell (Delrin) sealed with thin iron-free Kapton tape and frozen in liquid N_2 .

X-ray Absorption Spectroscopy Data Collection and Analysis

The X-ray Absorption measurements were collected at Stanford Synchrotron Radiation Lightsource (SSRL) under storage ring (SPEAR3) condition of 3 GeV and current of 80-100 mA. The iron K-edge XANES and EXAFS were collected on the unfocused a 20-pole, 2 T Wiggler beam line 7-3 (BL7-3) equipped with a Si(220) downward reflecting, double-crystal monochromator. A 30-element Ge solid-state detector windowed at the Fe- $\text{K}\alpha$ signal was used to collect data as fluorescence excitation spectra. The energy was calibrated using the first peak of the first derivative of an iron foil assigned to 7111.2 eV. During the measurement, the sample was placed in a liquid helium cryostat and maintained at a constant temperature of ~10 K. The beam line parameters were optimized at 8000 eV.

The sulfur K-edge XAS were collected on BL6-2. The measurements utilized the 54-pole wiggler beamline 6-2 operating in high field mode of 10 kG with a Ni-coated harmonic rejection mirror and a fully tuned Si(111) crystal monochromator. The energy was calibrated using the first peak of thiosulfate assigned to 2472.02 eV. During the measurement, the sample was placed in a liquid helium flow and maintained at a constant temperature of ~100 K. Details of the beamline optimization for S K-edge XAS studies have been published elsewhere [32].

The data is averages of at least five scans before background subtraction and normalization. Background correction and normalization of Fe and S K-edge XANES

was performed using ADRP (Automated Data Reduction Protocol), a program written in EXCEL by D.J. Gardenghi. The background removal for EXAFS was performed using and AUTOBK algorithm [33], implemented with ATHENA [34] as the graphical interface. FEFFIT [35] and FEFF 8.4 [36], implemented with ARTEMIS [34], were used to refine and model the EXAFS, respectively. The structural model used in calculation of amplitude and phase information was derived from combination of average Fe...Fe and Fe-S distances of reduced and oxidized [4Fe-4S] model compounds [34]. A non-linear least-squares minimization is used to vary the model and optimize the calculated fit to the observed EXAFS [35]. Due to FeS₄, [2Fe-2S], and [4Fe-4S] clusters presence in the samples which leads to various reasonable fits [defined as $R(\text{fit}) < 15\%$], the fits were constrained based upon corresponding Mössbauer data.

Results and Analysis

Mössbauer Spectroscopic Characterization of Anaerobic SP Lyase

The Mössbauer spectra of the ⁵⁷Fe enriched anaerobically purified SP lyase was analyzed for four states of the enzyme. The as-isolated (**A**), as-isolated with SAM (**B**), reduced (**C**) and reduced with SAM (**D**) are presented in Figure 5.1. The spectra were collected at 4.2 K in a magnetic field of 50 mT applied parallel to the γ radiation. Analysis of the data indicates that all four spectra are composed of mixture of cluster states. The as-isolated enzyme in the absence (**A**) and presence (**B**) of SAM are nearly the same and are comprised of three subspectral components. The presence of SAM did not seem to affect the composition and oxidation state of the cluster. The central quadrupole doublet (red line) was simulated as a superposition of two equal-intensity quadrupole

doublets and accounts for 40% of the total absorption. The parameters obtained [$\Delta E_Q(1) = 0.75$ mm/s, $\delta(1) = 0.27$ mm/s, and line width(1) = 0.27mm/s; $\Delta E_Q(2) = 0.46$ mm/s, $\delta(2) = 0.27$ mm/s, and line width(2) = 0.27mm/s] are typical of a $[2\text{Fe-2S}]^{2+}$ cluster. A smaller percentage (15%) was attributed to a $[4\text{Fe-4S}]^{2+}$ cluster (blue line) and was simulated as a superposition of two equal-intensity quadrupole doublets [$\Delta E_Q(1) = 1.00$ mm/s, $\delta(1) = 0.47$ mm/s, and line width(1) = 0.31mm/s; $\Delta E_Q(2) = 1.20$ mm/s, $\delta(2) = 0.48$ mm/s, and line width(2) = 0.32mm/s]. The remaining Fe species (45% of total absorption in **A** and **B**) were unresolved broad ferric species to which the composite simulation could not be obtained. This could be due to adventitious Fe binding to the N-terminal His₆ tag on SP lyase that is utilized for purification.

The reduced enzyme in the absence (**C**) and presence (**D**) of SAM were comprised of several subspectral components. The *solid black line* in the spectra **C** and **D** are the composite spectra including the simulated spectrum of a $[4\text{Fe-4S}]^{1+}$ cluster (*cyan line*: plotted at 60% of total Fe absorption in **C** and 45% in **D**), and the simulated spectrum of free Fe^{2+} (*green lines*: 10% contributed by ionic Fe^{2+} , 15% contributed by rubredoxin FeS_4 -type for **C** and 13% contributed by ionic Fe^{2+} , 12% contributed by rubredoxin FeS_4 -type for **D**) and Fe^{3+} (*orange line*: 15% of total Fe absorption for **C** and 25% of total Fe absorption for **D**). The $S=1/2$ $[4\text{Fe-4S}]^{1+}$ cluster was simulated using parameters from a Mössbauer study of the four-iron ferredoxin from *Bacillus stearothermophilus* [37]. The Fe^{2+} component was simulated using the following parameters, $\Delta E_Q = 2.92$ mm/s, $\delta = 1.32$ mm/s, for ionic Fe^{2+} and $\Delta E_Q = 3.26$ mm/s, $\delta = 0.72$ mm/s, for rubredoxin FeS_4 -type. The spectrum of the fast relaxing Fe^{3+} (*orange line*)

was simulated with a quadrupole doublet [$\Delta E_Q = 1.09$ mm/s, $\delta = 0.59$ mm/s, and a symmetric line width of 0.58 mm/s].

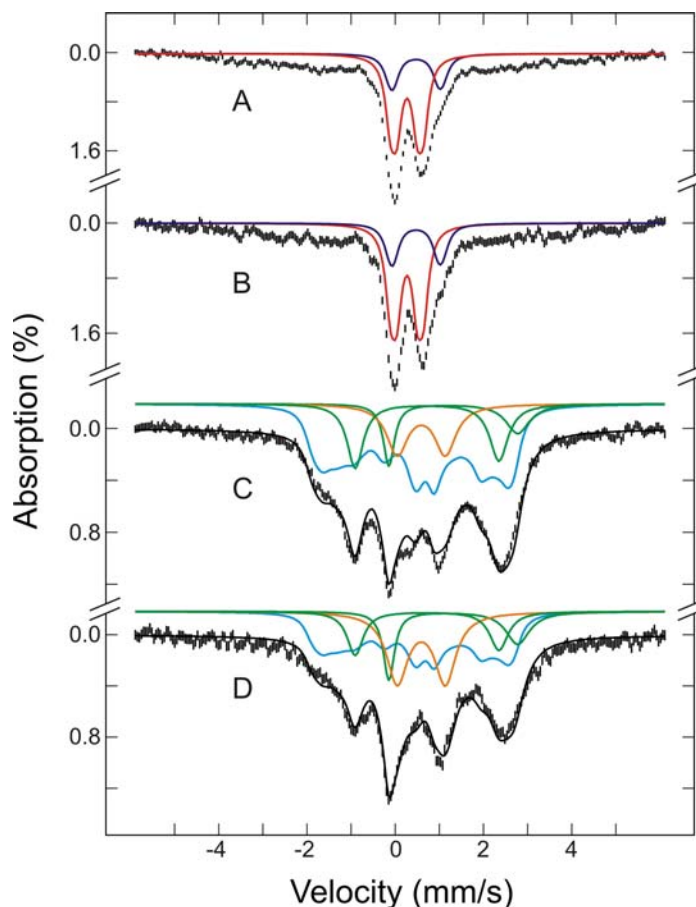


Figure 5.1. Mössbauer spectra of SP lyase as-isolated (**A**), after the addition of 3 mM SAM to as-isolated sample (**B**), reduced with 5-deazariboflavin in the presence of 5 mM DTT (**C**) and after the addition of 3 mM SAM to the reduced sample (**D**). The spectra (hatched marks) were recorded at 4.2 K in a magnetic field of 50 mT applied parallel to the γ radiation. The solid lines plotted above the data are simulated spectra for the $[2\text{Fe}-2\text{S}]^{2+}$ clusters (red), $[4\text{Fe}-4\text{S}]^{2+}$ clusters (blue), $[4\text{Fe}-4\text{S}]^{1+}$ clusters (cyan), mononuclear Fe^{2+} (green) and fast relaxing Fe^{3+} (orange). The black lines overlaid with the experimental spectra are composite spectra. Parameters used for the simulations are given in the text.

Anaerobically purified SP lyase is found to contain iron (between 2.3 and 3.1 ± 0.2) and acid-labile sulfide (between 2.4 and 3.6 ± 0.2) with content dependent upon preparation and determined per protein monomer. Since SP lyase requires a $[4\text{Fe}-4\text{S}]$

cluster for catalysis, the iron and sulfide numbers indicate that not all of the enzyme contains a fully assembled [4Fe-4S] cluster. Previous EPR and UV-vis studies indicate the presence of [Fe-S] clusters, but do not elucidate the types of clusters present. Here, the Mössbauer data demonstrates a mixture of cluster states present in the anaerobically prepared SP lyase. Table 5.1 illustrates the speciation of cluster types as determined by Mössbauer spectroscopy for the anaerobically prepared SP lyase. The incomplete cluster formation for SP lyase may be due to the procedures utilized to isolate pure enzyme and may not have any physiological implications.

Table 5.1. Percentage of total iron present in the iron-sulfur cluster of SP lyase determined by Mössbauer spectroscopy.

	[2Fe-2S] ²⁺	[4Fe-4S] ²⁺	[4Fe-4S] ¹⁺	Fe ²⁺ ^a	Fe ³⁺
(A) As-isolated	40%	15%			45%
(B) As-isolated + SAM	40%	15%			45%
(C) Reduced			60%	25%	15%
(D) Reduced + SAM			45%	25%	25%

^a: Free Fe²⁺ with contributions from ionic Fe²⁺ and rubredoxin FeS₄-type.

X-ray Absorption Spectroscopic Characterization of Anaerobic SP Lyase

Iron K-edge EXAFS

Samples of SP lyase (0.59 mM) were prepared as described above with photoreduction to produce the reduced SP lyase. A second set of samples were prepared utilizing SeMet labeled SP lyase (0.67 mM) with methyl viologen as the reductant in the reduced samples. This second sample set was prepared to perform Fe and S K-edge XAS on duplicate samples of SP lyase. Data collection at the SSRL BL 7-3 was performed on both sample sets with data collection performed at different times. The K-edge spectrum was reproducible for the independent protein samples.

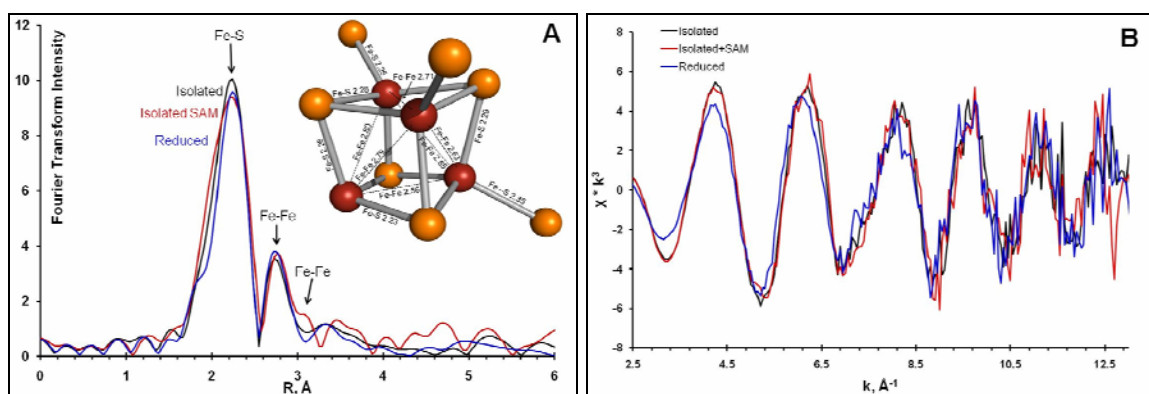


Figure 5.2. Fe K-edge EXAFS of as-isolated, as-isolated in the presence of SAM and reduced SP lyase. (A) FT of the EXAFS spectra shown in (B). (A) *Inset*: The [4Fe-4S] cluster of MoaA (PDB code: 1TV7).

The results of EXAFS analysis for the Fe K-edge spectra of the anaerobically purified SP lyase for three states of the enzyme are presented in Figure 5.2. Each Fourier transforms (FT) of Fe EXAFS data in panel B of Figure 5.2 shows two major peaks between ~ 1.5 Å and ~ 3.2 Å, suggesting at least two Fe-backscatter shells. The major peak at 2.25 Å for each protein sample is indicative of Fe-S scattering path. The as-isolated and reduced samples each show a major peak with a maximum intensity at 2.7 Å indicative of a Fe...Fe scattering path. The as-isolated SP lyase in the presence of SAM has a slightly longer Fe...Fe distance of ~ 2.74 Å. This sample also shows a shoulder on the Fe...Fe peak at ~ 3.0 Å. Modeling of the latter feature (Figure 5.3) suggests that this arises due to longer Fe...Fe scattering path in the cluster as the best fit was obtained with a Fe backscatter (Figures 5.3 B and C). This feature is only observed in the presence of SAM and only for the more concentrated sample. Interestingly, modeling of this feature with a sulfonium ion demonstrates the sulfonium would be out of phase with the data (Figure 5.3 C).

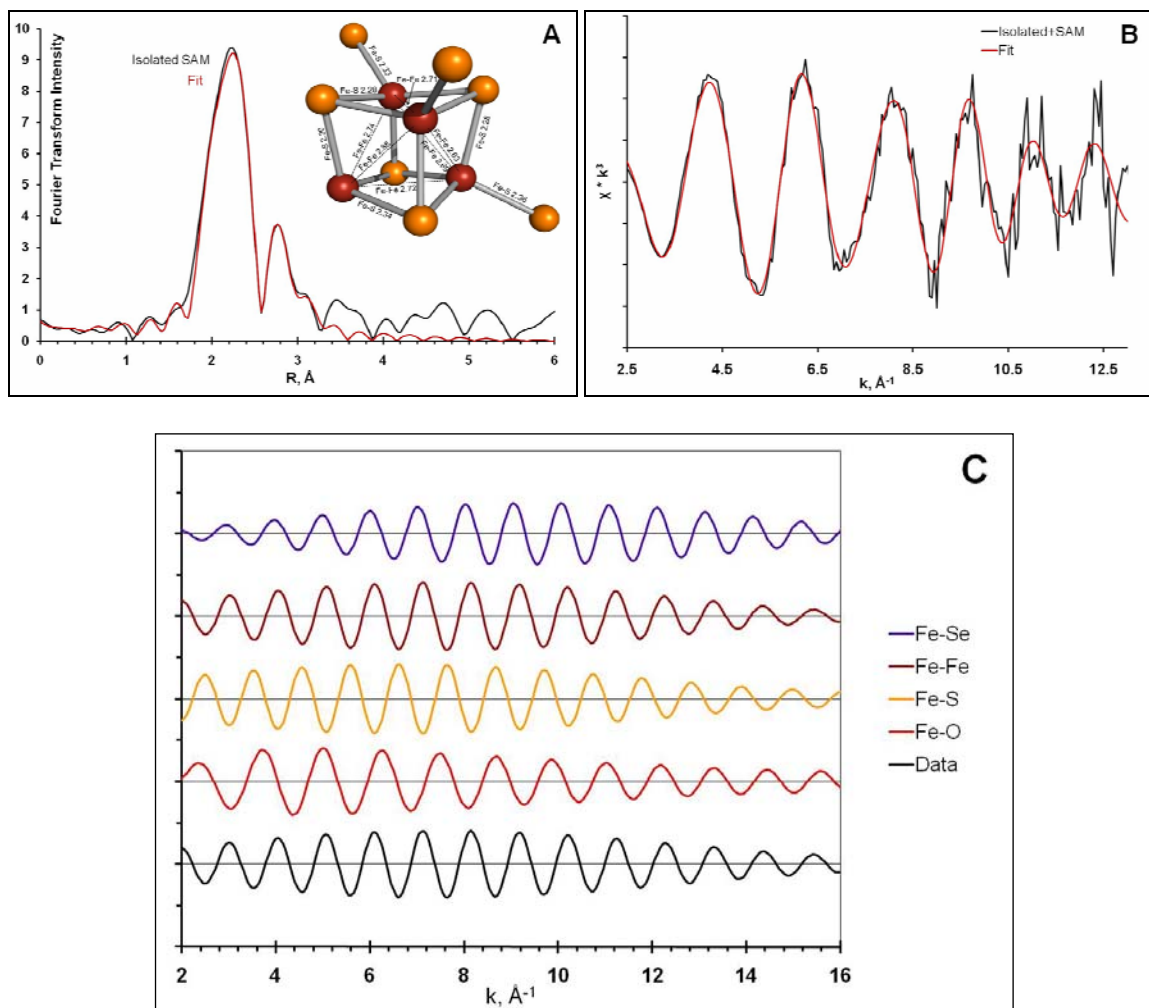


Figure 5.3. Fe K-edge EXAFS of as-isolated SP lyase in the presence of SAM. (B) FT of the EXAFS spectra shown in (A) with the data shown in black and the fit in red. (C) Data shown is the backtransformation of R 2.9-3.3 of FT shown in (A) with models of scattering paths. (A) *Inset:* The [4Fe-4S] cluster of MoaA ligated by SAM (PDB code: 1TV8).

The Mössbauer results demonstrate a mixture of cluster states present in SP lyase as well as unresolved iron species for which a simulation could not be obtained. While we initially suggested the observation of free iron could be due to adventitious iron binding to the N-His₆ tag present on SP lyase, Fe...N scatterers were not observed in the EXAFS spectra. These scatterers must be present if there is adventitious iron binding to

the His₆ tag. While the EXAFS results indicate the absence of free iron binding to the His₆ tag, the Fe...N scatterers, if present, may be unresolvable.

Iron K-edge XANES

The Fe K-edge XANES for as-isolated and reduced SP lyase in the absence and presence of SAM are presented in Figure 5.4. Also presented are the XANES for FeCl₂, FeCl₃, FeF₂ and FeF₃ to demonstrate the shift in energy between the different oxidation states of iron. The reduced Fe²⁺ shows a distinct difference in the rising edge energy position than the oxidized Fe³⁺ for all samples shown.

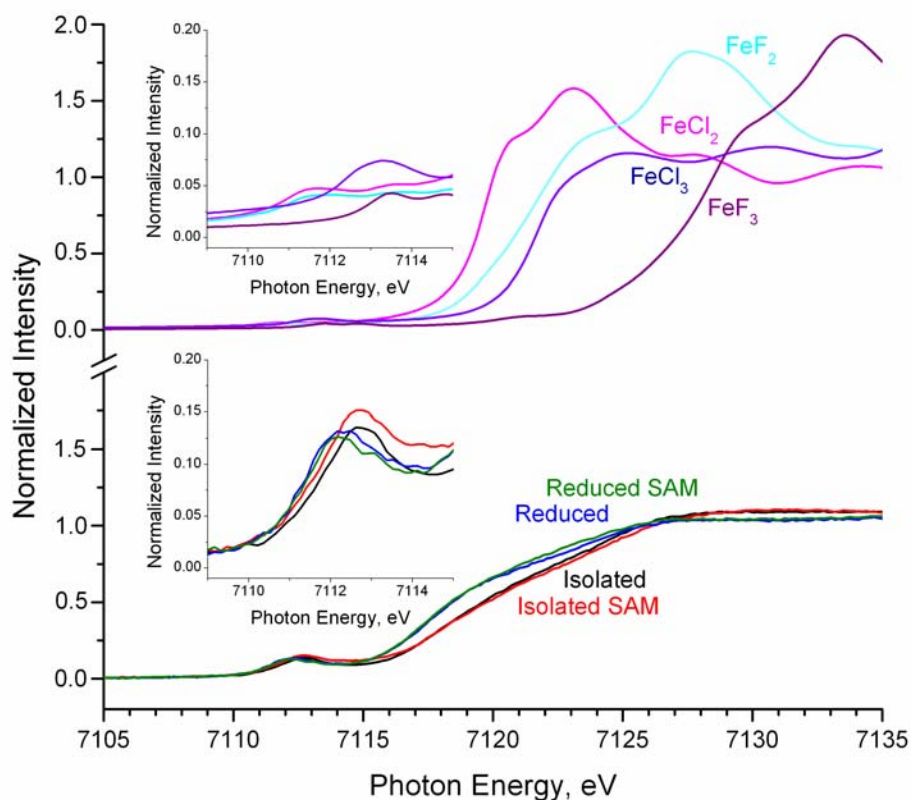


Figure 5.4. Normalized iron K-edge XANES of FeCl₂, FeCl₃, FeF₂ and FeF₃ (top) and as-isolated and reduced SP lyase in the absence and presence of SAM. Samples were prepared using 0.59 mM *C.a.* SP lyase. SAM was added to a final concentration of 3 mM.

The K-edge is a result of the $1s \rightarrow np$ transition, and therefore, it is very sensitive to the small change in the Z_{eff} . As the formal oxidation and ligand environment change, the energy position of the edge changes due to the change in Z_{eff} of the iron centers. Figure 5.4 summarizes some well-defined reference spectra of iron fluoride and chloride minerals. As the oxidation state goes from a formally $2+$ to $3+$, the edge position shift ~ 3 eV and ~ 5 eV higher for the chloride and fluoride minerals, respectively. Thus, as the formal oxidation of the iron increases, the ionization energy of the core electron increase cause a shift of the edge to a higher energy position. Changes in ligand environment can be also observed. Going from chloride to fluoride ligands, the energy position shifts ~ 2 eV and ~ 4 eV higher indicating a change in electron donation for the formally Fe(II) and Fe(III), respectively. Therefore, the oxidation of the SP lyase shows a shift ~ 1.2 eV higher going from the formally $[4\text{Fe-4S}]^{1+}$ to $[4\text{Fe-4S}]^{2+}$. The smaller shift in energy position is result of the charge being spread over four irons and sulfur being a better electron donor. While these energy differences are practically at the resolution limit of Fe K-edge XAS data, the change in spectral features of the pre-edge is indicative of minor electronic structure perturbation upon SAM binding.

The pre-edge features are a result of the $1s \rightarrow 3d$ quadrupole allowed transitions that gains intensity upon $3d-4p$ mixing due to the non-centrosymmetric coordination environment [38-39]. The reference minerals are all octahedral and no $3d-4p$ mixing occur. Thus, the pre-edge intensity is due only to the $1s \rightarrow 3d$ quadrupole allowed transitions [38]. Thus, the higher intensity of the pre-edge features of SP lyase is a result of the $3d-4p$ mixing that corresponds with the tetrahedral environment of the iron centers.

The intensity of the pre-edge feature is essentially the same for all spectra, except the as-isolated in the presence of SAM which increases slightly in intensity. This suggests a less symmetric overall Fe coordination, which is consistent with the presence of a unique Fe site in a 3:1 site-differentiated cluster.

Sulfur K-edge XAS

The sulfur XANES of free ligands are presented in Figure 5.5. The sulfur K-edge spectra of Na₂S, NaSH, and NaSET compounds are shown in Figure 5.5 A. The rising-edge region shows a shift in the edge position to higher energies in the order of sodium sulfide, sodium hydrosulfide, and thiolate. Previous work has demonstrated the positive energy shift, due to increased energy differences between the sulfur 1s and 4p orbitals, directly indicates an increase in the sulfur effective nuclear (Z_{eff}) charge in the same order [40].

The sulfur K-edge spectra of thiolate, cysteine, and methionine are shown in Figure 5.5 B. Cysteine and methionine show similar spectral features as well as similar rising edge energies. Both cysteine and methionine show higher Z_{eff} as compared to thiolate, with cysteine demonstrating a slightly higher Z_{eff} than methionine. These energy changes are in agreement with expected differences inductive effects of a proton vs. an alkyl group. The sulfur K-edge spectra of cysteine and SAM are demonstrated in Figure 5.5 C. SAM displays a characteristic high intensity spectrum due to the presence of three unoccupied C→S σ^* orbitals. The shift of the rising edge feature to higher energy is due to the higher Z_{eff} of the sulfonium ion.

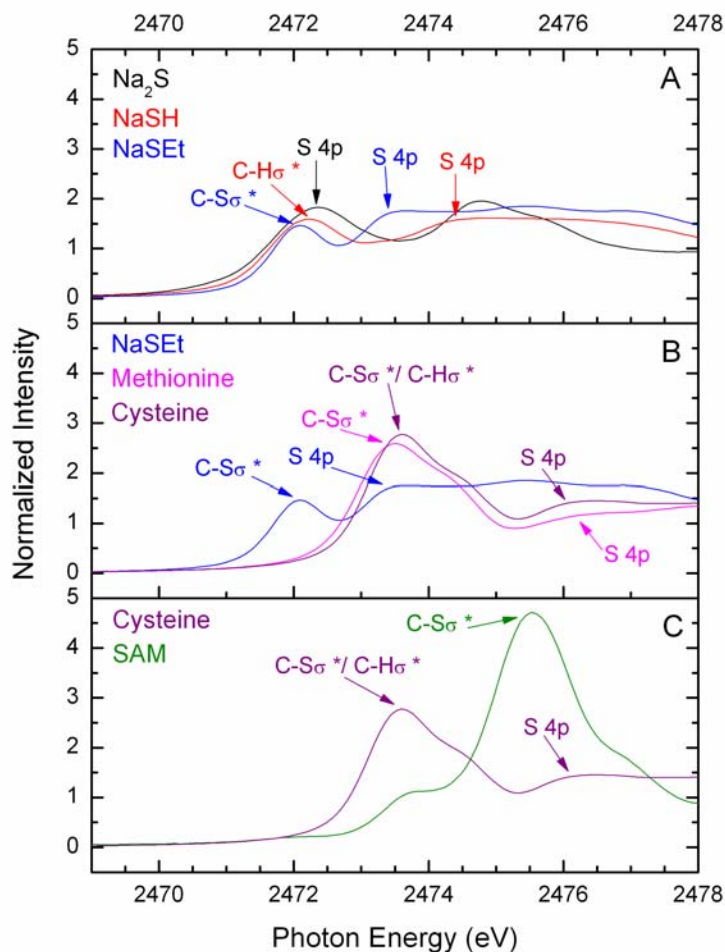


Figure 5.5. Sulfur K-edge XANES of free S-ligands (A) Na₂S, NaSH, NaSEt; (B) NaSEt, methionine, cysteine; (C) cysteine and SAM.

The sulfur K-edge XANES for as-isolated and reduced SP lyase in the absence and presence of SAM are presented in Figure 5.6. The samples were carefully prepared so as to remove all exogenous sulfur atoms. SP lyase was prepared by overexpressing SP lyase in B834(DE3)pLysS *E. coli* cells and grown in SeMet media to remove the contribution of 11 methionine sulfurs to the protein sulfur K-edge spectra. SP lyase contains four Cys residues, three of which ligate the [4Fe-4S] cluster. SP lyase was

purified and dialyzed in buffer lacking sulfur atoms and reduced samples were prepared in the absence of DTT and dithionite.

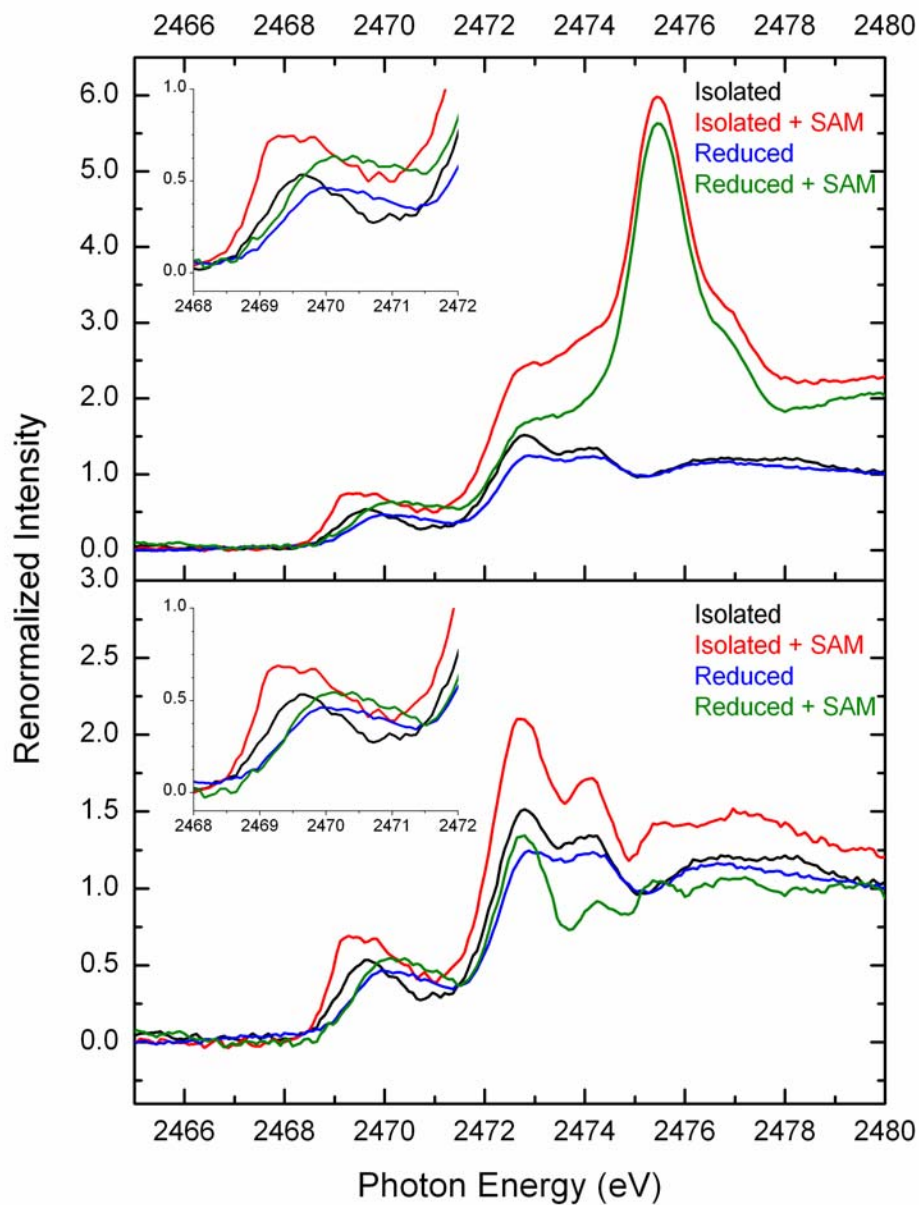


Figure 5.6. Renormalized S K-edge XANES of as-isolated and reduced SP lyase in the absence and presence of SAM (top panel). The renormalized spectra with SAM subtracted is presented in the lower panel. Samples were prepared using 0.49 mM *C.a.* SP lyase and SAM was added to a final concentration of 3 mM. In the lower panel, samples with SAM added have had the free ligand of SAM subtracted.

The total intensity of the pre-edge feature arises from transitions from the ligand 1s core level to the unoccupied metal d-orbitals that covalently mixed with the ligand p-orbitals. Contributing to this intensity for the sample of SP lyase are transitions from the three thiolates and the four sulfides. SP lyase utilized for these experiments was determined to contain $2.3 (\pm 0.2)$ Fe and $2.4 (\pm 0.2)$ labile S^{2-} per protein. Due to the mixed cluster states found in SP lyase pre-edge peaks for sulfide and thiolate contributions are not well resolved. Instead, these features are observed as broad envelope of features between 2468 and 2472 eV. Despite these limitations we attempted to provide a reasonable fit to the spectra (Figure 5.7). The as-isolated sample of SP lyase displays a pre-edge feature at ~ 2469.7 eV and the rising edge feature at ~ 2472.3 eV. The energies of the pre-edge features are presented in Table 5.2.

The addition of SAM to the as-isolated sample results in a spectrum with greater intensity and a pre-edge feature that appears to be shifted to lower energy. However, this spectrum appears to have another feature present in the lower energy side of the pre-edge feature. Oxidation of ferredoxin II has previously been observed to increase the S K-edge spectrum as compared to the reduced enzyme [41]. The observation of increased intensity in our spectrum may not be all that unexpected, however this observation is currently under investigation. It does seem that the addition of SAM may stabilize the [Fe-S] cluster present in SP lyase by providing a ligand to the unique Fe in the cluster. However, the Mössbauer results do not demonstrate the increased formation of [4Fe-4S] clusters in the as-isolated sample after the addition of SAM. Therefore, the presence of SAM would be unlikely to promote the formation of [4Fe-4S] clusters in SP lyase.

Reducing SP lyase unexpectedly results in a shift of the spectral features to higher energy. As demonstrated by the Mössbauer analysis, reducing SP lyase results in the conversion of [2Fe-2S] clusters to [4Fe-4S] clusters as has been previously demonstrated for other radical SAM enzymes [42-53]. The observation of the shift to higher energy for the pre-edge features of the reduced SP lyase samples may be due to the change in the cluster state of the enzyme. The addition of SAM to the reduced sample does not change the spectral features drastically. While the pre-edge features appear to be at similar peak energies, the addition of SAM appears to increase the intensity of the pre-edge feature implying an increase in the covalency of the iron-sulfur bonds. The addition of SAM to the as-isolated sample appears to have a similar effect.

Table 5.2. Pre-edge peak energies (eV), linewidths (eV) presented as full width half maximum (FWHM), amplitudes, and areas (eV) obtained from fits of the renormalized S K-edge XAS pre-edge features of SP lyase.

	S ²⁻	FWHM			RS ⁻	FWHM		
	Energy	Linewidth	Amplitude	Area	Energy	Linewidth	Amplitude	Area
As-isolated	2469.7	1.24	0.48	0.76	2471.0	1.24	0.16	0.26
As-isolated + SAM	2469.5	1.22	0.67	1.03	2470.8	1.22	0.31	0.49
Reduced	2469.9	1.32	0.37	0.62	2470.9	1.32	0.24	0.40
Reduced + SAM	2469.9	1.24	0.47	0.74	2471.0	1.24	0.36	0.56
SAM Subtracted Spectra								
As-isolated + SAM	2469.5	1.15	0.64	0.94	2470.7	1.15	0.32	0.46
Reduced + SAM	2470.0	1.25	.47	0.75	2471.0	1.25	.35	.55

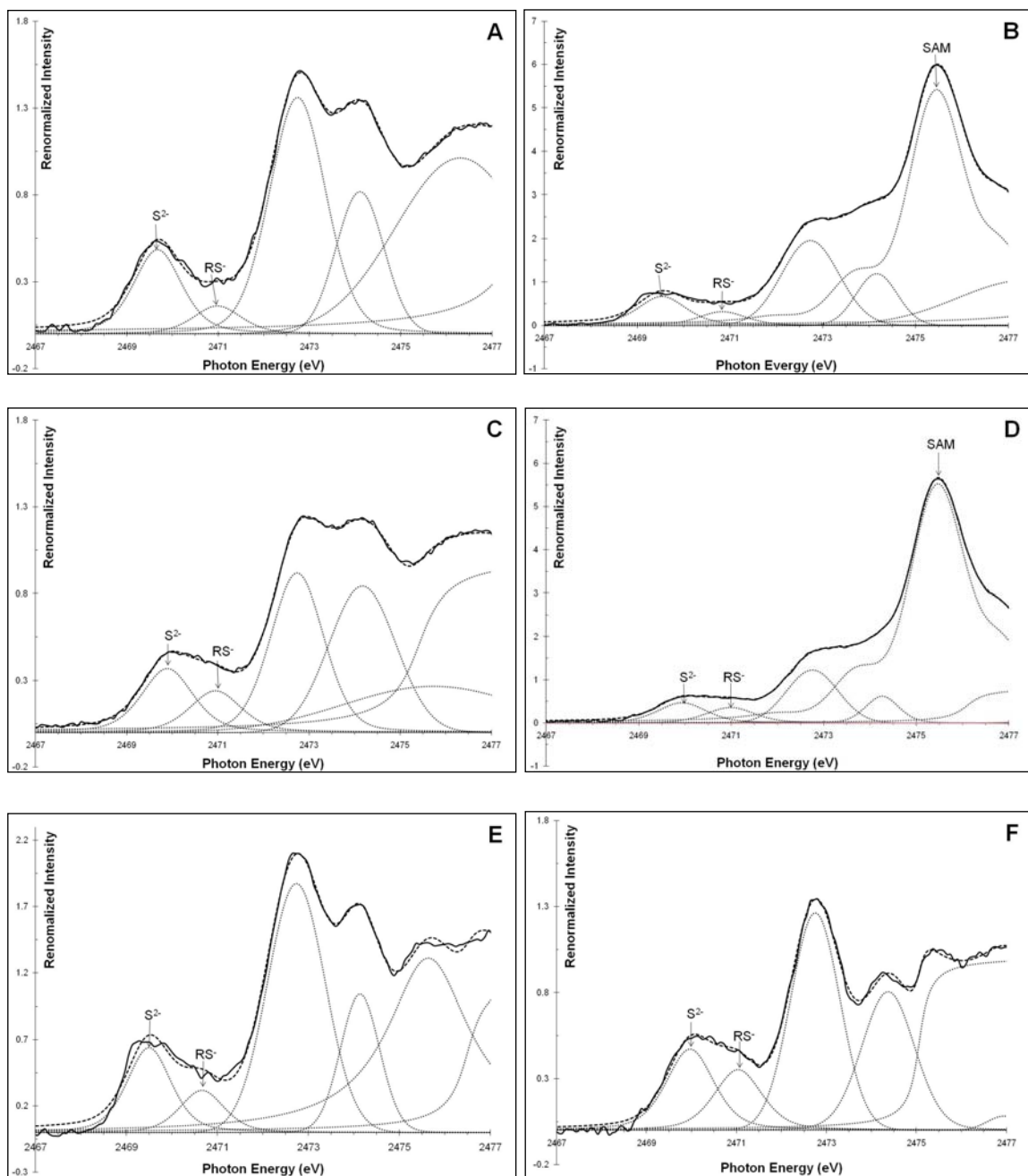


Figure 5.7. Fits of the S K-edge spectra of the as-isolated SP lyase (A), as-isolated SP lyase in the presence of 3 mM SAM (B), reduced SP lyase (C), and reduced SP lyase in the presence of 3 mM SAM (D). Fits of the S K-edge spectra of SP lyase with the free ligand of SAM subtracted from the spectra for as-isolated SP lyase in the presence of 3 mM SAM (E) and reduced SP lyase in the presence of 3 mM SAM (F). The pre-edge region of the S K-edge spectra of SP lyase: data (—), fit (---), and components of the fit (···). Note that the energy scale of (A) and (C) are different from that of (B), (D), (E) and (F).

The energies of pre-edge features of SP lyase as determined from fitting the renormalized data are displayed in Table 5.2 and are similar to those of other [Fe-S] clusters. The fits are based on two peaks in the pre-edge region, one peak for the sulfide and one peak for the thiolate. The pre-edge energies of the as-isolated samples are similar in values for the S^{2-} contribution of the model complex $[Fe_2S_2Cl_4]^{2-}$, which has a pre-edge feature at 2469.5 eV [41], the [2Fe-2S] rieske protein, which has an average pre-edge S^{2-} feature at 2469.6 eV [54], and the oxidized [2Fe-2S] ferredoxin I which has a pre-edge sulfide peak at 2469.8 eV [55]. This observation suggests a prevalence of $[Fe_2S_2]$ clusters as indicated by the Mössbauer analysis. The pre-edge energies of the reduced samples are similar in values for the $[4Fe-4S]^{2+}$ of ferredoxin, which has a S^{2-} pre-edge feature at 2469.9 eV and RS^- pre-edge feature at 2470.8 eV [56]. The ratio of the peak intensities for S^{2-} and RS^- of the as-isolated sample (3.0) is higher than that of the [2Fe-2S] ferredoxin I of 2.67 [55]. The $S^{2-}:RS^-$ intensity ratio for the reduced sample of 1.53 is lower than that observed for the [4Fe-4S] ferredoxin of 1.85 [56] and may be due to the mixed cluster states observed for SP lyase.

Discussion

In the absence of a crystal structure and despite the general structural knowledge of SAM chemistry, the interaction of SP lyase with its cofactor SAM remains to be elucidated. While previous studies have provided an initial characterization of the [4Fe-4S] cluster present in this enzyme, we provide here a more thorough investigation of the strictly anaerobic isolation of the enzyme using a combination of spectroscopic techniques. Mössbauer spectroscopy is a powerful tool to determine cluster states of [Fe-

S] proteins, especially those states which are inaccessible by EPR spectroscopy. In addition, iron and sulfur XAS studies provide complementary information regarding the geometric and electronic structure of the [Fe-S] cluster.

Anaerobically prepared SP lyase is isolated with iron (between 2.3 and 3.1 ± 0.2) and acid-labile sulfide (between 2.4 and 3.6 ± 0.2) with content dependent upon preparation and determined per protein monomer. The observation that SP lyase is isolated with less than four iron and sulfide atoms per monomer indicates the enzyme does not contain a fully loaded [4Fe-4S] cluster. While the initial analysis of anaerobically prepared SP lyase provided characteristic spectroscopic features of an iron-sulfur cluster [22], the results provided herein provide a more thorough understanding of the iron-sulfur cluster present in SP lyase.

Mössbauer analysis revealed a mixture of cluster states of the as-isolated and reduced SP lyase, which are converted to primarily [4Fe-4S] clusters upon reduction. Reductive cluster conversions (from [3Fe-4S]¹⁺ and [2Fe-2S]¹⁺ states to [4Fe-4S]^{2+/1+} have previously been reported for several radical SAM enzymes including biotin synthase [42-44], lipoyl synthase [45-46], lysine 2,3-aminomutase [47-48], and the activating enzymes of pyruvate formate lyase [49-52] and anaerobic ribonucleotide reductase [53], although the physiological relevance of these cluster conversions remain unknown. As-isolated SP lyase was determined to contain 40% [2Fe-2S]²⁺ clusters and 15% [4Fe-4S]²⁺ clusters. The remaining 45% was attributed to unresolvable broad ferric species. The addition of the cofactor SAM did not appear to have an effect on the cluster states of the as-isolated enzyme. Reduced SP lyase was determined to contain 60% [4Fe-4S]¹⁺ clusters as well as contributions from Fe²⁺ (10% ionic Fe²⁺ and 15% rubredoxin

FeS₄-type) and Fe³⁺ (15%). Upon adding SAM to the reduced SP lyase, it appears there may be some non-productive SAM cleavage as a 15% loss of the [4Fe-4S]¹⁺ state is observed as compared to the reduced spectrum. However, there does not appear to be a simple change to a [4Fe-4S]²⁺ state as would be expected if SAM cleavage was occurring.

Previous spectroscopic studies on radical SAM enzymes have provided a wealth of information regarding the requirement of SAM in radical catalysis. Mössbauer studies on pyruvate formate-lyase activating enzyme (PFL-AE) presented evidence for the interaction of SAM with the unique iron in the [4Fe-4S] cluster of the enzyme [49]. Electron nuclear double resonance (ENDOR) spectroscopy of PFL-AE then revealed the direct ligation of SAM to the unique iron of the cluster via the carboxyl and amino groups of the methionine moiety of SAM [2-3]. Resonance Raman, Mössbauer and EPR spectroscopic studies also provided evidence for the interaction of SAM with the unique iron of the [4Fe-4S]²⁺ cluster of biotin synthase (BioB) [57].

Conversely, a Se XAS study of lysine 2,3-aminomutase (LAM) indicated an interaction between the sulfonium ion and an Fe atom of the [4Fe-4S] cluster [58]. In this work, a feature at 2.7 Å was attributed to the interaction of the Se of SeMet (a cleavage product of Se-SAM) with a cluster Fe atom when [4Fe-4S]²⁺ LAM was incubated with Se-SAM, dithionite, and the substrate analog *trans*-3,4-dihydrolysine [58]. However, this feature was not observed when Se XAS studies were performed with Se-SAM and PFL-AE or BioB [59]. This led to the suggestion that this interaction may be specific to the enzymes that utilize SAM as a cofactor rather than as a substrate, since it is not a general property of radical SAM enzymes. Because these enzymes reform SAM during catalysis,

the cleavage products of SAM must remain in the active site and therefore may result in a different binding mode of SAM to the enzyme. However, a recent study by Nicolet et al. [60] suggests the role of SAM is determined by the relative affinity of the enzyme for [dAdo + Met] and SAM and not by the cleavage mechanism itself. Consequently, one of the interests of this work was to investigate the interaction of SAM with SP lyase, the other well characterized member of the radical SAM superfamily that also utilizes SAM as a cofactor.

Our EXAFS results demonstrate the emergence of a new feature at ~ 3.0 Å as a shoulder on the Fe...Fe shell when SAM is added to the as-isolated enzyme. This feature is only observed when SAM is present. Modeling of this shoulder feature fits well for an elongated Fe...Fe scatterer of 3.0 Å relative to the expected average Fe...Fe distance (2.72 Å) for a classical [4Fe-4S] cluster with tetrathiolate coordination. When modeled as a sulfonium, the feature is clearly not in phase (Figure 5.3 C). This observation indicates a longer Fe...Fe distance upon SAM binding to the cluster and the intensity suggests this feature is due to 1.5 Fe...Fe, or two Fe...Fe distances becoming elongated in the cluster. It appears the [4Fe-4S] cluster becomes slightly distorted upon SAM ligating the unique iron of the cluster with some Fe...Fe bond distances lengthening due to this interaction.

To determine if this observation is shared by other members of the radical SAM superfamily, we took a closer look at the Fe...Fe bond distances of the [4Fe-4S] radical cluster in the crystal structures solved for members of this superfamily. Of the handful of structures solved for this superfamily, only one (MoaA, resolution 2.8 Å) does not have SAM (or a cleavage product of SAM) bound to the radical [4Fe-4S] cluster, making it difficult to determine the geometry of the cluster of the other radical SAM enzymes when

the unique Fe atom is not ligated. However, from all of the available radical SAM crystal structures, it is apparent that the average Fe...Fe bond lengths are longer ($\sim 0.07 - 0.25 \text{ \AA}$) for the unique Fe when ligated by SAM than for the other cysteine bound Fe atoms in the cluster, resulting in a slightly distorted cluster conformation. The difference between the average bond lengths for the unique Fe atom and the protein bound Fe atoms in LAM (resolution 2.1 \AA) are less at 0.007 \AA , while HemN (resolution 2.07 \AA) is the only structure to not follow this general observation. Interestingly, both of these structures contain [4Fe-4S] clusters with significantly shorter ($0.14 - 0.32 \text{ \AA}$) Fe...Fe distances as compared to the other structures.

MoaA is the only radical SAM enzyme that has structures solved for both the SAM-bound and unbound forms of the enzyme in 2.2 and 2.8 \AA resolution, respectively. While the unligated unique Fe atom has slightly longer average Fe...Fe distances than the average protein bound Fe atoms (by $0.03 - 0.05 \text{ \AA}$), this distance is increased upon SAM ligation ($0.07 - 0.22 \text{ \AA}$). The slight distortion of the [4Fe-4S] cluster upon SAM binding observed in MoaA suggests that the elongated Fe...Fe distances are attributable to SAM ligating the unique Fe of the cluster. Specifically, the Fe₃...Fe₄ distance increases by 0.16 \AA for cluster A of the dimer and by 0.22 \AA for cluster B. The Fe₂...Fe₄ distance also increases for each cluster of the dimer by 0.09 \AA and 0.07 \AA (for cluster A and B, respectively). The changes in the clusters upon SAM binding MoaA are presented in Table 5.3. The distances that change for both clusters in the dimer upon SAM binding are indicated in bold. The observation that two of the Fe...Fe distances become elongated upon SAM binding agrees with our EXAFS data and suggests SP lyase may also have two Fe...Fe distances becoming elongated upon the unique Fe being ligated by SAM. The

Fe3...Fe4 distance of the SAM-bound PFL-AE structure is also elongated at 2.88 Å as compared to the other distances in the structure [12], while the HydE SAM-bound structure appears to have 3 elongated Fe...Fe distances for the unique Fe [60] (Table S1, Appendix B).

Table 5.3. Cluster changes in MoaA upon SAM binding.

Enzyme		MoaA	MoaA		MoaA	MoaA	
PDB code		1TV7	1TV8		1TV7	1TV8	
Resolution		2.8	2.2		2.8	2.2	
cluster		A	A		B	B	
			SAM bound	Change		SAM bound	Change
Fe-Fe Distances	Fe1...Fe2	2.71	2.71	0.00	2.72	2.80	0.08
	Fe2...Fe3	2.63	2.63	0.00	2.66	2.47	-0.19
	Fe3...Fe4	2.56	2.72	0.16	2.62	2.84	0.22
	Fe4...Fe1	2.80	2.74	-0.06	2.76	2.82	0.06
	Fe1...Fe3	2.65	2.69	0.04	2.66	2.50	-0.16
	Fe2...Fe4	2.79	2.88	0.09	2.76	2.83	0.07

Resolution of the X-ray structures and distances are given in Å. Cluster numbering as in PDB code 3CIW with the unique Fe labeled as Fe4.

A similar observation is made for aconitase when the unique Fe atom in the [4Fe-4S] cluster is ligated by citrate [61]. In the unligated form, the average Fe...Fe distances for the unique Fe atom are ~ 0.01 Å shorter than the protein bound Fe atoms [62]. However, upon ligation by citrate, the average Fe...Fe distances for the unique Fe atom are 0.2 Å longer than the average Fe...Fe distances for the protein bound Fe atoms, suggesting distortion of the [4Fe-4S] cluster. Several of the Fe...Fe distances increase in the S642A aconitase crystal structure in the presence of the citrate substrate. The

Fe1...Fe2 distance increases by 0.17 Å, Fe3...Fe4 increases by 0.18 Å, the Fe4...Fe1 distance increases by 0.23 Å and the Fe2...Fe4 distance increases by a surprising 0.38 Å (Table S1 Appendix B).

The Fe K-edge XANES in Figure 5.4 show two oxidation states for the as-isolated and reduced samples as clearly observed with shifts in the rising edge. The higher intensity of the pre-edge feature for as-isolated in the presence of SAM may also indicate the distortion of the [4Fe-4S] cluster upon interacting with SAM as pre-edge features gain intensity when the symmetry is reduced and thus Fe 4p orbitals are allowed to mix with Fe 3d orbitals. A noteworthy observation of the spectra is the small differences in the spectral features between the reduced sample and the reduced sample in the presence of SAM. EPR spectroscopy of the reduced enzyme in the presence of SAM shows a broadened signal of the [4Fe-4S]¹⁺ signal with a striking decrease in intensity [19, 22]. Previous studies have suggested the decreased EPR intensity is due to non-productive SAM cleavage, meaning SAM is reductively cleaved by the [4Fe-4S]¹⁺ cluster to produce methionine, 5'deoxyadenosine and a [4Fe-4S]²⁺ cluster without turnover of substrate to product occurring [13]. However, a recent study demonstrated little dAdo production in the absence of dithionite and substrate, as is the case in these samples [22]. The spectra presented in Figure 5.4 demonstrate upon the addition of SAM to the reduced enzyme, there is no apparent oxidation of the cluster. In fact, the addition of SAM shifts the features of the rising edge to slightly lower energy, away from the oxidized spectra of the as-isolated SP lyase samples. This supports the previous observations in our laboratory that the interaction of SAM with the [4Fe-4S]¹⁺ cluster of SP lyase is not due to SAM cleavage and the accompanied oxidation of the cluster [22].

The sulfur K-edge spectra of free ligands (Figure 5.5) demonstrates the shift in energy of the edge position to higher energies, directly indicating an increase in the sulfur effective nuclear charge (Z_{eff}). The Na_2S , NaSH and NaSET compounds show shifts in the rising-edge region displaying lower Z_{eff} as compared to methionine and cysteine. Methionine and cysteine display similar spectral features as well as similar rising edge energies. SAM displays a high intensity feature ~ 2475.5 eV due to 3 C-S σ^* interactions as well as a large shift of the rising edge feature to higher energy due to the higher Z_{eff} of the sulfonium ion. The lower energy shoulder just below 2474 eV in the SAM spectrum is most likely due to the presence of 5'-methylthioadenosine (MTA) present in the sample.

Rigorous evaluation of the S K-edge XAS spectra for anaerobically isolated SP lyase (Figure 5.6) is hindered by the presence of mixture of cluster states as demonstrated by Mössbauer spectroscopy. In agreement with the Mössbauer data, the pre-edge peak energies for the as-isolated SP lyase indicate primarily [2Fe-2S] clusters present in this sample while the pre-edge peak energies for the reduced sample are more indicative of a [4Fe-4S] cluster. The addition of SAM to the as-isolated sample results in a spectrum with greater intensity and significant changes in the pre-edge spectral features. When the free ligand of SAM is subtracted from the spectra of samples containing SAM, the resulting pre-edge fits have nearly the same peak energies of those before the free ligand of SAM subtracted.

Overall the combined spectroscopic analysis of anaerobically isolated SP lyase indicate that the specific interaction of the Fe-S cluster of SP lyase with its cofactor SAM as observed by EPR is not due to non-productive SAM cleavage and formation of a [4Fe-4S]²⁺ cluster. The interaction between the cluster and SAM appears to produce a slight

distortion of the cluster with some of the Fe...Fe distances increasing. This observation may include other members of the radical SAM superfamily and may be critical for reducing the cluster or initiating radical catalysis.

References

1. Sofia HJ, Chen G, Hetzler BG, Reyes-Spindola JF, Miller NE (2001) *Nucleic Acids Res.* 29:1097-1106
2. Walsby CJ, Hong W, Broderick WE, Cheek J, Ortillo D, Broderick JB, Hoffman BM (2002) *J. Am. Chem. Soc.* 124:3143-3151
3. Walsby CJ, Ortillo D, Broderick WE, Broderick JB, Hoffman BM (2002) *J. Am. Chem. Soc.* 124:11270-11271
4. Walsby C, Ortillo D, Yang J, Nnyepi M, Broderick WE, Hoffman BM, Broderick JB (2005) *Inorg. Chem.* 44:727-741
5. Layer G, Moser J, Heinz DW, Jahn D, Schubert W-D (2003) *EMBO J.* 22:6214-6224
6. Chen D, Walsby C, Hoffman BM, Frey PA (2003) *J. Am. Chem. Soc.* 125:11788-11789
7. Berkovitch F, Nicolet Y, Wan JT, Jarrett JT, Drennan CL (2004) *Science* 303:76-79
8. Hänzelmann P, Schindelin H (2004) *Proc. Natl. Acad. Sci. U.S.A.* 101:12870-12875
9. Hänzelmann P, Schindelin H (2006) *Proc. Natl. Acad. Sci. U.S.A.* 103:6829-6834
10. Lepore BW, Ruzicka FJ, Frey PA, Ringe D (2005) *Proc. Natl. Acad. Sci. U.S.A.* 102:13819-13824
11. Nicolet Y, Rubach JK, Posewitz MC, Amara P, Mathevon C, Atta M, Fontecave M, Fontecilla-Camps JC (2008) *J. Biol. Chem.* 283:18861-18872
12. Vey JL, Yang J, Li M, Broderick WE, Broderick JB, Drennan CL (2008) *Proc. Natl. Acad. Sci. U.S.A.* 105:16137-16141
13. Rebeil R, Nicholson WL (2001) *Proc. Natl. Acad. Sci. U.S.A.* 98:9038-9043

14. Munakata N, Rupert CS (1972) *J. Bacteriol.* 111:192-198
15. Munakata N, Rupert CS (1974) *Mol. Gen. Genet.* 130:239-250
16. Cheek J, Broderick JB (2002) *J. Am. Chem. Soc.* 124:2860-2861
17. Varghese AJ (1970) *Biochem. Biophys. Res. Commun.* 38:484-490
18. Donnellan JE, Jr., Setlow RB (1965) *Science* 149:308-310
19. Buis JM, Cheek J, Kalliri E, Broderick JB (2006) *J. Biol. Chem.* 281:25994-26003
20. Mehl RA, Begley TP (1999) *Org. Lett.* 1:1065-1066
21. Chandra T, Silver SC, Zilinskas E, Shepard EM, Broderick WE, Broderick JB (2009) *J. Am. Chem. Soc.* 131:2420-2421
22. Silver SC, Chandra T, Zilinskas E, Ghose S, Broderick WE, Broderick JB (2010) *J. Biol. Inorg. Chem.* 15:943-955
23. Mantel C, Chandor A, Gasparutto D, Douki T, Atta M, Fontecave M, Bayle P-A, Mouesca J-M, Bardet M (2008) *J. Am. Chem. Soc.* 130:16978-16984
24. Chandor A, Berteau O, Douki T, Gasparutto D, Sanakis Y, Ollagnier-de-Choudens S, Atta M, Fontecave M (2006) *J. Biol. Chem.* 281:26922-26931
25. Chandor A, Douki T, Gasparutto D, Gambarelli S, Sanakis Y, Nicolet Y, Ollagnier-de-Choudens S, Atta M, Fontecave M (2007) *C. R. Chimie* 10:756-765
26. Broderick JB, Henshaw TF, Cheek J, Wojtuszewski K, Smith SR, Trojan MR, McGhan RM, Kopf A, Kibbey M, Broderick WE (2000) *Biochem. Biophys. Res. Comm.* 269:451-456
27. Miller JR, Busby RW, Jordan SW, Cheek J, Henshaw TF, Ashley GW, Broderick JB, Cronan JE, Jr., Marletta MA (2000) *Biochemistry* 39:15166-15178
28. Ugulava NB, Sacanell CJ, Jarrett JT (2001) *Biochemistry* 40:8352-8358
29. Bradford M (1976) *Anal. Biochem.* 72:248-254
30. Beinert H (1978) *Methods Enzymol.* 54:435-445
31. Beinert H (1983) *Anal. Biochem.* 131:373-378

32. Solomon EI, Hedman B, Hodgson KO, Dey A, Szilagyi RK (2005) *Coord. Chem. Rev.* 249:97-129
33. Newville M, Liviņš P, Yacoby Y, Rehr JJ, Stern EA (1993) *Phys. Rev. B* 47:14126-14131
34. Ravel B, Newville M (2005) *J. Synchrotron Radiat.* 12:537-541
35. Newville M, Ravel B, Haskel D, Rehr JJ, Stern EA, Yacoby Y (1995) *Physica B* 208:154-156
36. Ankudinov AL, Nesvizhskii AI, Rehr JJ (2003) *Phys Rev B* 67:-
37. Middleton P, Dickson DP, Johnson CE, Rush JD (1978) *Eur. J. Biochem.* 88:135-141
38. Westre TE, Kennepohl P, DeWitt JG, Hedman B, Hodgson KO, Solomon EI (1997) *J. Am. Chem. Soc.* 119:6297-6314
39. Shulman RG, Yafet Y, Eisenberger P, Blumberg WE (1976) *Proc. Natl. Acad. Sci. U.S.A.* 73:1384-1388
40. Shadle SE, Hedman B, Hodgson KO, Solomon EI (1995) *J. Am. Chem. Soc.* 117:2259-2272
41. Dey A, Glaser T, Moura JGG, Holm RH, Hedman B, Hodgson KO, Solomon EI (2004) *J. Am. Chem. Soc.* 126:16868-16878
42. Ugulava NB, Gibney BR, Jarrett JT (2000) *Biochemistry* 39:5206-5214
43. Duin EC, Lafferty ME, Crouse BR, Allen RM, Sanyal I, Flint DH, Johnson MK (1997) *Biochemistry* 36:11811-11820
44. Tse Sum Bui B, Florentin D, Marquet A, Benda R, Trautwein AX (1999) *FEBS Lett.* 459:411-414
45. Busby RW, Schelvis JPM, Yu DS, Babcock GT, Marletta MA (1999) *J. Am. Chem. Soc.* 121:4706-4707
46. Ollagnier-de Choudens S, Fontecave M (1999) *FEBS Lett.* 453:25-28
47. Lieder K, Booker S, Ruzicka FJ, Beinert H, Reed GH, Frey PA (1998) *Biochemistry* 37:2578-2585

48. Petrovich RM, Ruzicka FJ, Reed GH, Frey PA (1992) *Biochemistry* 31:10774-10781
49. Krebs C, Broderick WE, Henshaw TF, Broderick JB, Huynh BH (2002) *J. Am. Chem. Soc.* 124:912-913
50. Krebs C, Henshaw TF, Cheek J, Huynh B-H, Broderick JB (2000) *J. Am. Chem. Soc.* 122:12497-12506
51. Broderick J, Duderstadt R, Fernandez D, Wojtuszewski K, Henshaw T, Johnson M (1997) *J. Am. Chem. Soc.* 119:7396-7397
52. Yang J, Naik SG, Ortillo DO, Garcia-Serres R, Li M, Broderick WE, Huynh BH, Broderick JB (2009) *Biochemistry* 48:9234-9241
53. Ollagnier S, Meier C, Mulliez E, Gaillard J, Schuenemann V, Trautwein A, Mattioli T, Lutz M, Fontecave M (1999) *J. Am. Chem. Soc.* 121:6344-6350
54. Rose K, Shadle SE, Glaser T, de Vries S, Cherepanov A, Canters GW, Hedman B, Hodgson KO, Solomon EI (1999) *J. Am. Chem. Soc.* 121:2353-2363
55. Anxolabéhère-Mallart E, Glaser T, Frank P, Aliverti A, Zanetti G, Hedman B, Hodgson KO, Solomon EI (2001) *J. Am. Chem. Soc.* 123:5444-5452
56. Glaser T, Bertini I, Moura JJG, Hedman B, Hodgson KO, Solomon EI (2001) *J. Am. Chem. Soc.* 123:4859-4860
57. Coper MM, Jameson GN, Davydov R, Eidsness MK, Hoffman BM, Huynh BH, Johnson MK (2002) *J. Am. Chem. Soc.* 124:14006-14007
58. Coper NJ, Booker SJ, Ruzicka F, Frey PA, Scott RA (2000) *Biochemistry* 39:15668-15673
59. Coper MM, Coper NJ, Hong W, Shokes JE, Broderick WE, Broderick JB, Johnson MK, Scott RA (2003) *Protein Sci.* 12:1573-1577
60. Nicolet Y, Amara P, Mouesca JM, Fontecilla-Camps JC (2009) *Proc. Natl. Acad. Sci. U.S.A.* 106:14867-14871
61. Lloyd SJ, Lauble H, Prasad GS, Stout CD (1999) *Protein Sci.* 8:2655-2662
62. Robbins AH, Stout CD (1989) *Proc. Natl. Acad. Sci. U.S.A.* 86:3639-3643

CHAPTER 6

CONCLUDING REMARKS

Spore photoproduct lyase repairs a unique thymine dimer found to accumulate in spore forming organisms and is largely responsible for the high resistance of these organisms to UV light. This enzyme is the first nonphotoactivatable pyrimidine dimer lyase and is found in *Bacillus*, *Clostridium* and other spore-forming organisms. The UV resistance of spores poses a major health risk to humans as these organisms are responsible for a variety of diseases including tetanus, botulism, and anthrax, but are difficult to kill due to their unusually high resistance to UV light. Therefore, understanding the mechanism of DNA repair by which these spore forming organisms confer their UV resistance is of great interest. The goal of this work was to develop a molecular-level understanding of the repair of this unique DNA damage by SP lyase. The work presented in this dissertation provides a deeper understanding of the formation and repair of the unique thymine dimer formed in sporulating bacteria.

One of the outstanding questions regarding repair of SP by SP lyase was the substrate upon which SP lyase acts. While in theory two stereoisomers of SP could be formed and repaired, it would be quite surprising that both were being formed *in vivo* and even more surprising that SP lyase would be able to repair two very different conformations of SP. In order to identify the substrate for SP lyase, both the 5*R*- and 5*S*-SP dinucleosides and dinucleotides were synthesized and characterized. The ability of SP lyase to repair each of these stereochemically defined substrates was then investigated.

The work presented in Chapter 2 demonstrated the repair of the synthetic *5R*-SP, but not the *5S*-SP dinucleoside (lacking a phosphodiester bridge) by SP lyase. This finding provided the first definitive evidence for the stereochemical requirement for SP repair by SP lyase. However, repair was quite slow ($0.4 \text{ nmol min}^{-1} \text{ mg}^{-1}$) and did not proceed to completion. Following this work, we characterized for the first time the ability of SP lyase to repair the pure stereochemically defined dinucleotide (containing a phosphodiester bridge) substrates. The results, presented in Chapter 3, supported our previous conclusions with the repair of the *5R*-SPTpT but not the *5S*-SPTpT dinucleotide. The repair of the *5R*-SPTpT dinucleotide went to completion with 10 turnovers in less than 40 minutes. This relatively rapid repair was determined to be 18 fold higher than the observed repair of the dinucleoside with a specific activity of $7.1 \text{ nmol min}^{-1} \text{ mg}^{-1}$. The turnover rate was lower than that observed using “native” substrate ($0.33 \text{ } \mu\text{mol min}^{-1} \text{ mg}^{-1}$) generated by irradiating DNA with UV light under appropriate conditions. These results demonstrate the necessity of a complete substrate for optimal enzyme efficiency.

Our results demonstrating the repair of the *5R*-SP dinucleoside and dinucleotide provide the most convincing evidence to date for the repair reaction catalyzed by SP lyase. However, our results contradict earlier reports that the *5S*-SP but not the *5R*-SP is a substrate for SP lyase. While we can not be certain what precisely led to the different conclusion in the previously published work, the turnover of *5R*-SPTpT reported here is both rapid and complete, allowing for complete characterization of turnover and providing definitive evidence for our conclusion that SP lyase is stereospecific for *5R*-SP. Our conclusion that the *5R* isomer of SP is the only one repaired by SP lyase is further

supported by a recent report that UV irradiation of TpT produced only 5*R*-SPTpT. The study utilized a combination of NMR techniques combined with DFT analysis to unambiguously determine the assignment of the 5*R*-SPTpT in UV-irradiated TpT.

Work in our lab is now being conducted to incorporate SP into a 14-mer DNA oligo. We have previously synthesized the SP amidite and the Barton group is attempting to complete the custom synthesis. This will allow a characterization of turnover with a more complete and physiologically relevant substrate. Furthermore, it will be of interest to characterize the role of SAM using this complete substrate. Previous repair assays using “native” substrate prepared by UV-irradiating DNA demonstrated the role of SAM as a cofactor. However, when synthetic substrates were utilized in repair assays, cleavage products of SAM were observed indicating the role of SAM as a co-substrate. The difference between the observed roles of SAM in these assays may be due to the incomplete substrate utilized when synthetic substrates are used as compared to the complete “native” substrate. The DNA backbone may play a critical role in sealing off the active site of SP lyase, eliminating non-productive SAM cleavage during turnover. Incorporating SP into a DNA oligo may aid in elucidating the role of SAM during repair of SP.

To elucidate the parameters of SP formation as well as repair, we performed repair assays using SP pUC18 DNA grown in media enriched with [*C*-6-³H] thymidine. A previous study utilizing this particular substrate demonstrated the incorporation of ³H into AdoMet during the course of turnover with SP lyase. During these assays we took aliquots and determined the amount of ³H transferred to AdoMet. The results indicated a

primary kinetic isotope effect of 15 – 17.2, which lies in the expected range for enzymes which catalyze reactions where the isotopically sensitive step is considerably rate limiting. The results suggested the nonstereospecific formation of SP with regards to the C-6 H atom with subsequent stereospecific abstraction of a H atom by SP lyase. These results provide some of the first experimental evidence regarding the formation of SP.

One of the difficulties of this reaction is quantitatively determining the amount of SP repaired during the course of the reaction. The amount of SP in a reaction mixture is determined by LSC, which measures the amount of ^3H in thymidine or SP. However, the ^3H is being abstracted from C-6 of SP by AdoMet over the course of the reaction. Therefore, the assays could be repeated with substrate labeled with ^3H and ^{14}C to quantify the amount of SP remaining in the reaction mixture.

While this study determined a kinetic isotope effect for the abstraction of the C-6 H atom from SP, it did not determine which H atom is abstracted from the C-6 position. We hypothesize that the pro-*S* H atom is being abstracted as discussed in Chapter 4. However, experimental studies would be required to demonstrate this action. This could be determined by utilizing SP specifically deuterated at the C-6 position. However, this would require an involved and expensive synthesis which may not yield the desired substrate. Other possible experiments include separating the SP from the reaction mixture of the kinetic isotope assay and subject it to NMR analysis. Because of the KIE, the 50% reaction time point would have a buildup of the substrate with a ^3H atom in the position that was being abstracted. Therefore, we could in theory analyze this aliquot with the aim of determining which H atom is being abstracted. Unfortunately, this analysis would be

limited by the amount of SP present, which may not be the minimum required to determine the stereochemistry utilizing NMR techniques.

The thorough characterization of the [Fe-S] cluster present in anaerobically isolated SP lyase revealed an inhomogenous mix of cluster states. While the addition of SAM did not appear to change any of the oxidation states of the [Fe-S] cluster present in the as-isolated enzyme, it did appear to change the geometry of the cluster as indicated by Fe K-edge EXAFS analysis. The EXAFS results indicate a shoulder on the Fe-Fe shell around 3.0 Å. Modeling of this feature provided evidence for longer Fe-Fe distances present in the as-isolated form of SP lyase in the presence of SAM. This observation may not be unique to SP lyase and may indicate an important step of initiating radical catalysis in the radical SAM superfamily. This observation is currently under further investigation to elucidate its importance.

The Fe K-edge XANES provided evidence for two oxidation states of the as-isolated and reduced samples with different shifts in the rising edge. The higher intensity of the preedge feature for as-isolated in the presence of SAM may also indicate the distortion of the [4Fe-4S] cluster upon interacting with SAM as preedge features gain intensity when the symmetry is reduced. The specific interaction between the [Fe-S] cluster of SP lyase and its cofactor SAM were first investigated in an EPR study in Chapter 3. Interestingly, the EPR spectrum of reduced SP lyase in the presence of SAM results in broadening of the spectral features and a marked decrease in intensity. Previously, this observation has been attributed to SAM cleavage to form methionine and 5'-deoxyadenosine with an electron from the [4Fe-4S]¹⁺ cluster to form a [4Fe-4S]²⁺

cluster. However, the investigation of SAM cleavage in the absence of dithionite and substrate presented evidence for only a small amount of SAM cleavage. Furthermore, Mössbauer analysis provided a decrease in the amount of $[4\text{Fe-4S}]^{1+}$ clusters in the presence of SAM, but not formation of any $[4\text{Fe-4S}]^{2+}$ clusters. The Fe K-edge XANES demonstrate upon the addition of SAM to the reduced enzyme, there is no apparent oxidation of the cluster. In fact, the addition of SAM shifts the features of the rising edge to slightly lower energy, away from the oxidized spectra of the as-isolated SP lyase samples. This supports the previous observations in our laboratory that the unique interaction of SAM with the $[4\text{Fe-4S}]^{1+}$ cluster of SP lyase is not due to SAM cleavage and the accompanied oxidation of the cluster.

The studies presented in this dissertation have provided some key insights into how SP is formed and repaired in bacterial spores. We have demonstrated the substrate for SP lyase is the 5*R*-SP and the completeness of the substrate directly affects the repair activity of SP lyase. The KIE study has provided some of the first experimental evidence regarding the stereospecificity of SP formation as well as important kinetic information regarding the repair of SP. Our spectroscopic analysis has provided insights not only into SP lyase, but perhaps for many of the other radical SAM enzymes as well.

APPENDICES

APPENDIX A

SUPPORTING INFORMATION FOR CHAPTER 2

Chapter 2: Specific Repair of the 5R but not the 5S Spore Photoproduct by Spore Photoproduct Lyase

Published: *Journal of the American Chemical Society*, **2009**, *131*, 2420-2421

Further Supporting Information is available free of charge via the Internet at <http://pubs.acs.org>. This contains synthetic methods and NMR characterization of all synthetic SPs mentioned herein; NOESY and ROESY of selected compounds; molecular modeling of SPs; mass spec data on T and SP peaks from the HPLC-based assay.

Enzyme Assays

Assays were conducted under strictly anaerobic conditions in an MBraun glove box operating at <1 ppm. Assays included *R* or *S* SP (1.0 mM), AdoMet (1.0 mM), DTT (5 mM), and dithionite (1 mM) in buffer (45 mM Hepes, 362 mM NaCl, 30 mM KCl, pH 7.5). SPL (50 μ M) was added to initiate the reaction, and aliquots were taken at specific time points, boiled for 45 s, centrifuged, and diluted prior to injecting onto an HPLC column (Waters ODS2 C18) for analysis. Samples were eluted using a gradient of acetonitrile in water (0% to 10% from 2 min to 20 min, then to 20% from 20 to 25 min).

Analysis of Turnover

HPLC was used to analyze turnover of the synthetic SP substrates, as described in the text of the communication. The peak eluting at 14.4 min was initially identified as thymidine by co-injection with an authentic thymidine sample. To confirm this identification, the 14.4 min peaks from several assays of the 5R-SP were combined, concentrated, and subjected to QTOF MS; the results of this analysis are shown in Fig S1. As can be seen in the mass spectrum, a peak corresponding to thymidine ($M + Na = 265$) is observed. The peak eluting at ~15 – 17 minutes in the chromatograms has been analyzed by MS and found to comprise an inhomogenous mixture of small peptides that

whose composition is consistent with the sequence of SPL. We presume that these peptides are generated as a result of sample workup after the assay.

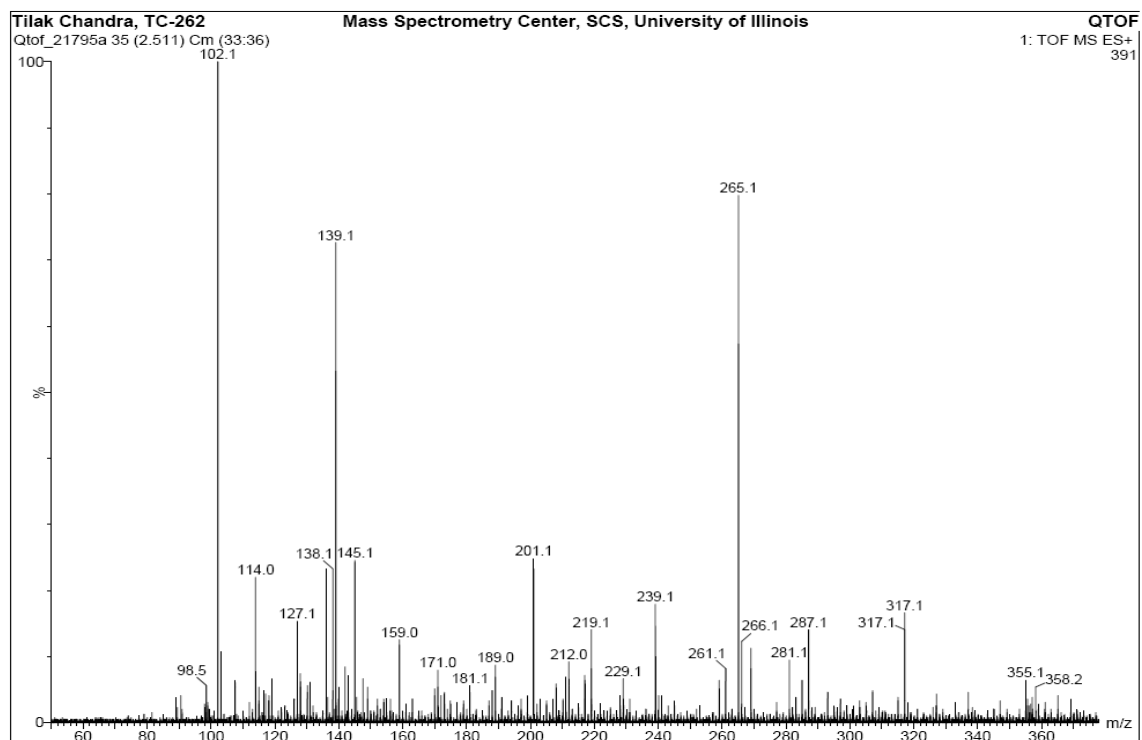


Figure S1. Mass spectrum of thymidine isolated from the assay mixture ($M + Na = 265$).

APPENDIX B

SUPPORTING INFORMATION FOR CHAPTER 5

Chapter 5: Combined Mössbauer and Multi-Edge X-Ray Absorption Spectroscopic Study of the Fe-S Cluster in Spore Photoprotein Lyase

Table S1. EXAFS fit parameters.

Scatter	Fit A	Fit B	Fit C
Fe-S ^s			
N	1.86	1.92	2.69
R (Å)	2.25	2.26	2.26
s ² (Å ²)	0.001	0.002	0.00
Fe-S ^t			
N	1.16	1.44	1.31
R (Å)	2.12	2.13	2.12
s ² (Å ²)	0.001	0.002	0.00
Fe...Fe			
N	0.85	0.75	1.20
R (Å)	2.70	2.74	2.70
s ² (Å ²)	0.006	0.00	0.01
Fe...Fe			
N		0.59	
R (Å)		3.00	
s ² (Å ²)		0.005	
SO ₂	1.0	1.0	0.64
E ₀ (eV)	-9.69	-10.00	-9.57
k-range	2 - 13	2 - 13	2 - 13
R(fit)	7.8%	11.8%	10.7%

A: As-isolated SP lyase, B: As-isolated SP lyase + SAM, C: Reduced SP lyase

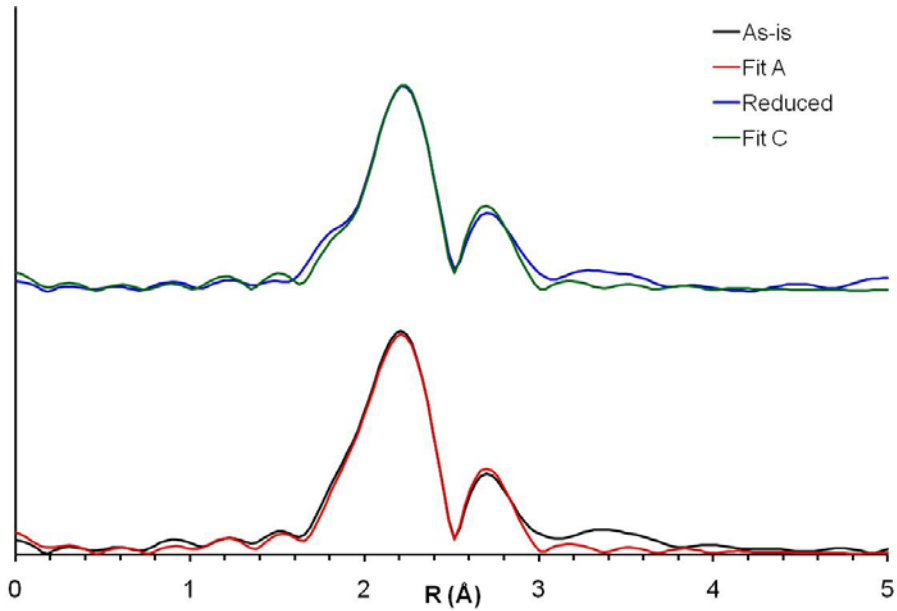


Figure S2. FT of EXAFS shown in S3. Fits of the as-isolated SP lyase (Fit A) and reduced SP lyase (Fit C).

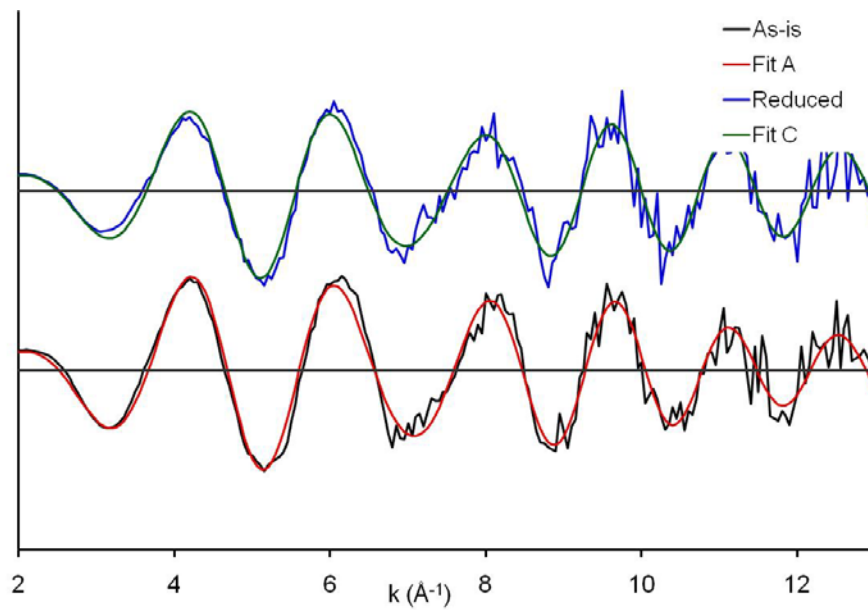


Figure S3. Fe K-edge EXAFS for the as-isolated SP lyase (Fit A) and reduced SP lyase (Fit C).

Table S2. Fe...Fe, Fe-S Distances in radical SAM enzymes and aconitase (Ac). Resolution of the X-ray structures and distances are given in Å.

	Enzyme	MoaA		MoaA SAM		PFL-AE SAM	HydE SAM	HydE Met dAdo	HemN SAM	LAM SAM	Ac	Ac Citrate
	PDB code	1TV7		1TV8		3CB8	3IZ	3IIX	1OLT	2A5H	6ACN	1C96
	Resolution	2.8		2.2		2.77	1.62	1.25	2.07	2.1	2.5	1.81
	Cluster	A	B	A	B					A		
Fe-Fe Distances	Fe1...Fe2	2.71	2.72	2.71	2.80	2.68	2.71	2.72	2.48	2.56	2.62	2.79
	Fe2...Fe3	2.63	2.66	2.63	2.47	2.70	2.72	2.73	2.45	2.52	2.70	2.72
	Fe3...Fe4	2.56	2.62	2.72	2.84	2.88	2.83	2.88	2.56	2.55	2.62	2.80
	Fe4...Fe1	2.80	2.76	2.74	2.82	2.74	2.84	2.96	2.49	2.52	2.71	2.94
	Fe1...Fe3	2.65	2.66	2.69	2.50	2.76	2.67	2.68	2.66	2.58	2.70	2.65
	Fe2...Fe4	2.79	2.76	2.88	2.83	2.74	2.83	2.96	2.37	2.61	2.66	3.04
Fe-S Distances	Fe1-S1	2.28	2.34	2.28	2.33	2.29	2.32	2.31	2.24	2.21	2.29	2.24
	Fe1-S2	2.33	2.31	2.30	2.31	2.31	2.24	2.27	2.12	2.13	2.27	2.24
	Fe1-S3	2.28	2.27	2.32	2.32	2.30	2.30	2.29	2.21	2.13	2.33	2.28
	Fe2-S1	2.23	2.25	2.29	2.28	2.30	2.26	2.29	2.22	2.15	2.32	2.17
	Fe2-S2	2.27	2.27	2.25	2.47	2.30	2.30	2.33	2.10	2.13	2.31	2.28
	Fe2-S4	2.28	2.35	2.30	2.22	2.30	2.33	2.32	2.30	2.15	2.31	2.49
	Fe3-S2	2.29	2.27	2.28	2.32	2.29	2.32	2.32	2.22	2.12	2.30	2.30
	Fe3-S3	2.22	2.29	2.30	2.30	2.29	2.24	2.25	2.12	2.14	2.34	2.25
	Fe3-S4	2.25	2.29	2.23	2.36	2.29	2.31	2.32	2.24	2.17	2.34	2.47
	Fe4-S1	2.28	2.29	2.30	2.35	2.31	2.33	2.44	2.28	2.33	2.38	2.32
	Fe4-S3	2.29	2.34	2.32	2.34	2.31	2.35	2.39	2.17	2.16	2.39	2.28
Fe4-S4	2.23	2.24	2.34	2.37	2.31	2.28	2.35	2.26	2.15	2.33	2.38	
Fe-SR Distances	Fe1-S	2.25	2.25	2.33	2.24	2.23	2.28	2.27	2.32	2.29	2.32	2.42
	Fe2-S	2.23	2.38	2.20	2.50	2.25	2.34	2.29	2.49	2.30	2.31	2.29
	Fe3-S	2.35	2.39	2.36	2.53	2.31	2.26	2.32	2.35	2.30	2.30	2.24
Fe-SAM Distances	Fe4-O	NA	NA	1.97	2.18	2.12	2.25	2.27	2.24	1.98	NA	NA
	Fe4-N	NA	NA	2.30	2.24	2.17	2.33	2.24	2.55	1.98	NA	NA
	Fe4-S+	NA	NA	3.19	3.18	3.22	3.25	2.67	3.49	3.15	NA	NA
	S3-S+	NA	NA	3.45	3.64	4.18	3.90	3.51	3.70	3.86	NA	NA
	S4-S+	NA	NA	3.84	3.62	3.97	3.66	3.50	4.04	3.79	NA	NA